Max-Planck-Institut für Metallforschung
Stuttgart

Characterization of the conduction properties of alkali metal ion conducting solid electrolytes using thermoelectric measurements

Devendraprakash Gautam

Dissertation
an der
Universität Stuttgart

Bericht Nr. 190
September 2006

Characterization of the conduction properties of alkali metal ion conducting solid electrolytes using thermoelectric measurements

Dissertation

Von der Fakultät Chemie der Universität Stuttgart

zur Erlangung der Würde eines

Doktors der Naturwissenchaften (Dr. rer. nat.)

genehmigte Abhandlung

Vorgelegt von

Devendraprakash Gautam

Aus Deori Hatai, Indien

Hauptberichter: Prof. Dr. rer. nat. F. Aldinger

Mitberichter: Prof. Dr. rer. nat. E. Roduner

Tag der mündlichen Prüfung: 19. September 2006

Institut für Nichtmetallische Anorganische Materialien der Universität Stuttgart

Max-Planck-Institüt für Metallforschung, Stuttgart

Pulvermetallurgisches Laboratorium

2006

Dedicated to my teachers and to my family and specially to my Bulbul

One’s ignorance does not change reality; it simply alters the perception of reality, resulting in misperception and misconception of what is and what is not, what can be done and what can not be done.

Acknowledgements

This doctoral work was done from June 2002 to June 2006 at Max-Planck-Institut für Metallforschung, Stuttgart, supported by a scholarship of the Max-Planck-Gesellschaft which is gratefully acknowledged.

I wish to express my deep gratitude to my advisor Prof. Dr. Fritz Aldinger for giving me an opportunity to realize this thesis in his department. He encouraged me with much kindness throughout the work. In particular, I appreciate his support, confidence and the remarkable patience he had with me.

I express my sincere heartfelt thanks to Dr. Helfried Näfe for introducing me to the beauty of solid state electrochemistry, the initiation and subject of this work. This thesis would not have been possible without the scientific support, the trenchant critiques, the probing questions and patience of Dr. Näfe. I cherish, the most, the excellent lively scientific discussions, sometimes heated, which I had with him during the course of my work. I benefited and learnt a lot from him in approaching a problem not only in scientific matters but life in general.

Prof. Dr. E. Roduner is gratefully acknowledged for giving his consent to be “Mitberichter’’ for the final examination. I also express my profuse thanks to Prof. Dr. E. J. Mittemeijier for accepting to be “Prüfungsvorsitzender’’ for the final examination.

My heartfelt thanks I want to give to Prof. Kamal Singh from Department of Physics, Nagpur University, Nagpur, who was my supervisor during postgraduate and continued to give her guidance, her blessings and incitement to perform my best.

Special thanks to Mrs. Gisela Feldhofer for her technical support of the experimental work. I am greatly indebted to her not only for the motherly affection which she showered on me but also for her encouragement during the difficult times.

Further there are many people who helped me in many ways during my stay. My thanks are given to all colleagues in Powder Metallurgical Laboratory (PML) who made my work here comfortable. In particular, to Mrs. S. Paulsen and Ms. M. Henschke for

administrative work; to Mr. G. Kaiser and Mr. H. Labitzke for their help and advice in carrying out the chemical analyses and SEM; to Mr. H. Eckstein, Mr. I. Kozmon, Mr. M. Zeindelmeir for technical assistance; Ms. M. Thomas for XRD analyses; Mr. E. Bruckner for providing the computer services.

I would like to thank my friends and colleagues from “Functional Ceramics Working Group”: Krenar Shqau, Bogdan Khorkounov, Vladimir Plashnitsa, Natalia Karpukhina, Subasri Raghavan, Steffi Gollhofer, Ruhul Amin, Michael Feldhofer, Amit Sinha and Yude Wang who made my days at PML memorable and also my life comfortable.

I also thank all my Indian friends Ravi, Nana, Manga, Atul, Mohapatra, Vinodh, Santosh, Nachi, Vijay, Kailash and Gourishankar for making my stay wonderful and full of fun.

Finally, I would like to remember the affection of my family, in particular my mother who continuously inspired me to do my best. Without their support and encouragement, I could not have accomplished what I have today.

Contents

Acknowledgements
Contents 1
List of Figures 4
List of Tables 9
1 Introduction 10
1.1 Electronic conduction properties of cation conductors: Current status 10
1.2 Focus of the literature with respect to thermoelectric power 11
1.3 Motivation 12

2 Theoretical considerations 14
2.1 Solid electrolyte 14
2.1.1 Conductivity 14
2.1.1.1 Ionic conductivity 15
2.1.1.1.1 Defect chemistry 18
2.1.1.1.2 Structural aspects 20
2.1.1.1.2.1 Structure of sodium- and potassium-beta-alumina 20
2.1.1.1.2.2 Structure of NASICON 23
2.1.1.1.2.3 Structure of Na_2CO_3 and K_2CO_3 25
2.1.1.2 Electronic conductivity 26
2.1.1.2.1 Electronic defects 26
2.1.1.2.2 Mechanism of electronic conduction 31
2.1.1.2.2.1 Broad-band conduction 31
2.1.1.2.2.2 Narrow-band conduction 31
2.1.1.3 Ionic domain 32

2.2 Electrode systems 33
2.2.1 Carbonate electrodes 33
2.2.2 Silicate electrodes 34
2.2.3 Molybdenum electrode 35
2.3 Solid electrolyte galvanic cell under isothermal condition 36
2.4 Solid electrolyte galvanic cell under non-isothermal condition 38
2.4.1 Heterogeneous part of the voltage 39
2.4.2 Homogeneous part of the voltage 40
2.4.2.1 Pure electronic conductors 40
2.4.2.2 Mixed ionic-electronic conductors 40
2.4.3 Thermo voltage and thermoelectric power 41
2.4.3.1 Data evaluation 42

2.4.3.2 Calculation of d(ln a_{Me})/dT 43
2.4.3.3 Polarity of thermoelectric power 44
2.5 Thermodynamic stability of NASICON 44
2.6 Fundamentals of impedance spectroscopy 46

3 Experimental 49
3.1 Characterization Techniques 49
3.1.1 Chemical analysis 49
3.1.2 X-ray analysis 49
3.1.3 Scanning electron microscopy (SEM) 49
3.2 Solid electrolytes 50
3.2.1 Na-beta-alumina 50
3.2.2 K-beta-alumina 52
3.2.3 NASICON 53
3.2.4 Na_2CO_3 and K_2CO_3 54
3.3 Electrodes 54
3.3.1 Carbonate/gas electrode 54
3.3.2 Silicate/SiO_2/O_2 electrode 55
3.3.3 Na-Mo-O/O_2 electrode 58
3.3.4 Sputtering method 59
3.4 Galvanic cells 60
3.4.1 Cells under isothermal condition 60
3.4.2 Cells under non-isothermal condition 63
3.4.3 Cells for impedance spectroscopy measurements 65

4 Results and discussion 66
4.1 Thermodynamic stability of NASICON 66
4.2 Thermoelectric power of NASICON 74
4.2.1 Thermo voltage 74
4.2.2 Thermoelectric power 75
4.2.3 Temperature dependence of $a_{\oplus}$ 78
4.3 Thermoelectric power of Na_2CO_3 and K_2CO_3 80
4.3.1 Thermo voltage 80
4.3.2 Thermoelectric power 81
4.3.3 Temperature dependence of $a_{\oplus}$ 84
4.4 Thermoelectric power of NBA 87
4.4.1 System NBA/Na-silicate/O_2 87
4.4.1.1 Thermo voltage 87
4.4.1.2 Thermoelectric power 90
4.4.1.3 Temperature dependence of $a_{\oplus}$ 91

4.4.2 System NBA/Na-Molybdate/O_2 93
4.4.2.1 Thermo voltage 93
4.4.2.2 Thermoelectric power 95
4.4.2.3 Temperature dependence of $a_{\oplus}$ 96
4.4.3 Sodium chemical potential dependence of $a_{\oplus}$ 97
4.5 Thermoelectric power of KBA 99
4.5.1 System KBA/K_2CO_3/CO_2/O_2 99
4.5.1.1 Thermo voltage 99
4.5.1.2 Thermoelectric power 99
4.5.1.3 Temperature dependence of $a_{\oplus}$ 102
4.5.2 System KBA/K-Silicate/O_2 103
4.5.2.1 Thermo voltage 103
4.5.2.2 Thermoelectric power 104
4.5.2.3 Temperature dependence of $a_{\oplus}$ 105
4.5.3 Potassium chemical potential dependence of $a_{\oplus}$ 107
4.6 Impedance spectroscopy measurement on Na_2CO_3 108

5 Conclusions and Outlook 113

6 Summary 115

7 Zusammenfassung 120

8 References 125

Curriculum Vitae 130

List of Figures

1-1	Temperature dependence of the logarithm of p-electronic conduction parameter of Na-beta-alumina (adopted from [14])	11
2-1	Vacancy mechanism for transport of ions	15
2-2	Interstitial mechanism for transport of ions	15
2-3	Interstitialcy mechanism showing the two possible locations of ions after movement	16
2-4	Temperature dependence of the conductivity for polycrystalline Na-beta-alumina and NASICON	17
2-5	Temperature dependence of the conductivity of Na_2CO_3 and K_2CO_3	18
2-6	Structure of Na-β-Al_2O_3 (left) and Na-β"-Al_2O_3 (right)	20
2-7	Oxide ion packing arrangement in β-Al_2O_3 (left) and β"-Al_2O_3 (right) (letters refer to stacking arrangement where ABC represent face-centered cubic packing while ABAB represents hexagonal packing)	21
2-8	Ideal structure of the conducting plane of β-alumina. Solid circles are columns of oxygen ions; open circles are mobile cations on BR sites; unoccupied hexagon vertices are aBR sites; and sites between neighbouring BR and aBR are mO sites. A mobile cation in an ideal structure is in a deep potential well indicated by dotted lines	22
2-9	View of the rhombohedral $R\bar{3}c$ structure of NASICON showing $(ZrP_3O_{12})^-$ units parallel to c_r and Na^+ ions in Na1 positions octahedrally coordinated by O^{2-} ions. The Na1 positions are also octahedrally coordinated by empty Na2 positions in the same basal planes as the nearest-neighbour O^{2-} ions	24
2-10	Composition dependence of specific resistivity of dense ceramic NASICON with graphite electrodes at high frequencies [62]	24
2-11	Definition of sites of cations around CO_3^{2-}-anions	26
2-12	Electronic energy level of crystalline solid omitting lattice imperfections	27
2-13	Electronic energy level of crystalline solid exhibiting lattice imperfections	27
2-14	Brouwer diagram for undoped K-beta-alumina [18]	29
2-15	Brouwer diagram for Mg doped Na-beta-alumina [18]	30
2-16	Conductivity diagram of undoped K-beta-alumina	32
2-17	A typical impedance spectrum (b) and corresponding equivalent circuit (a) [87]	47
3-1	XRD pattern of the commercial Na-beta-alumina tube	51
3-2	SEM image of the commercial Na-beta-alumina tube	51
3-3	XRD pattern of the commercial K-beta-alumina tube	52
3-4	XRD pattern of NASICON material	53
3-5	XRD pattern of Na_2CO_3	54

3-6	Schematic set-up of thermo cells	56
3-7	Schematic sketch of experimental apparatus	57
3-8	Phase diagram of the MoO_3-Na_2MoO_4 system constitute an eutectic mixture of Na_2MoO_4+$Na_2Mo_2O_7$ [93]	58
3-9	XRD pattern of the eutectic phase mixture Na_2MoO_4+$Na_2Mo_2O_7$	59
3-10	DTA traces of the eutectic phase mixture Na_2MoO_4+$Na_2Mo_2O_7$. 1 and 2 are the endothermic while 3, 4 and 5 are the exothermic peaks	59
3-11	Top and front view of the NASICON pellet sputtered with Au where the hatched area represents the Au layer together with schematic arrangement of the galvanic cell	60
3-12	Galvanic cell along with schematic sketch of the placement of cell in the non-uniform temperature zone of the furnace	62
3-13	Experimental apparatus	62
3-14	Schematic set-up of thermo cells	64
3-15	Schematic sketch of the thermo-cell in the non-uniform temperature zone of the furnace. S.E. denotes solid electrolyte, R.E. is reversible electrode	65
4-1	Temperature dependence of voltage of the galvanic cell (VIII) at p_{CO_2} = 19.4 · 10^{-6} bar and p_{O_2} = 19.7 · 10^{-6} bar	66
4-2	Time dependence of the voltage of cell (VIII) at 550 °C for different sodium activities from one extreme to the other. The different values of logarithm of sodium activity established by experimental conditions are displayed	67
4-3	Time dependent change of logarithm of sodium oxide activity as a function of logarithm of the sodium activity after heating up the cell and exposing it to the experimental conditions for the first time. (T = 550 °C, a_{Na} established according to Eq. 2-24 and adjusted by the gas composition. a_{Na_2O} evaluated according to Eq. 2-79)	68
4-4	Sodium oxide activities as a function of sodium chemical potential at various temperatures	69
4-5	Temperature dependence of the sodium oxide activity dissolved in NASICON ($Na_3Zr_2Si_2PO_{12}$) in comparison with literature data: (1) [82], (2) present study	70
4-6	Time dependent change of logarithm of sodium oxide activity as a function logarithm of sodium activity after stepwise cooling the cell from T = 550 °C to T = 350 °C	71
4-7	Difference of the standard Gibbs free energy of formation of the phases coexisting in NASICON ($Na_3Zr_2Si_2PO_{12}$) as a function temperature	73
4-8	Non isothermal voltage of cell (II) against ΔT at T = 700 and 400 ° C	74
4-9	Offset voltages (U_0) of cell (II) as a function of the sodium activity for T = 700 and 500 ° C (Curve 1: after heating up cell (II) and exposing the cell for the first time, curve 2: about 3600 h after curve 1)	75
4-10	Variation of the total thermoelectric power of NASICON with the sodium chemical potential at T = 550 °C	76

4-11	Sodium chemical potential dependence of the thermoelectric power of NASICON at T= 700 °C (solid line curve fitting according to Eq. 2-70)	76
4-12	Sodium chemical potential dependence of the thermoelectric power of NASICON at T= 400 °C (solid line curve fitting according to Eq. 2-70)	77
4-13	Typical fitted results for the thermoelectric power illustrating contribution of partial thermoelectric power on total ($\varepsilon = t_{ion}\ \varepsilon_{ion} + t_p\ \varepsilon_p$) at T = 575 °C	78
4-14	Temperature dependence of p-electronic conduction parameter of NASICON evaluated by thermoelectric power measurements (curve 1) compared with that obtained by potentiometric measurements (curve 2 [15]) (dashed line: lower limit of the sodium activity of the sodium carbonate electrode)	79
4-15	Thermo voltage vs ΔT (Na_2CO_3, T = 700, 400 °C and K_2CO_3 T = 625, 425 °C)	81
4-16	Sodium chemical potential dependence of the thermoelectric power of Na_2CO_3 at T= 625 °C (solid line curve fitting according to Eq. 2-70)	82
4-17	Potassium chemical potential dependence of the thermoelectric power of K_2CO_3 at T= 525 °C (solid line curve fitting according to Eq. 2-70)	82
4-18	Sodium chemical potential dependence of the thermoelectric power at T= 400 °C for Na_2CO_3 (solid line curve fitting according to Eq. 2-70. Curves 1, 3 are obtained after stepwise increasing the sodium activity, curve 2 is due to decreasing the sodium activity stepwise)	83
4-19	Temperature dependence of p-electronic conduction parameter for Na_2CO_3 (dashed line: upper limit of the sodium activity covered by the sodium carbonate electrode)	84
4-20	Temperature dependence of p-electronic conduction parameter for K_2CO_3 (dashed line: upper limit of the potassium activity covered by the potassium carbonate electrode)	85
4-21	Non isothermal voltage of cell (V) dependence on ΔT at T = 600 and 700 °C	87
4-22	Offset voltages (U_0) of cell (V) as a function of the sodium activity of the $NaSi_xO_{2x+0.5}/SiO_2/O_2$ (curves 1a, 2a) and $NaSi_xO_{2x+0.5}/SiO_2/H_2/H_2O$ (curves 1b, 2b) electrodes at T = 650 °C (Curve1 is obtained after stepwise increasing the chemical potential and curve 2 is due to decreasing the sodium activity stepwise)	88
4-23	Schematic sketch of the sodium chemical potential profile inside the solid electrolyte (Na-beta-alumina) under the conditions of cell (V)	89
4-24	Sodium chemical potential dependence of the thermoelectric power of Na-beta-alumina at T= 650 °C with $NaSi_xO_{2x+0.5}/SiO_2/O_2$ electrode (solid line curve fitting according to Eq. 2-70)	90
4-25	Sodium chemical potential dependence of the thermoelectric power of Na-beta-alumina at T= 650 °C with $NaSi_xO_{2x+0.5}/SiO_2/H_2/H_2O$ electrode (solid line curve fitting according to Eq. 2-70)	90

4-26	Temperature dependence of p-electronic conduction parameter for Na-beta-alumina with $NaSi_xO_{2x+0.5}/SiO_2/O_2$ electrode (dashed line: upper limit of the sodium activity covered by the electrode)	92
4-27	Temperature dependence of p-electronic conduction parameter for Na-beta-alumina with $NaSi_xO_{2x+0.5}/SiO_2/H_2/H_2O$ electrode (dashed line: upper limit of the sodium activity covered by the electrode)	92
4-28	Non isothermal voltage of cell (VI) as a function of ΔT at T = 500 °C under various sodium activity	94
4-29	Non isothermal voltage of cell (VI) as a function of ΔT at T = 500 °C under different sodium chemical potential	94
4-30	Sodium chemical potential dependence of the thermoelectric power of Na-beta-alumina T= 500 °C (solid line curve fitting according to Eq. 2-70, dashed line represents pure ionic conduction slope)	95
4-31	Temperature dependence of p-electronic conduction parameter for Na-beta-alumina with $Na_2Mo_2O_7/Na_2MoO_4/O_2$ electrode (curve1) compared with that of Na-beta-alumina with $Na_2CO_3/CO_2/O_2$ electrode (curve 2 [16]) (dashed line: upper limit of the sodium activity region covered by the electrode of cell (VI))	97
4-32	Sodium chemical dependence of p-electronic conduction parameter for Na-beta-alumina with different electrodes	98
4-33	Non isothermal voltage of cell (III) dependence on ΔT at T = 650 & 400 °C	99
4-34	Potassium chemical potential dependence of the thermoelectric power of cell (III) at T = 550°C (curve fitting according to Eq. 2-70 demonstrated by solid lines)	100
4-35	Potassium chemical potential dependence of the thermoelectric power of cell (III) at T = 700 and 450 °C (curve fitting according to Eq.2-70 demonstrated by solid lines)	101
4-36	Temperature dependence of p-electronic conduction parameter for K-beta-alumina with K_2CO_3, CO_2, O_2 electrode compared with that obtained from potentiometric measurement [23]	102
4-37	Non isothermal voltage dependence on ΔT of cell (VII) under O_2 (Ar) and H_2/H_2O (Ar) atmosphere at T = 650 °C	103
4-38	Potassium chemical potential dependence of the thermoelectric power of cell (VII) at T = 650 °C (solid lines demonstrate the fitting according to Eq. 2-70)	104
4-39	Temperature dependence of p-electronic conduction parameter for K-beta-alumina with $KSi_xO_{2x+0.5}$, SiO_2, H_2/H_2O and $KSi_xO_{2x+0.5}$, SiO_2, O_2 electrodes	106
4-40	Potassium dependence of p-electronic conduction parameter for K-beta-alumina with different electrodes at 650 °C	107
4-41 (a)	Impedance spectrum of Na_2CO_3 at lg a_{Na} = -13.105, T = 650 °C	108
4-41 (b)	An enlarged view of high frequency semicircle Z_1Z_2	108
4-42	Variation of the impedance spectra of Na_2CO_3 under various sodium activities at T = 650 °C	109

4-43	Influence of sodium activity on the conductivities σ_1 (left) and σ_2 (right) of cell (I) at T = 450 °C and 650 °C	110
4-44	Total conductivity of Na_2CO_3 as a function of the temperature (σ_1: curve 1, σ_2: curve 2) in comparison with literature data (curve 3 [43])	111

List of Tables

2-1	Defect formation reactions along with mass action law	28
2-2	Sodium activity dependence of the concentration of charge species in different regions of the Brouwer diagram for Mg-doped Na-beta-alumina	31
3-1	Ceramographic preparations of K and Na-beta-Al_2O_3 and NASICON	50
3-2	Solid electrolytes under investigation	50
3-3	Elemental composition of K-beta-alumina	52
3-4	Elemental composition of NASICON material	53
3-5	Elemental composition of Na-silicate ($NaSi_xO_{2x+0.5}$) glass	55
3-6	Elemental composition of K-silicate ($KSi_xO_{2x+0.5}$) glass	56
3-7	Sputtering conditions	60

1. Introduction

1.1 Electronic conduction properties of cation conductors: Current status

Cation conducting solid electrolytes like Na-beta-alumina, K-beta-alumina and NASICON employed in batteries, alkali metal thermal-to-electrical converter and electrochemical gas sensors as well as any other solid electrolytes should be both good ionic conductors and electronic insulators. Basically it is important to know in the aforementioned applications to what extent the material is electronically conducting. Depending on the application the level of electronic conductivity in the electrolyte can be tolerated or is detrimental. For instance, in the case of fuel cells a slight amount of electronic conductivity might be acceptable. In contrast, in sensors or thermodynamic investigations based on the electrochemical technique the electronic conduction results in data distortion and must be avoided. However, for the sake of simplicity the electronic conductivity is often neglected and the electrolyte is considered as an ideal ionic conductor. The region with respect to the activity or the partial pressure of the potential determining species and temperature within which the electronic contribution to the total conductivity of a solid electrolyte is less than 1% is defined as electrolytic domain. Beyond that the electronic conductivity of the solid electrolyte influences the behaviour of galvanic cells. The effect can be taken quantitatively into account by knowing the electronic conduction parameters i.e., the electronic and ionic conductivities as a function of the chemical potential of neutral species and temperature.

The electronic conductivity of alkali ion conducting solid electrolytes was not acknowledged in the literature until the development of alkali metal thermal-to-electric converter and sodium sulfur batteries. De Jonghe [1] and Virkar [2] argued a possible impact of the electronic conductivity, in particular the n-type conductivity, and this was measured by Weber [3] for the first time. Until now, the conduction properties of Na-beta-alumina have been quite intensively studied [4-14]. A substantial amount of knowledge regarding the p-type electronic conduction property of Na-beta-alumina has been obtained by Näfe and coworkers [7-14] by undertaking various investigations. The results span more than a decade of the electronic conduction parameter $a_{\oplus}$ as depicted in Fig. 1-1.

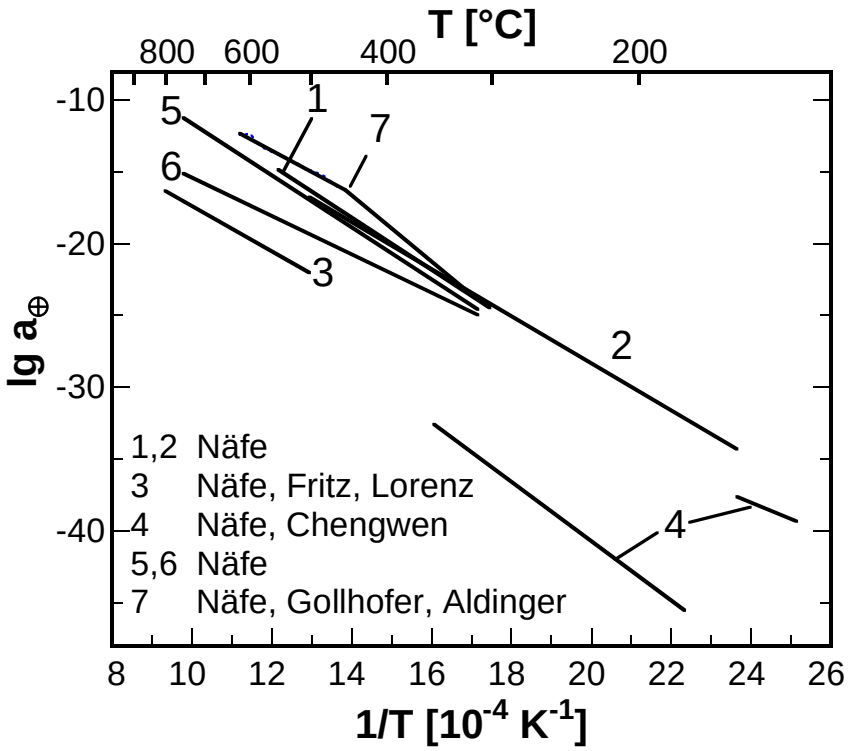

Fig. 1-1 Temperature dependence of the logarithm of the p-electronic conduction parameter of Na-beta-alumina (adopted from [14])

However, in the case of other cation conductors like NASICON, K-beta-alumina [15, 23] or alkali carbonates either little or nothing is known in regard to the electronic conduction properties. Even though the substantial influence of the electronic conductivity of Na-beta-alumina used as a solid electrolyte in a number of galvanic cells is well proven, the situation is very complex insofar as under certain conditions the electronic conduction phenomenon may be completely hidden. This is at least known from the previous studies on Na-beta-alumina and K-beta-alumina [9, 10, 14, 22] that points out a kind of adaptation of the electronic conduction parameter to the surrounding chemical potential.

1.2 Focus of the literature with respect to thermoelectric power

As shown in [16] the thermoelectric power determinations may yield valuable information about the conduction properties of a solid electrolyte. Till date, the only aim of all the studies in the literature concerning thermoelectric power measurements on solid electrolytes was to obtain information about the heat of transport and the

transported entropy of the charge species. The theoretical framework about the relationship between thermoelectric power and the mixed ionic-electronic conduction properties of a solid was laid by Wagner [17] and appropriately advanced by Näfe [18] in view of the dependence of the thermoelectric power on the chemical potential in the surroundings of the material under consideration. The impact of the surrounding conditions was first observed by Tallan and Bransky [19] who determined the thermoelectric power of ThO_2 over a range of oxygen partial pressure. Since then anion conductors especially oxygen ion conductors have been studied extensively with regard to the thermoelectric power. However, in case of cation conductors, especially Na-beta-alumina only few reports on the thermoelectric power study exist in the literature [20-22] with the goal to obtain only the information about the heat of transport of the species. There is only one report [23] in which the thermoelectric power, in this case of Na-beta-alumina has been measured as a function of the chemical potential of the neutral species in the surroundings i.e., under a broad sodium activity interval with the view to assess the conduction properties of the material. For other cation conductors like K-beta-alumina and NASICON nothing is known as far as the thermoelectric power is concerned.

1.3 Motivation

Näfe et al. [9, 15] demonstrated the existence of non-negligible electronic conductivity in Na-beta-alumina, K-beta-alumina and NASICON, which have been treated as pure ionic conductors in the literature so far, under the condition of measurement prevalent in any solid-state CO_2 sensor. The previous findings on Na-beta-alumina [9, 10, 14] do indicate that $a_{\oplus}$ is a function of the chemical potential in the surroundings, in contradiction to the assumptions of the conventional defect chemical considerations. Since thermoelectric measurements, under certain prerequisites, promise to determine the proportion of the electronic charge carriers to the total conductivity of the material [16], this technique might give further insight into the topic. The advantage of the approach is that the surfaces of the material need not to be exposed to different chemical potentials in contrast to solid state potentiometry. This is of utmost importance especially when the impact of the chemical potential in the ambience of the solid on the conduction behaviour is in the focus of interest.

As a sequel to the previous findings on the characteristics of electronic conduction and with a view to check the general relevance of the previous knowledge about the

behaviour of the electronic conduction parameter as a function of the surroundings, the present work has been undertaken. The aim of the current investigation is the quantitative determination of the p-electronic conduction parameter $a_{\oplus}$ of Na-beta-alumina, K-beta-alumina, NASICON, Na_2CO_3 and K_2CO_3 by thermoelectric power measurements under a large spectrum of the chemical potential of the potential determining species and temperature thereby to establish further proofs for substantiating the previous findings on the anomalous behaviour of the p-electronic conduction parameter.

In view of the fragmentary knowledge about the thermodynamic stability of one of the electrolytes under investigation, namely NASICON, and in view of possible interrelationships between thermodynamic stability and electronic conduction, a part of the present work aims at the characterization of the thermodynamic stability of NASICON. In none of the previous studies on this topic the establishment of the phase equilibrium was really checked, which is why the present work focuses on that. In addition, impedance spectroscopy was performed to get an independent information about the conduction properties of the materials under investigation and to support the results of the thermoelectric power measurements, qualitatively.

2. Theoretical considerations

2.1 Solid electrolyte

Solid electrolytes, in principle, carry most of their currents by ions, existing as defects. The general requirements for practical solid electrolytes are (1) high ionic conductivity with negligible electronic conductivity, (2) stability with respect to thermal and electrochemical decomposition and (3) ease of fabrication and cost effectiveness. In the subsequent sections the conduction phenomena, their description by defect chemical considerations and the structure of solid electrolytes are dealt with.

2.1.1 Conductivity

There are two types of conduction processes that occur in solid electrolytes, namely ionic that involves matter transport and electronic that does not involve matter transport. Electronic conductivity is omnipresent no matter how low it is, whereas ionic conduction requires presence of ions in the material. In the solid electrolyte, ion movement differs from the gas or liquid phase in that one type of charged particle is often much more mobile than the oppositely charged one and the availability of free electrons. The total electrical conductivity (σ) of a solid electrolyte can be expressed as [24]

$$\sigma = F\left[\sum_i c_i |z_i| u_i + n|z_e| u_e + p|z_h| u_h\right] \qquad \text{Eq. 2-1}$$

where c_i, n and p are the ionic, electron and hole concentration, z is the charge number, F is Faraday constant, u is the mobility i.e., the mean particle velocity per unit electric field and the subscripts i, e and h denote ions, electrons and electron holes, respectively.

In the crystal, in general, one sublattice is mobile while the other is immobile. In case of K-beta-Al_2O_3, the K^+ ions are moving with the Al^{3+} and O^{2-} fixed while in yttria doped ZrO_2 O^{2-} ions are mobile with Zr^{2+} and Y^{3+} being practically immobile. It is thus apparent from Eq. 2-1 that two parameters namely the carrier concentration and the mobility of a carrier can be modified to enhance the conductivity. The carrier concentration is determined by the defect chemistry of a material (section 2.1.1.1.1 and section 2.1.1.2.1) while the defect mobility is mainly a function of crystal structure that will be discussed in section 2.1.1 1.2.

2.1.1.1 Ionic conductivity

Ionic conduction i.e. movement of ions from one position to another after application of an electric field (migration), or under a concentration gradient (diffusion) needs the presence of inherent disorder in the solid. The disorder exists intrinsically in any solid by thermodynamic reasons. The degree of disorder can be varied (increased) by doping. Ionic conduction results by hopping of ions from site to site through a crystal structure (section 2.1.1.1.2). The conduction mechanism can be classified broadly into three types. These are interstitial, interstitialcy and vacancy diffusion [25].

In the vacancy mechanism, a number of sites that would be occupied in the ideal crystal are empty. An adjacent ion may jump into it leaving its own site vacant as illustrated in Fig. 2-1. In the case of interstitial motion ions may be displaced from their lattice sites into interstitial sites (Fig. 2-2). This is energetically less favourable than vacancy migration [25]. The third type of motion involves a possible combination of vacancy and interstitial mechanisms, as shown in Fig. 2-3.

If there is simply an exchange of positions of a mobile ion with the near neighbouring one of the same kind then no net ion flow is detected. To observe a detectable flow a series of ionic movements should occur that produces a net change in charge and/or mass over the material. This movement of ions or atoms is usually modelled as a process of discrete jumps over potential energy barriers.

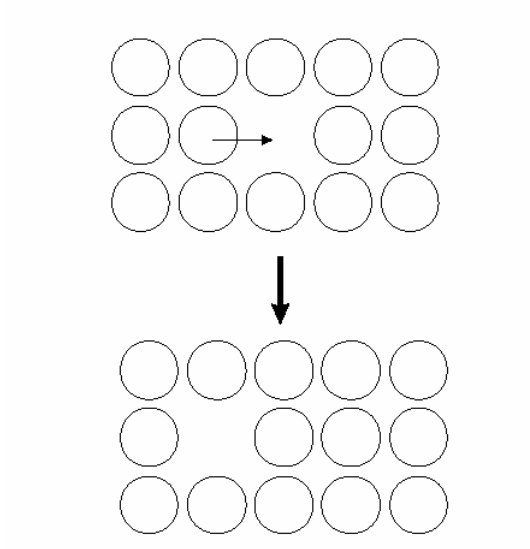

Fig. 2-1 Vacancy mechanism for transport of ions

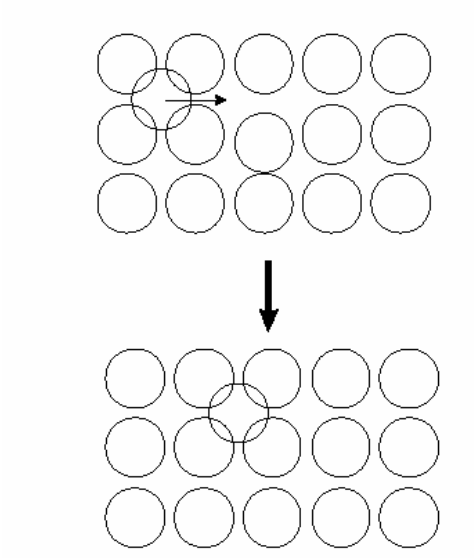

Fig. 2-2 Interstitial mechanism for transport of ions

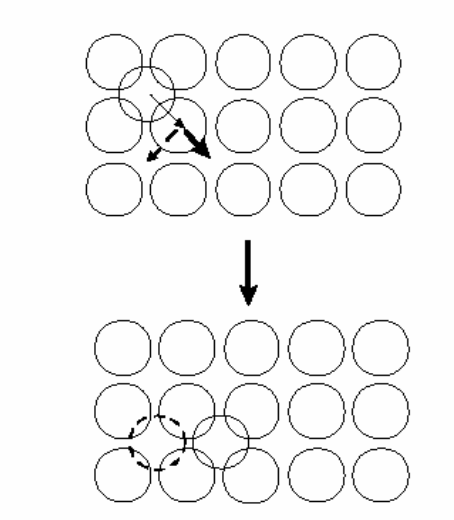

Fig. 2-3 Interstitialcy mechanism showing two possible locations of ions after movement

The conductivity depends on mobility, concentration and charge of the species involved. The mobility of electrons is significantly larger than that of ions; hence for the predominance of ionic conductivity, the concentration of ionic defects should be considerably larger than of the electronic defects. The concentration of ionic defects can be increased by a) doping with aliovalent impurities and/or b) interaction of the solid with the surroundings.

However, it should be noted that the latter process simultaneously produces electronic species thereby leading to a mixed conduction.

The conductivity of ionically conducting solid electrolytes like Na-beta-Al_2O_3 or NASICON is significantly difficult to measure because of the precondition of having suitable reversible electrodes at one's disposal. Moreover, it is often not clear to what extent and to which species the electrodes are reversible. In addition, the thermodynamic stability and compatibility of many electrode systems are not known. An alternative approach is to use non-reversible electrodes at high frequency with a frequency range where the conductivity is independent of frequency. Conductivity data for single crystals of K-beta-alumina has been reported by Briant and Farrington [26] and Roth et al. [27] using blocking electrodes and in the range of 0.1–10 MHz. The temperature dependence of the conductivity reported in literature is shown in Fig. 2-4 for polycrystalline Na-beta-alumina, NASICON and for Na_2CO_3, K_2CO_3 in Fig. 2-5. The ionic conductivity of Na-beta-alumina at room temperature may reach values of about log (σ[S/cm]) = -0.255.

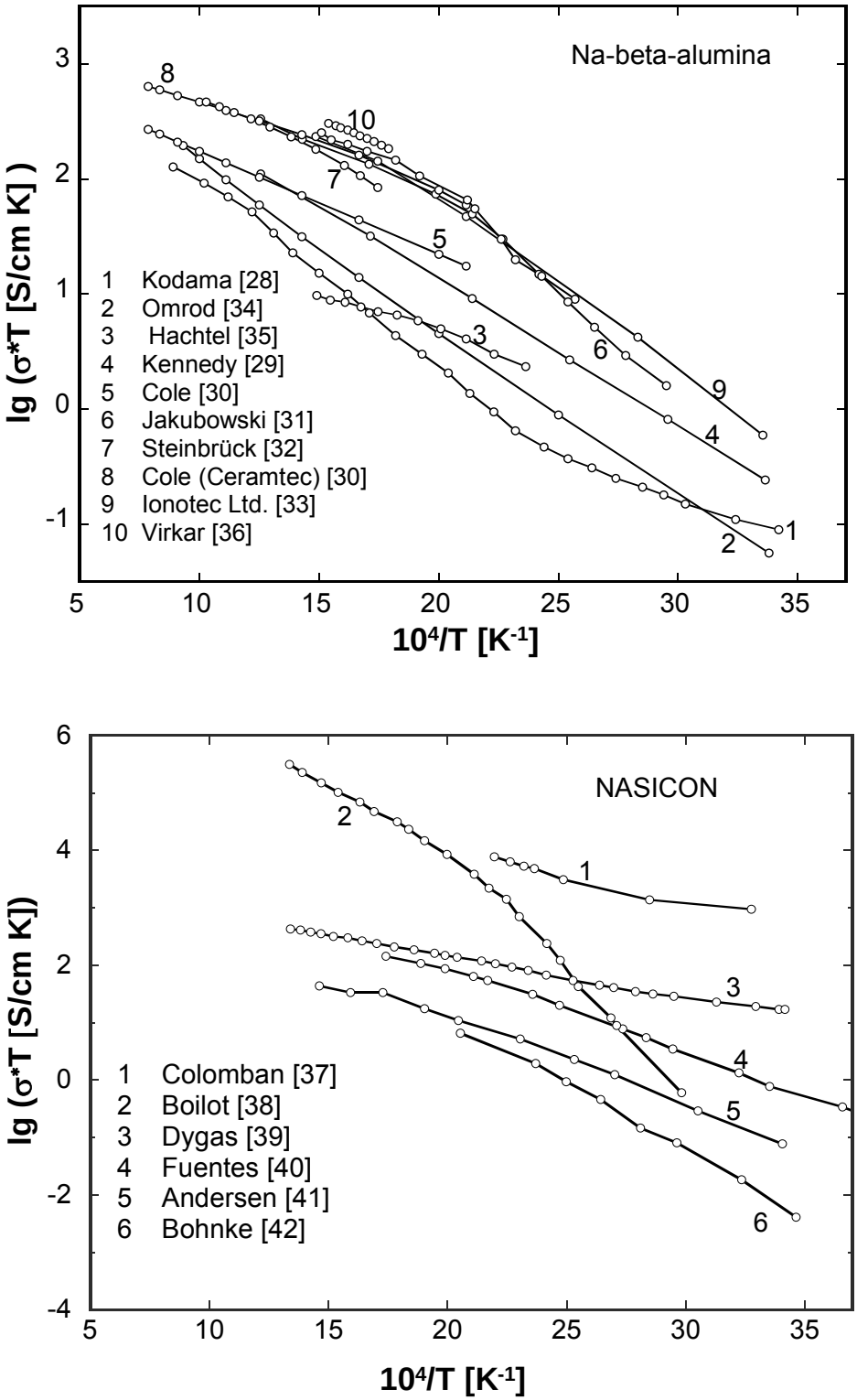

Fig. 2-4 Temperature dependence of the conductivity for polycrystalline Na-beta-alumina and NASICON

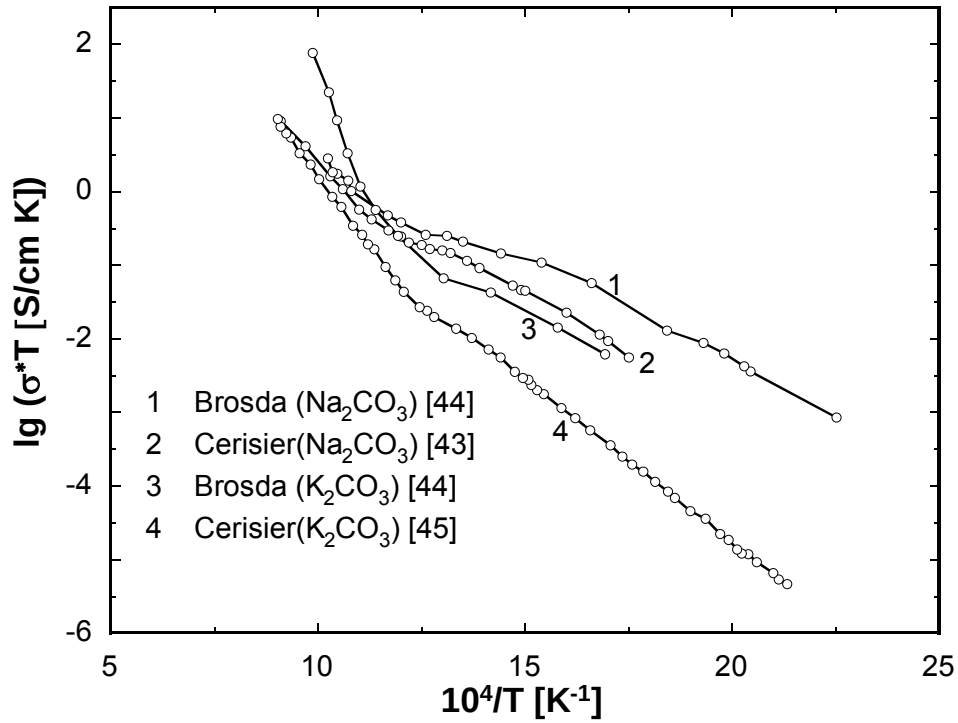

Fig. 2-5 Temperature dependence of the conductivity of Na_2CO_3 and K_2CO_3

2.1.1.1.1 Defect chemistry

The state of lowest energy of a crystal is characterised by the fact that the constituents are arranged as per a purely periodic pattern [46]. As discussed in the preceding section, the entropy contribution to the Gibbs free energy requires the presence of a finite concentration of point defects in solids at any temperature above 0 K. The commonly used nomenclature for the description of point defects has been proposed by Kröger and Vink in 1956 [47]. The point defects are considered as solute and the solid as the solvent. Bulk defect chemical reactions must obey mass balance, charge balance (global electrical neutrality), and lattice-site balance.

There are essentially three kinds of establishment of equilibrium of defects in ionic crystals:

(i) Intrinsic defects; i.e., the defects present in the bulk of a crystal are in thermodynamic equilibrium, which includes the Frenkel and Schottky defects.

(ii) Doping; i.e. the intentional manipulation of defect types and concentration by incorporation of specific species into the bulk of the crystal.

(iii) Defect reactions at interfaces, e.g. the incorporation of neutral species from the "outside" into the crystal via defects or the opposite, the loss of crystal atoms to the ambience generating defects in the crystal.

In cation conductors, like beta-Al_2O_3 and NASICON lattice disorder occurs predominantly in the cation sublattice. The assumed intrinsic lattice defects are Frenkel pairs [9, 48], i.e. pair of a metal interstitial and a metal vacancy, $M_i^{\bullet}$ and V_M, respectively, while the anionic defects are immobile.

The relationship between defect equilibria and conductivity is described using K-beta-alumina as an example but is also valid for other mono-valent cation conductors. It is assumed here that the concentration of interstitial potassium ions and vacancies is much larger than those of electrons and defect electrons (holes). The intrinsic defect occurring in K-beta-alumina is fixed by thermodynamic equilibrium and given below along with mass action law.

Type of reaction	Reaction	Law of mass action	Eq.
Intrinsic defect formation	$K_K + V_i \leftrightarrow K_i^{\bullet} + V_K'$	$K_F = \frac{[K_i^{\bullet}]\cdot[V_K']}{[K_K]\cdot[V_i]}$	2-2

V_i and V_K are the interstitial and potassium vacancies, respectively. K_F is the constant of the above equilibrium, having the form

$$K(T) = K_0 \exp\left(-\frac{\Delta H}{RT}\right), \qquad \text{Eq. 2-3}$$

where K_0 is the pre-exponential factor that includes the entropy term, ΔH is the reaction enthalpy, T is the absolute temperature and R is the gas constant.

The extrinsic ionic defects in solid electrolytes in this case K-beta-alumina can be formed by doping with aliovalent ions. Charge balance in undoped K-beta-alumina has been attributed to Al^{3+} vacancies and O^{2-} interstitials. If a metal ion for instance Mg^{2+} having a charge less than +3 substitutes an aluminium ion [27, 49], additional potassium ions for example in K-beta-alumina could be incorporated for charge balance according to the reaction

$$K + Mg + \frac{1}{3}V_{Al}''' \leftrightarrow K_i^{\bullet} + Mg_{Al}' \qquad \text{Eq. 2-4}$$

This will affect the defect concentrations of the K^+ ions and in turn the ionic conductivity [50, 51]. However, the effect of doping on the concentration of the electronic defects is not well understood [52].

2.1.1.1.2 Structural aspects

2.1.1.1.2.1 Structure of sodium- and potassium-beta-alumina

Beta-alumina is a general term that refers to a family of sodium aluminates with closely related structures and chemical properties. The two most important structures of the family are the hexagonal form (designated β-alumina) and the rhombohedral form (designated β″-alumina) and represented by the general formula $Na_{1+x+y}Mg_xAl_{11-x}O_{17+y/2}$. The structure of beta-aluminas has been studied mostly by X-ray diffraction, although several other experimental probes have been applied to obtain details of the structure in the recent years. The main characteristics of the β-alumina have been determined already in 1931 by Bragg et al. [53] and in 1937 by Beevers et al. [54]. The structure of Na or K-β/β″-alumina is shown in Fig. 2-6.

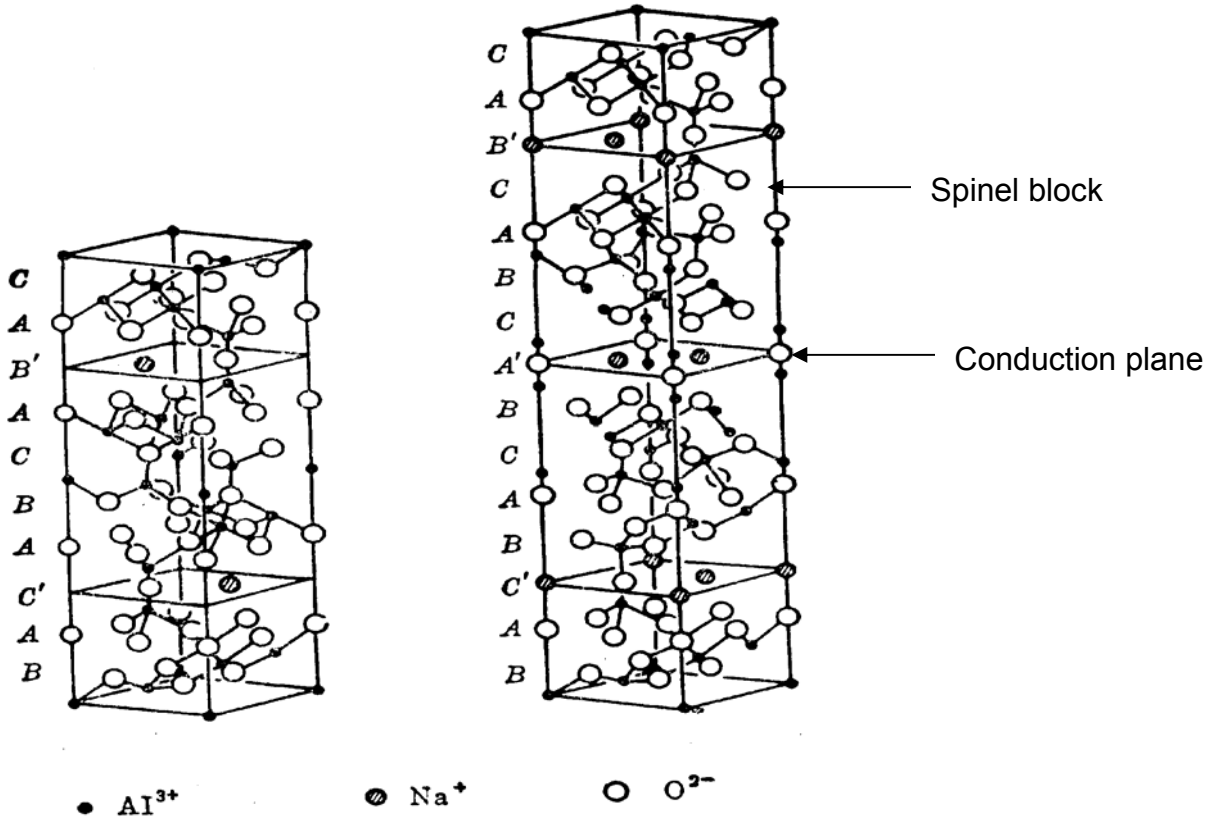

Fig. 2-6 Structure of Na-β-alumina (left) and Na-β"-alumina (right)

The blocks of Al^{3+} and O^{2-} are packed in the same fashion as in spinel ($MgAl_2O_4$). They are usually called "spinel block". The unit cell is composed of two spinel blocks

separated by a mirror plane (Fig. 2-6). These blocks result from the stack of four layers of O^{2-} ions in the c direction and are connected by Al-O-Al bonds i.e. O^{2-} ions in the conduction plane form a bridge between Al^{3+} ions in the adjacent spinel blocks. Al^{3+} ions occupy the octahedral sites; the tetrahedral sites are occupied by Mg^{2+} ions. The spinel-type blocks are separated from each other by a loosely packed plane containing Na^{+} (or K^{+}) and O^{2-}. Because of the loose packing, sufficient space is available for movement of the alkali ions which enhances the mobility of alkali ions thereby leading to a high ionic conductivity. However, the conductivity is limited to these planes only and movement along the c axis is exceedingly difficult. The conductivity of the material, therefore, is highly anisotropic. The conduction plane of beta-alumina is a mirror plane, with the face centred cubic packing arrangement of oxygen ions in the ambience shown in Fig. 2-7.

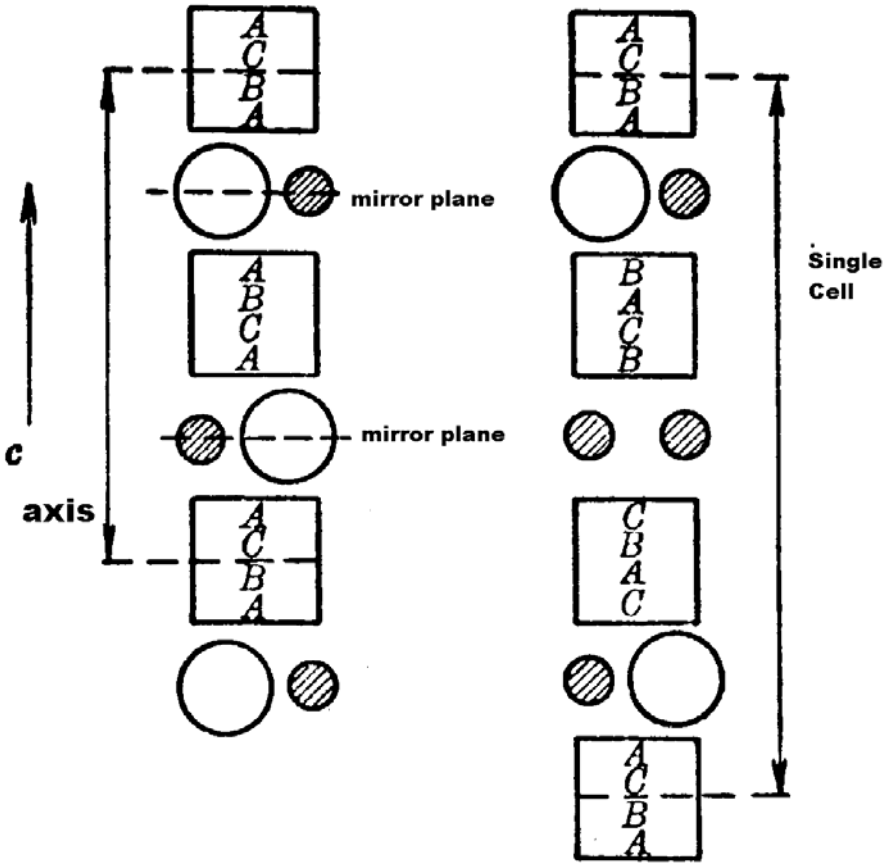

Fig. 2-7 Oxide ion packing arrangement in β-alumina (left) and β"-alumina (right) (letters refer to stacking arrangement where ABC represent face-centered cubic packing while ABAB represents hexagonal packing)

This packing arrangement is slightly different in β"-alumina since the conduction plane is not a mirror plane. As can be seen in Fig. 2-7, it takes three spinel-type blocks before the stacking arrangement is repeated, and for this reason, β"-alumina is called "3-block" while the β-alumina is called "2-block" material.

Although spinel is cubic, the intermediate conduction planes lead to a hexagonal crystal structure for β-alumina and a rhombohedral structure for β"-alumina. Other modifications of the spinel block stacking arrangement have been reported [55] and given the names β"'-alumina and β""-alumina.

The conduction plane of β–alumina is characterised by three distinct crystallographic sites for the sodium ions. For Na-β-alumina the most probable position determined by Beevers and Ross [54] is shown in Fig. 2-8 and is called BR ("Beevers Ross") position.

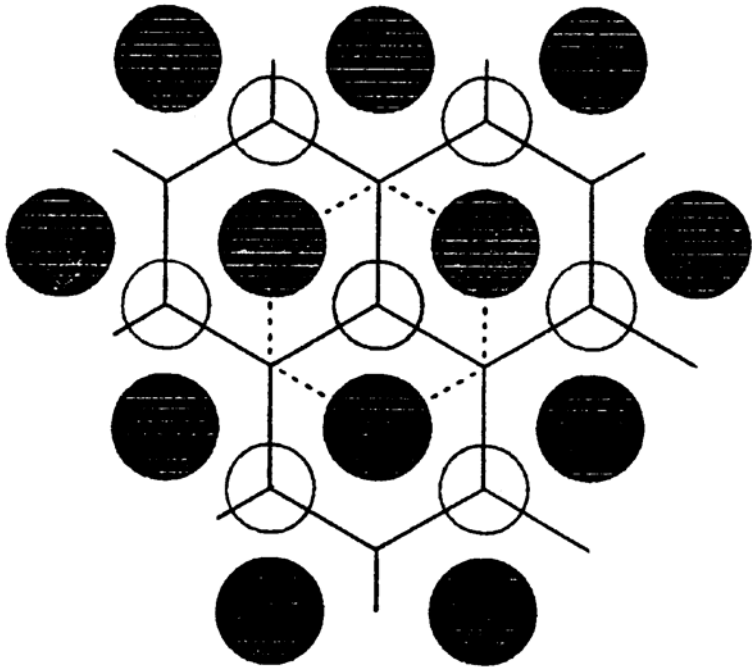

Fig. 2-8 Ideal structure of the conducting plane of β-alumina. Solid circles are columns of oxygen ions; open circles are mobile cations on BR sites; unoccupied hexagon vertices are aBR sites; and sites between neighbouring BR and aBR are mO sites. A mobile cation in an ideal structure is in a deep potential well indicated by dotted lines

The other positions lie between the oxide ions and are labelled mO for "mid-oxygen". All these sites would ordinarily be filled in the stoichiometric $NaAl_{11}O_{17}$ material. However, Felsche [56] found using a three-dimensional refinement method that the sodium sites are only partially occupied. In case of excess sodium, the charge is compensated by aluminium vacancies as postulated by Peters et al. [57].

Two possible positions for the excess sodium are shown in Figure 2-8. The sites labelled aBR refer to "anti Beevers-Ross" positions since Beevers and Ross rejected this type of site. The other positions lie between the oxide ions and are labelled mO for "mid-oxygen". The measurement of the electron density due to sodium revealed that BR

sites are 75% occupied, aBR sites are unoccupied and the remaining Na^+ electron density was found in a diffuse fashion around the mO sites [57].

The three-dimensional neutron diffraction analysis on β- and β″-alumina (Mg stabilized) studied by Roth et al. [58, 59] showed that Na^+ was distributed in two equivalent sites in β″-alumina. The interstitial O^{2-} ions reside on the conduction plane in β-alumina that would impede the mobility of Na^+ and account for charge compensation. However, no blocking O^{2-} ions were found in β″-alumina and charge compensation is accomplished by stabilizing Mg^{2+} in the spinal block. A similar single crystal X-ray diffraction study of K-β-alumina and cobalt doped K-β-alumina was carried out by Derier and Remeika [60]. They showed that potassium behaved in a similar fashion to sodium with regard to occupying BR and mO sites with no occupation of aBR sites.

Thus the structure of Na-beta-alumina provides a basic framework for the movement of alkali ions thus playing an important role in imparting exceptionally high conductivity of such material.

2.1.1.1.2.2 Structure of NASICON

NASICON is the acronym for Na superionic conductor consisting of a non-stoichiometric framework of sodium zirconophosphosilicate [61]. It is primarily a solid solution between isostructural $NaZr_2(PO_4)_3$ and $Na_4Zr_2(SiO_4)_3$, in which the phosphorus may be partially replaced by silicon, resulting in a solid solution $Na_{1+x}Zr_2P_{3-x}Si_xO_{12}$ in the range of $0< x < 3$.

NASICON has primarily rhombohedral symmetry with space group $R\bar{3}c$, with eventually a slight distortion to monoclinic *C2/c* group, except in the interval $1.8< x <2.2$ at room temperature [61]. The structure consists of a three-dimensional skeletal network of PO_4 tetrahedra corner-sharing with ZrO_6 octahedra. In the $(Zr_2P_{3-x}Si_xO_{12})^{(1+x)-}$ skeleton, each Zr^{4+} octahedron shares its six corners with tetrahedral, and each tetrahedron shares its four corners with octahedral sites (Fig. 2-9). Thus each anion bonds strongly to a tetrahedral and an octahedral cation of the skeleton. In the rhombohedral phase, two Na^+-ion sites are distinguishable in the interstitial space: close-packed-hexagonal Na2 layers (Fig. 2-9) in the basal plane connected by one-third as many Na1 sites between the Na2 layers as illustrated in Fig. 2-9.

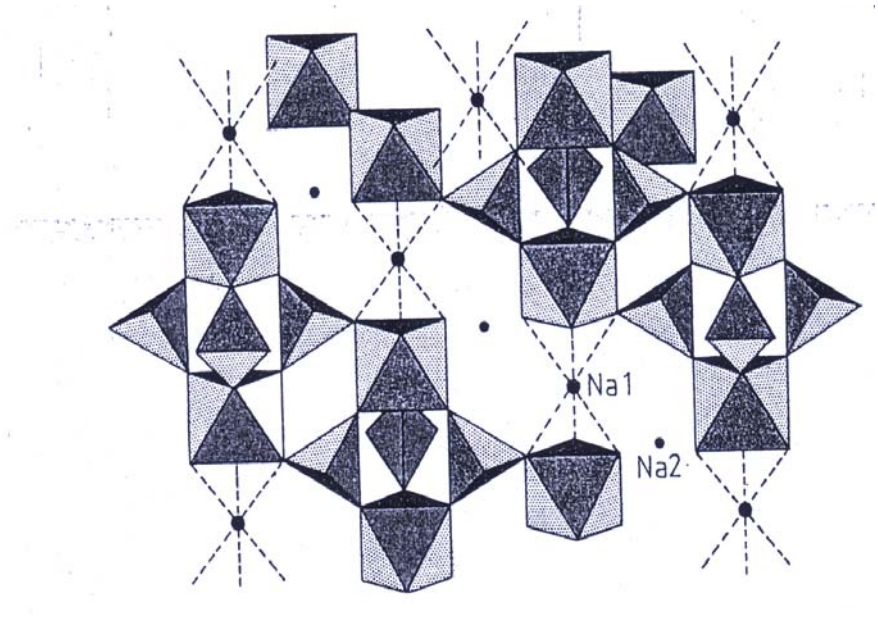

Fig. 2-9 View of the rhombohedral $R\bar{3}c$ structure of NASICON showing $(ZrP_3O_{12})^-$ units parallel to c_r and Na^+ ions in Na1 positions octahedrally coordinated by O^{2-} ions. The Na1 positions are also octahedrally coordinated by empty Na2 positions in the same basal planes as the nearest-neighbour O^{2-} ions

In the compound $NaZr_2P_3O_{12}$, Na1 sites are filled and the Na2 sites are empty. Substitution of Si for P is charge compensated by the introduction of Na^+ ions on Na2 sites, which are linked to one another via Na1 sites. The specific resistivity due to Na^+ ions passes through a minimum at intermediate x~2 (Fig. 2-10) [62].

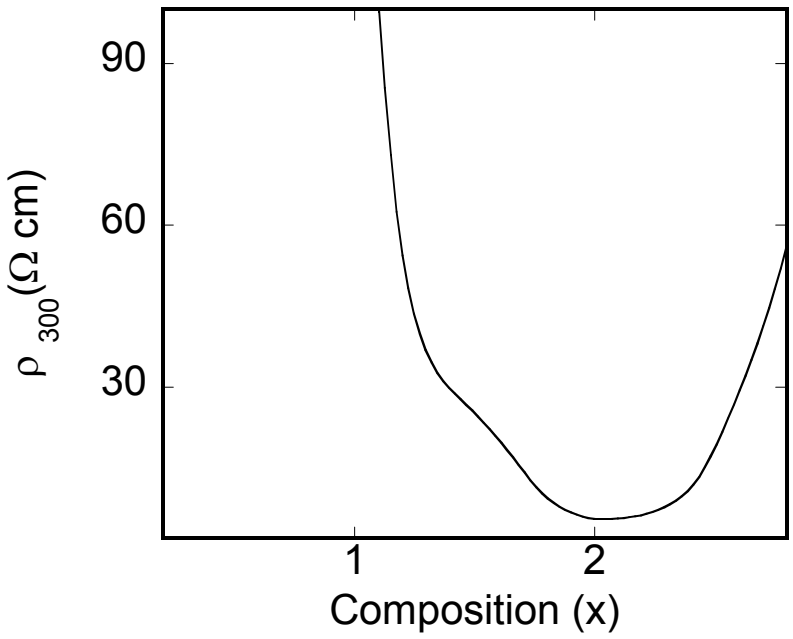

Fig. 2-10 Composition dependence of specific resistivity of dense ceramic NASICON with graphite electrodes at high frequencies [62]

This fact occurs if the rhombohedral axis c_r and cell volume are maximum [62] suggesting that Na^+-Na^+ electrostatic interactions reduce the Na1-site preference energy with increasing x. For $x > 2$, both Na1 and Na2 vacancies must coexist. The fact that the crystal cell volume reaches a maximum with increasing x suggests that the electrostatic forces between Na ions at adjacent Na1 and Na2 sites may displace Na ions towards bottleneck position between Na1 and Na2 sites, which will correspond to a high resistivity.

2.1.1.1.2.3 Structure of Na_2CO_3 and K_2CO_3

Much information regarding the structure of sodium and potassium carbonate is acquired from X-ray and neutron diffraction studies [63]. The structural changes in these alkali carbonates are substantiated by various techniques such as differential thermal analysis, electrical conductivity [43, 64, 65] due to lack of clarity with regard to structural changes at high temperatures by X-ray diffraction. Still there exists some obscurity with respect to the structural polymorphism displayed by alkali carbonates and the specific distribution of alkaline cations around the anions.

At room temperature Na_2CO_3 has a C-centred monoclinic unit cell. This so called γ phase has a space group *C2/m* that changes to another phase with a monoclinic structure (phase β) at 360 °C. This phase is retained till 489 °C and finally transforms to a phase with primitive hexagonal structure (phase α) which is stable till fusion. The transition to the β form is gradual and is characterised by large temperature coefficients of the unit cell parameters while the transition to the α form is sharp [66].

The crystallography of K_2CO_3 is similar to that of Na_2CO_3. At room temperature K_2CO_3 has a monoclinic structure with space group $P2_1/c$ and above 425±5 °C it crystallizes in the hexagonal structure. However, there is still uncertainty in the literature regarding the existence of structural transformations in K_2CO_3. The reason for the uncertainty lies in the fact that measurements are performed under different conditions and utilising various techniques [67]. The arrangement of favourable sites for alkali metal ions surrounding CO_3^{2-} ions has been analysed [63]. The CO_3^{2-} anion can be considered as rigid units built up of 3 interpenetrating oxygen as shown in Fig. 2-11. A cation can occupy various positions around such a unit. Hence more sites are available for movement of cation facilitating the conduction of ionic species in the materials.

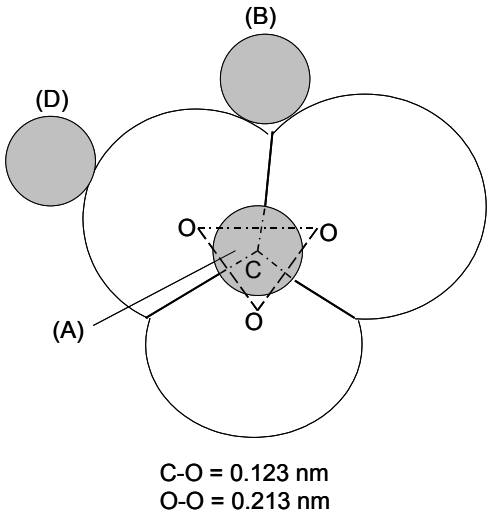

Fig. 2-11 Definition of sites of cations around CO_3^{2-}-anions

Under the assumption that the cation remains in contact with the anion, three principal sites of the cation may be considered that are designated as A, B and D. They correspond to symmetrical positions of a cation in contact with oxygen of the same anion (Fig. 2-11). Increasing the ionic radius e.g. from Li^+ to K^+, the predominant positions show an increasing tendency to occupy the D site close to the corner of the anions while the site A becomes depleted. As a consequence the free rotation of the anions is more likely to occur for the Na and K carbonates in the molten state. The occupancy of cation around an anion is still uncertain [63] and there is no clear indication in the literature about the predominant site of alkali metals.

2.1.1.2 Electronic conductivity

2.1.1.2.1 Electronic defects

At 0 K all electrons are in the state of lowest energy level. Electronic defects can be formed by thermal excitation of electrons from the valence band to the conduction band constituting intrinsic defects. Equilibrium between free electrons (e') in the conduction band and electron holes ($h^{\bullet}$) in the valence band can be expressed as

$$0 \leftrightarrow e' + h^{\bullet} \qquad \text{Eq. 2-5}$$

and are shown in Fig. 2-12.

The expression for thermal equilibrium of electrons and holes leads to the equation [46]:

$$K_e = np = 4\left(\frac{2\pi\, m_h^{1/2} m_e^{1/2} kT}{h^2}\right)^3 \exp\left(-\frac{E_g}{kT}\right), \qquad \text{Eq. 2-6}$$

where n and p denote the concentrations of electrons and electron holes, respectively, K_e is the equilibrium constant, E_g is the energy difference between the valence and the conduction band (band gap energy), m_h and m_e are the effective masses of free holes and electrons, k and h are the Boltzmann and Planck's constant.

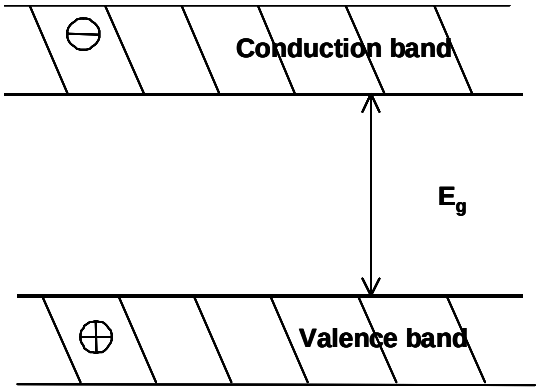

Fig. 2-12 Electronic energy level of crystalline solid omitting lattice imperfections

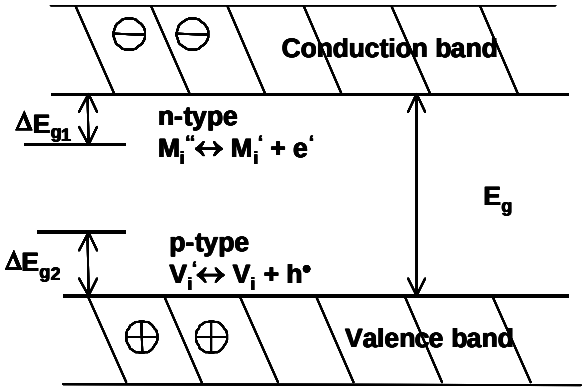

Fig. 2-13 Electronic energy level of crystalline solid exhibiting lattice imperfections

The larger the value of the bandgap energy, the smaller is the value of K_e in Eq. 2-6 and the lower is the concentration of electronic defects. Therefore, materials which exhibit predominately ionic conduction usually have a bandgap energy greater than 3 electron volts (eV).

Another way to produce electronic disorder is the involvement of atomic imperfections. Atomic imperfections may make additional electronic excitation processes possible, namely:

a) excitation in which electrons associated with the imperfections are brought into states in which they can move freely through the crystal and
b) excitation in which normal valence electrons of the crystal are transferred to the imperfections as illustrated in Fig. 2-13.

Thus, the ionic defects in the solid electrolyte produces additional energy levels in the gap that reduces the activation energy required for the formation of defect electrons as compared to the intrinsic case and increases the concentration of extrinsic electronic charge carrier. If the chemical potential or the activity of the mobile species of the solid electrolyte in the surroundings is changed then the charged defects are compensated by electronic carriers, such as excess electrons e', and electron holes, $h^{\bullet}$.

When the chemical potential of the potassium is high, potassium is incorporated into the lattice of the electrolyte (K-beta-alumina). This leads to the enhancement of the concentrations of excess electrons (e') in the solid owing to charge neutrality requirement. However, at low potassium potential, potassium is released from the solid. As result, electron holes ($h^{\bullet}$) are formed. The relevant defect chemical reactions along with the mass action relations are given in Table 2-1.

Table 2-1 Defect formation reactions along with mass action law

Type of reaction	Reaction	Law of mass action	Eq.
Interaction with the surroundings	$K_K \leftrightarrow K + V_K' + h^{\bullet}$	$K_p = \frac{[V_K'] \cdot [h^{\bullet}]}{[K_K]} a_K$	2-7a
	$K + V_K' \leftrightarrow K_K + e'$	$K_n = \frac{[K_K] \cdot [e']}{[V_K'] \cdot a_K}$	2-7b

In Table 2-1 a_K represents the potassium activity in the surroundings, [ ] denote concentration of the defects and K_p and K_n are the constants of above equilibriums, having the form described by Eq. 2-3.

Additionally, the electro-neutrality condition must be fulfilled

$$[V_K'] + [e'] = [h^{\bullet}] + [K_i^{\bullet}] \qquad \text{Eq. 2-8}$$

Eqs. 2-2, 2-5, 2-7 and 2-8 allow to calculate the defect concentration as a function of the potassium chemical potential and temperature.

The Brouwer diagram is the graphical representation of the interrelation of the concentration of all the defects existing in a solid electrolyte taking into account all possible defect reactions and the electro-neutrality condition. Fig. 2-14 represents the Brouwer diagram for undoped K-beta-Al_2O_3. The diagram can be splitted into three intrinsic regions. In each of them, one of the defects on either side of Eq. 2-8 controls the neutrality equation, and thus, the potassium activity dependence of the defects involved.

At low chemical potential of potassium, the excess electron concentration ([e']) becomes negligible while the level of the hole concentration becomes comparable to that of the potassium vacancy concentration. However, owing to the interaction with the surroundings the charge balance can also be achieved by increasing the concentration of the positively charged potassium interstitial and decreasing the concentration of negatively charged potassium vacancies that is a kind of internal rearrangement in the crystal.

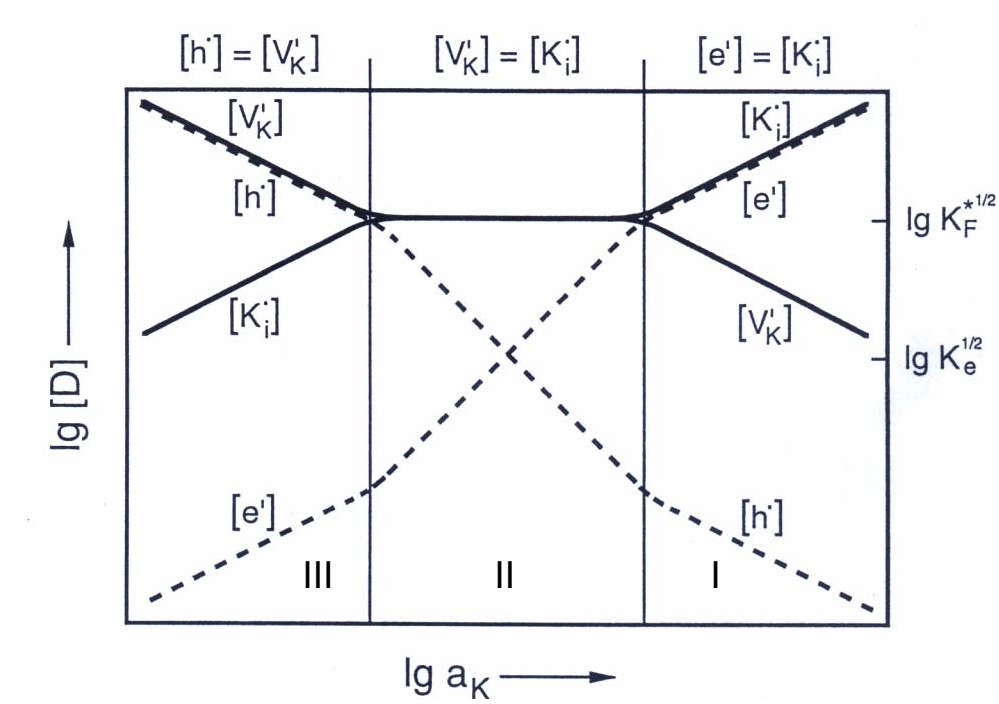

Fig. 2-14 Brouwer diagram for undoped K-beta-alumina [18]

Considering the extreme case of charge balance, for charge neutrality

$$[h^{\bullet}] = [V_K'] . \qquad \text{Eq. 2-9}$$

Inserting the new neutrality condition into the mass action equation i.e. Eq. 2-2, Eq. 2-5 and Eq. 2-7, the defect concentration in the solid electrolyte can be calculated. With the assumption that the concentration of potassium ion on potassium sites is constant, the concentration of electron holes is proportional to the second root of the potassium chemical potential with what solid electrolyte is equilibrated and the region is labelled as hole conduction region.

In the vicinity of the stoichiometric point, the concentrations of potassium ions on interstitial sites and vacancies are much larger than the concentrations of electrons and defect electrons, the relative changes in the concentrations of electronic charge carriers are much larger than that of the interstitial ions ($K_i^{\bullet}$) and the vacancies (range II in Fig. 2-14). Hence the concentrations of potassium ion vacancies and potassium ions in the interstitial site may be considered as virtually being constant:

$$[V_K'] = [K_i^{\bullet}] \cong \text{const} . \qquad \text{Eq. 2-10}$$

Applying the law of mass action to Eq. 2-7a and taking Eq. 2-10 into consideration one obtains the relation

$$[h^{\bullet}] \propto a_K^{-1} , \qquad \text{Eq. 2-11}$$

i.e., the concentration of electron defects is proportional to the inverse of the potassium activity in the surroundings.

Proceeding in a similar fashion the expression for the concentration of the electrons in this range can be obtained by taking into account Eq. 2-7b and Eq. 2-10

$$[e'] \propto a_K . \qquad \text{Eq. 2-12}$$

The situation is totally different for large deviations from the ideal stoichiometry. If the chemical potential of potassium is very high, the concentration of the holes and potassium vacancies may be neglected, hence the electro neutrality condition 2-8 reduces to

$$[e'] = [K_i^{\bullet}]. \qquad \text{Eq. 2-13}$$

Applying the law of mass action to Eq. 2-7b and taking into account the above relation one obtains

$$[e'] \propto a_K^{1/2}, \qquad \text{Eq. 2-14}$$

i.e., the concentration of excess electrons, now equal to the concentration of interstitial ions, is proportional to the square root of the potassium activity.

These results are shown schematically in Fig. 2-14. In case of doped material like MgO doped Na-beta-alumina, the concentration of charge species in different regions of the Brouwer diagram is shown in Table 2-2 and plotted in Fig. 2-15.

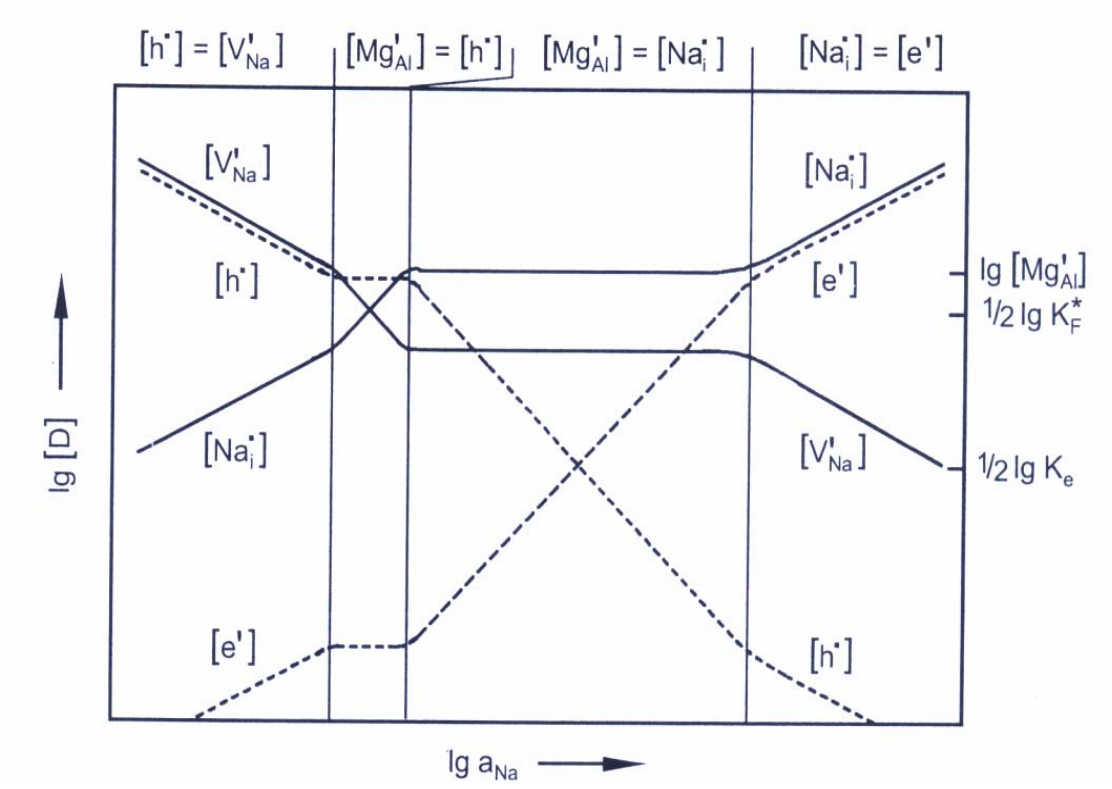

Fig. 2-15 Brouwer diagram for Mg doped Na-beta-alumina [18]

Table 2-2 Sodium activity dependence of the concentration of charge species in different regions of the Brouwer diagram for Mg-doped Na-beta-alumina

Electro-neutrality condition	a_{Na}	$[V'_{Na}]$	$[Na_i^{\bullet}]$	$[h^{\bullet}]$	$[e']$
$[h^{\bullet}] = [V'_{Na}]$	low	$\propto a_{Na}^{-1/2}$	$\propto a_{Na}^{1/2}$	$\propto a_{Na}^{-1/2}$	$\propto a_{Na}^{1/2}$
$[Mg'_{Al}] = [h^{\bullet}]$	middle	$\propto a_{Na}^{-1}$	$\propto a_{Na}$	$\cong$ const	$\cong$ const
$[Mg'_{Al}] = [Na_i^{\bullet}]$	middle	$\cong$ const	$\cong$ const	$\propto a_{Na}^{-1}$	$\propto a_{Na}$
$[e'] = [Na_i^{\bullet}]$	high	$\propto a_{Na}^{-1/2}$	$\propto a_{Na}^{1/2}$	$\propto a_{Na}^{-1/2}$	$\propto a_{Na}^{1/2}$

2.1.1.2.2 Mechanisms of electronic conduction

The mechanism of electronic migration in a cation conductor such as Na-beta-alumina and K-beta-alumina is not known properly. However, the mechanism of hole and electron conduction in solid electrolytes is described by different models that are discussed in the following.

2.1.1.2.2.1 Broad-band conduction

Quasi free excess electrons (e') and electron holes ($h^{\bullet}$) move within the conduction and valence band respectively as depicted in Fig. 2-12. They move through the crystal without the need of activation energy. Such conduction is termed as broad band conduction. In this case the charge carriers possess a relatively high mobility.

2.1.1.2.2.2 Narrow-band conduction

A polaron is a defect in the crystal that is formed when an excess of charge polarizes or distorts the lattice in its immediate vicinity. The combination between charge carriers and distorted field leads to energetically favourable conditions. Hence with the charge carrier the distorted field also moves. This polarization essentially slows down and therefore obstructs the motion of electronic charge carrier through the lattice. Depending on the range of lattice distortion the polaron can be termed as large polaron or small polaron. In case of large polarons, the distortion is not large enough to totally bind an electron or mobile holes completely but is still large enough to retard its motion and thus the lattice distortion generated extends over several atomic distances. Large polarons behave as free carriers except that they have a higher effective mass than a free electron. In case of small polarons, the lattice distortion is localized and the carriers

i.e. electrons or holes are trapped or strongly bound to the lattice. The migration in this case occurs by hopping of the carrier from one ion core to the other due to lattice vibrations and the process is thermally activated.

2.1.1.3 Ionic domain

The total conductivity σ_t of an electrolyte for e.g. K-beta-alumina is the sum of the partial ionic conductivity σ_i and the partial electronic conductivity σ_e and σ_n as discussed in section 2.1.1 and expressed by Eq. 2-1.

The ratio of the partial conductivity σ_j of charge carrier 'j' to the total conductivity σ_t is defined as the transference number t_j of this type of charge carrier:

$$t_j = \frac{\sigma_j}{\sigma_t} \qquad \text{Eq. 2-15}$$

The region within which the electronic contribution to the total conductivity of solid electrolyte is less than 1% with respect to the activity or partial pressure of the potential determining species and temperature is defined as electrolytic domain. The ionic domain represents the region for which the transference number of ions $t_i \geq 0.5$ as shown in Fig. 2-16 for K-beta-alumina.

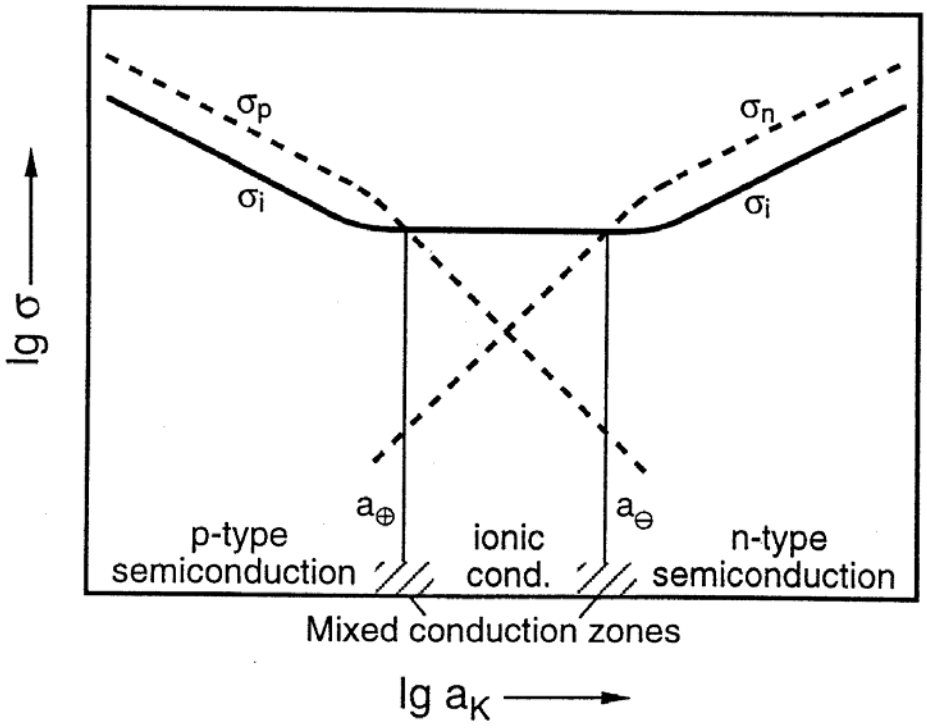

Fig. 2-16 Conductivity diagram of undoped K-beta-alumina

Taking into consideration the defect chemical considerations (section 2.1.1.1.1, 2.1.1.2.1), the definition of conductivity (Eq. 2-1) and supposing that the mobility of the ionic and electronic defect is independent of their concentrations, it follows that the conductivities of electronic defects are related to potassium activities as (K_n and K_p are constants)

$$\sigma_i = \text{const}\,, \qquad \text{Eq. 2-16}$$

$$\sigma_p \propto \left(a_K\right)^{-1} \;\rightarrow\; \sigma_p = K_p \left(a_K\right)^{-1} \quad \text{and} \qquad \text{Eq. 2-17a}$$

$$\sigma_n \propto \left(a_K\right) \;\rightarrow\; \sigma_n = K_n \left(a_K\right). \qquad \text{Eq. 2-17b}$$

These results based on the considerations of section (sections 2.1.1.1 and section 2.1.1.2) are shown schematically in Fig. 2-16 for K-beta-alumina. The electronic conduction parameters $a_{\oplus}$ and $a_{\ominus}$ [7, 68, 69] denote those potassium activities at which the partial electronic conductivities σ_p and σ_n are equal to the ionic conductivity (Fig. 2-16). Thus, they are the limits of the potassium activity range over which the ionic conduction prevails. By using Eqs. 2-16, 2-17, the parameters are given by

$$\frac{\sigma_p}{\sigma_i} = \left(\frac{a_{\oplus}}{a_K}\right) \qquad a_{\oplus} = a_K \;\left(\sigma_p = \sigma_i\right). \qquad \text{Eq. 2-18}$$

and

$$\frac{\sigma_n}{\sigma_i} = \left(\frac{a_K}{a_{\ominus}}\right) \qquad a_{\ominus} = a_K \;\left(\sigma_n = \sigma_i\right). \qquad \text{Eq. 2-19}$$

According to equations 2-15, 2-18 and 2-19, the ionic transference number can be represented in terms of the electronic conduction parameters ($a_{\oplus}$, $a_{\ominus}$) as

$$t_i = \frac{1}{1 + \frac{a_{\oplus}}{a_K} + \frac{a_K}{a_{\ominus}}} \quad . \qquad \text{Eq. 2-20}$$

2.2 Electrode systems

2.2.1 Carbonate electrodes

The establishment of potassium and sodium activity (a_K and a_{Na}) of the carbonate used in this study as electrode, i.e. at the interface between the gas sensitive layer and the

electrolyte, results from the dissociation of K_2CO_3 or Na_2CO_3 into K/Na and gas components CO_2 and O_2 according to the following equilibria

$K_2CO_3 = 2K + CO_2 + 1/2\ O_2$ Eq. 2-21

and

$Na_2CO_3 = 2Na + CO_2 + 1/2\ O_2$ Eq. 2-22

Proceeding from these equilibria the alkali metal activities can be calculated according to the relationships:

$$\ln a_K = \frac{\Delta_f G^\circ_{K_2CO_3} - \Delta_f G^\circ_{CO_2}}{2RT} - \frac{1}{2}\ln\ p_{CO_2} - \frac{1}{4}\ln\ p_{O_2} \qquad \text{Eq. 2-23}$$

$$\ln a_{Na} = \frac{\Delta_f G^\circ_{Na_2CO_3} - \Delta_f G^\circ_{CO_2}}{2RT} - \frac{1}{2}\ln\ p_{CO_2} - \frac{1}{4}\ln\ p_{O_2} \qquad \text{Eq. 2-24}$$

where $\Delta_f G^\circ_{K_2CO_3}$, $\Delta_f G^\circ_{Na_2CO_3}$ and $\Delta_f G^\circ_{CO_2}$ denote the standard Gibbs energies of formation of K_2CO_3, Na_2CO_3 and CO_2, respectively. In the present work numerical data for these quantities are taken from [70]. p_{CO_2} and p_{O_2} are the CO_2 as well as O_2 partial pressure of the gas atmosphere.

2.2.2 Silicate electrodes

With the view to expand the range of chemical potential of the alkaline metal (Na, K) silicate electrodes were used. The alkaline metal chemical potential of the electrode is the consequence of the equilibrium between $MeSi_xO_{2x+0.5}$, SiO_2 and the ambient oxygen atmosphere where Me = Na, K:

$$Me + \frac{1}{4}O_2 + xSiO_2 \leftrightarrow MeSi_xO_{2x+0.5}\,. \qquad \text{Eq. 2-25}$$

As a consequence

$$\ln a_{Me} = \frac{\left(\Delta_f G^\circ_{MeSi_xO_{2x+0.5}} - x\Delta_f G^\circ_{SiO_2}\right)}{RT} - \frac{1}{4}\ln pO_2 + \ln\left(\frac{a_{MeSi_xO_{2x+0.5}}}{a^x_{SiO_2}}\right) \qquad \text{Eq. 2-26}$$

where $\Delta_f G^\circ_{MeSi_xO_{2x+0.5}}$, $\Delta_f G^\circ_{SiO_2}$, $a_{MeSi_xO_{2x+0.5}}$ and a_{SiO_2} denote the standard Gibbs energies of formation of the respective pure substances and the Raoultian activities of $MeSi_xO_{2x+0.5}$ and SiO_2, respectively. p_{O_2} represents the O_2 partial pressure in the gas atmosphere (section 3.3.2) in contact with the solid phases.

By definition, in a pure compound the values of the activity are equal to unity and hence Eq. 2-26 can be rewritten as

$$\ln a_{Me} = \frac{\left(\Delta_f G^\circ_{MeSi_xO_{2x+0.5}} - x\Delta_f G^\circ_{SiO_2}\right)}{RT} - \frac{1}{4}\ln pO_2 . \qquad \text{Eq. 2-27}$$

Eq. 2-27 holds true provided that both the silicate and SiO_2 remain as pure phases during the establishment of equilibrium (Eq. 2-25).

There are literature data on the standard Gibbs energy of formation of $MeSi_xO_{2x+0.5}$ given in [23, 71, 72].

2.2.3 Molybdenum electrode

The sodium chemical potential of the electrode results from the equilibrium between the eutectic mixture of Na_2MoO_4 + $Na_2Mo_2O_7$ and the ambient oxygen atmosphere:

$$Na_2MoO_4 \Leftrightarrow Na + \frac{1}{4}O_2 + \frac{1}{2}Na_2Mo_2O_7 . \qquad \text{Eq. 2-28}$$

The particularity of the eutectic mixture is that it is a homogeneous mixture of two heterogeneous phases. Hence the sodium chemical potential can be given by the following equation

$$\ln a_{Na} = \frac{\left(\Delta_f G^\circ_{Na_2MoO_4} - \frac{1}{2}\Delta_f G^\circ_{Na_2Mo_2O_7}\right)}{RT} - \frac{1}{4}\ln pO_2 + \ln\left(\frac{a^{1/2}_{Na_2Mo_2O_7}}{a_{Na_2MoO_4}}\right). \qquad \text{Eq. 2-29}$$

For pure phases the activities are equal to unity; that is why Eq. 2-29 can be simplified as

$$\ln a_{Na} = \frac{\left(\Delta_f G^\circ_{Na_2MoO_4} - \frac{1}{2}\Delta_f G^\circ_{Na_2Mo_2O_7}\right)}{RT} - \frac{1}{4}\ln pO_2 . \qquad \text{Eq. 2-30}$$

The standard Gibbs energy of formation of the substances involved in Eq. 2-30 is taken from [73]; p_{O_2} represents the O_2 partial pressure in contact with the solid phases.

2.3 Solid electrolyte galvanic cell under isothermal condition

The voltage of a galvanic cell can be described according to Wagner [74]. If the conduction takes place by electrons in the solid electrolyte in addition to ionic conduction then the voltage U is calculated from the balance of the ionic and electronic current densities. The electrical current density for a particle 'k' can be expressed according to the principle of irreversible thermodynamics [17, 75] as

$$i_k = -\frac{\sigma_k}{z_k F}\left[\frac{d\eta_k}{dx}\right] \qquad \text{Eq. 2-31}$$

where σ_k is the partial conductivity, z_k is the charge of species k, F is the Faraday constant, x is the distance coordinate and η_k is the electrochemical potential of species k defined by

$$\eta_k = \mu_k + z_k F\varphi \qquad \text{Eq. 2-32}$$

where μ_k is chemical potential of k and φ is the electrostatic potential.

Under open circuit condition, the partial current densities due to alkali ions (M^+ = Na^+, K^+; z =1) i_{M^+} and electrons i_{e^-} must be equal to each other owing charge neutrality reason:

$$i_{M^+} = -i_{e^-}\,. \qquad \text{Eq. 2-33}$$

Using equations 2-31, 2-32, Eq. 2-33 can be written as

$$\sigma_{M^+}.d\eta_{M^+} = -\sigma_e.d\eta_{e^-}\,. \qquad \text{Eq. 2-34}$$

A local equilibrium can be assumed to exist between the alkali ions, the electrons, e′ and the respective neutral metals [76]:

$$M^+ + e' \leftrightarrow M. \qquad \text{Eq. 2-35}$$

Accordingly, the electrochemical potentials,η, of these species are interrelated as

$$\text{grad}\,\eta_{M^+} + \text{grad}\,\eta_{e^-} = \text{grad}\,\mu_M. \qquad \text{Eq. 2-36}$$

Since solid electrolytes are heavily doped materials with high concentrations of mobile ionic charge carriers, the chemical potential of ions may be assumed to be constant with respect to changes of the chemical potential μ_M throughout the electrolyte. Hence

$$\text{grad}\,\mu_M \approx 0 \quad [77] \qquad \text{Eq. 2-37}$$

Eqs. 2-34, 2-36 and 2-37 result in the expression:

$$d\eta_e = t_{M^+} d\mu_M \qquad \text{Eq. 2-38}$$

Integrating Eq. 2-38 over the thickness of the solid electrolyte and using the definition of the chemical potential of the metal,

$$\mu_M = \mu^\circ_M + RT\ln a_M \qquad \text{Eq. 2-39}$$

the cell voltage U generated across the solid electrolyte can be expressed in terms of the chemical potential of the alkali metal as:

$$U = -\frac{RT}{F}\int_{a'_M}^{a''_M} t_{M^+}\, d(\ln a_M) \qquad \text{Eq. 2-40}$$

where a''_M and a'_M define metal chemical activities at the two ends of the solid electrolyte that is established by electrodes.

Eq. 2-40 allows the information about the transference number to be obtained by measuring the voltage U. Substituting the expression for the transference number expressed by Eq. 2-20 (section 2.1.1.3) into relationship Eq. 2-40 enables the Wagner equation to be integrated [11, 68]. Under the boundary conditions

$$\left(\frac{a_\oplus}{a_\ominus}\right) \ll \frac{1}{4}. \qquad \text{Eq. 2-41}$$

The integration yields:

$$U = -\frac{RT}{F}\ln\left[\frac{(a''_M + a_\oplus)(a'_M + a_\ominus)}{(a''_M + a_\ominus)(a'_M + a_\oplus)}\right]. \qquad \text{Eq. 2-42}$$

Eq. 2-42 is the most general form of the integrated Wagner cell voltage equation for a galvanic cell and holds over the entire range of the metal chemical potential in which the relationships Eq. 2-18 and Eq. 2-19 are valid. Depending on the magnitudes of the chemical activities a″ and a′ in comparison with the parameters $a_\oplus$ and $a_\ominus$, Eq. 2-42 can be simplified into various forms [11]. It results in the classical Nernst equilibrium voltage if the electrolyte has an infinitely extended width of the ionic domain, i.e.

$a_\oplus \to 0$ and $a_\ominus \to \infty$.

Hence, Eq. 2-42 reduces to

$$U_{eq} = -\frac{RT}{F}\ln\frac{a''_M}{a'_M}. \qquad \text{Eq. 2-4}$$

2.4 Solid electrolyte galvanic cell under non-isothermal condition

A thermo cell is defined as a galvanic cell in which temperature is not uniform. To determine the p-electronic conduction parameter of solid electrolytes various thermo cells with cation conducting solid electrolytes are investigated.

A thermo cell involving a solid electrolyte can be represented schematically as follows:

$$\overset{T_0}{\underset{\varphi_1|\varphi_2}{Cu}}\ \Big|\ \overset{T_1}{\underset{\varphi_3|\varphi_4}{Pt}}\ \Big|\ \overset{T}{\underset{\varphi_5|\varphi_6}{Au}}\ \Big|\ \overset{T}{\underset{\varphi_7|\varphi_8}{RE}}\ \Big|\ \underset{\varphi_9|\varphi_{10}}{SE}\ \Big|\ \overset{T+\Delta T}{\underset{\varphi_{11}|\varphi_{12}}{RE}}\ \Big|\ \overset{T+\Delta T}{\underset{\varphi_{13}|\varphi_{14}}{Au}}\ \Big|\ \overset{T_2}{\underset{\varphi_{15}|\varphi_{16}}{Pt}}\ \Big|\ \overset{T_0}{\underset{}{Cu}} \qquad (A)$$

The non-isothermal voltage is generated across cell (A) due to the temperature gradient ΔT applied to the solid electrolyte (SE) along the x-axis. One end of the solid electrolyte is at controlled temperature T while the other end is at temperature $T+\Delta T$. RE represents the reversible electrode used to establish the chemical potential of the neutral species that are mobile in the solid electrolyte. T_1 and T_2 are the temperatures established at the phase boundaries between Au and Pt leads on either side of the solid electrolyte while T_0 is the temperature at the phase boundary of Pt leads with Cu contacts. The quantities φ_j (j =1-16) represent the electrical potential in the respective phases.

The potential difference U developed across cell (A) can be written as follows

$$\begin{aligned} U = {} & (\varphi_1 - \varphi_2) + (\varphi_2 - \varphi_3) + (\varphi_3 - \varphi_4) + (\varphi_4 - \varphi_5) + (\varphi_5 - \varphi_6) + (\varphi_6 - \varphi_7) + (\varphi_7 - \varphi_8) \\ & + (\varphi_8 - \varphi_9) + (\varphi_9 - \varphi_{10}) + (\varphi_{10} - \varphi_{11}) + (\varphi_{11} - \varphi_{12}) + (\varphi_{12} - \varphi_{13}) + (\varphi_{13} - \varphi_{14}) + (\varphi_{14} - \varphi_{15}) \\ & + (\varphi_{15} - \varphi_{16}) \end{aligned}$$

Eq. 2-44

The different types of potential differences result from three contributions namely:

1) The homogeneous contribution arising due to potential difference within pure electronic conductors (Au, Pt, Cu) i.e. $\Delta\varphi_{\ Hom_1}$
2) The homogeneous contribution arising due to the potential difference within mixed conductors containing ions and electrons i.e. the solid electrolyte i.e. $\Delta\varphi_{\ Hom_2}$
3) The heterogeneous contribution arising due to the potential difference at the boundaries between different phases i.e. $\Delta\varphi_{\ Het}$.

Hence the overall generated potential difference across cell (A) can be clumped in terms of homogeneous and heterogeneous parts as

$$U = \Delta\varphi_{Het} + \Delta\varphi_{Hom_1} + \Delta\varphi_{Hom_2} \qquad \text{Eq. 2-45}$$

Both parts will be discussed in detail in the following sections.

2.4.1 Heterogeneous part of the voltage

The heterogeneous part of cell (A) comprises

$$\Delta\varphi_{Het} = (\varphi_1 - \varphi_2) + (\varphi_3 - \varphi_4) + (\varphi_5 - \varphi_6) + (\varphi_7 - \varphi_8) + (\varphi_9 - \varphi_{10}) + (\varphi_{11} - \varphi_{12}) + (\varphi_{13} - \varphi_{14}) + (\varphi_{15} - \varphi_{16}). \qquad \text{Eq. 2-46}$$

At the phase boundaries, an electrochemical equilibrium can be assumed to exist. Hence the electrochemical potential on both sides of the interfaces is identical:

$$\eta_e^{(n)} = \eta_e^{(n+1)} \qquad \text{Eq. 2-47}$$

where $\eta_e^{(n)}$ and $\eta_e^{(n+1)}$ are the electrochemical potential of electrons in the n^{th} and $(n+1)^{th}$ phase.

Invoking the definition of the electrochemical potential as expressed by Eq. 2-32 into Eq. 2-47 leads to

$$\varphi_e^{(n)} - \varphi_e^{(n+1)} = \frac{1}{F}\left[\mu_e^{(n)} - \mu_e^{(n+1)}\right]. \qquad \text{Eq. 2-48}$$

By making use of Eq. 2-48, Eq. 2-46 can be rewritten as follows:

$$\Delta\varphi_{het} = \frac{1}{F}\left[\begin{matrix}\mu_{e_{Pt,T_1}} - \mu_{e_{Au,T_1}} + \mu_{e_{Au,T}} - \mu_{e_{SE,T}} + \mu_{e_{SE,T+\Delta T}} \\ - \mu_{e_{Au,T+\Delta T}} + \mu_{e_{Au,T_2}} - \mu_{e_{Pt,T_2}}\end{matrix}\right]. \qquad \text{Eq. 2-49}$$

Taking into account that the chemical potential is a function of temperature and pressure, i.e., μ_e = f [p, T (x)], it follows from basic relationships of chemical thermodynamics:

$$\left(\frac{\partial\mu_e}{\partial T}\right)_p = -S_e \qquad \text{Eq. 2-50}$$

where S_e is the partial molar entropy of an electron.

Using Eq. 2-50, Eq. 2-49 can be modified into

$$\Delta\varphi_{Het.} = \frac{1}{F}\left[\mu_{e_{SE,T+\Delta T}} - \mu_{e_{SE,T}}\right] + \frac{1}{F}\int_{T_1}^{T_2}\left[S_{e_{Pt}} - S_{e_{Au}}\right] dT + \frac{1}{F}\int_{T}^{T+\Delta T} S_{e_{Au}}\, dT \quad . \qquad \text{Eq. 2-51}$$

Eq. 2.51 represents the heterogeneous part of the thermo voltage of cell (A).

2.4.2 Homogeneous part of the voltage

2.4.2.1 Pure electronic conductors

The homogeneous part of the voltage of cell (A) of the electronically conducting phases is

$$\Delta\varphi_{Hom_1} = (\varphi_2 - \varphi_3) + (\varphi_4 - \varphi_5) + (\varphi_{12} - \varphi_{13}) + (\varphi_{14} - \varphi_{15}). \quad \text{Eq. 2-52}$$

The flux of electrons under a temperature gradient is given as

$$j_e = -\frac{\sigma_e}{z_e^2 F^2}\left[\frac{d\eta_e}{dx} + \left(S_e + \frac{Q_e^*}{T}\right)\frac{dT}{dx}\right] \quad \text{Eq. 2-53}$$

where $S_e^* = S_e + \frac{Q_e^*}{T}$, Q_e^* represents the transported entropy and the heat of transport of an electron respectively. η_e and σ_e are electrochemical potential and partial electrical conductivity of the electrons.

Under open circuit condition the flux of electrons, in a pure metallic conductor must be zero i.e.,

$$j_e = 0. \quad \text{Eq. 2-54}$$

Therefore making use of equations 2-48, 2-50, 2-53 and 2-54, we obtain

$$\varphi = \frac{1}{F}\int\left(S_e^* - S_e\right) dT. \quad \text{Eq. 2-55}$$

The homogenous part of the voltage comprising a pure electronic conductor can be expressed using Eqs. 2-55 and 2-52 as

$$\Delta\varphi_{Hom_1} = \frac{1}{F}\int_{T_1}^{T_2}\left[\left(S_{e_{Pt}}^* - S_{e_{Pt}}\right) - \left(S_{e_{Au}}^* - S_{e_{Au}}\right)\right]dT + \frac{1}{F}\int_{T}^{T+\Delta T}\left(S_{e_{Au}}^* - S_{e_{Au}}\right)dT. \quad \text{Eq. 2-56}$$

2.4.2.2 Mixed ionic-electronic conductors

The flux of charge particle ‘k’ under a temperature gradient can be written as

$$j_k = -\frac{\sigma_k}{z_k^2 F^2}\left[\frac{d\eta_k}{dx} + S_k^*\frac{dT}{dx}\right] \quad \text{Eq. 2-57}$$

where $S_k^* = S_k + \frac{Q_k^*}{T}$ is the transported entropy of particle ‘k’, z_k is the charge on the species that is equal to unity in case of mono-valent cation conductors i.e. for Na, K considered in the present investigation.

Under steady state the fluxes of the ions (i) and electrons (e′) must be oppositely identical, as each volume element of the solid electrolyte must remain electrically neutral (cf. section 2.3):

$$j_i = -j_e . \qquad \text{Eq. 2-58}$$

An electrochemical equilibrium can be assumed to exist inside the solid electrolyte between ions, electrons and neutral atoms without ambiguity (cf. section 2.3)

$$i + e' \leftrightarrow Me \qquad \text{Eq. 2-59}$$

where Me represents the neutral counter part of the mobile species in the solid electrolyte.

Hence the electrochemical potentials η, of these species are interrelated to each other

$$\frac{d\eta_i}{dx} + \frac{d\eta_{e'}}{dx} = \frac{d\mu_{Me}}{dx} . \qquad \text{Eq. 2-60}$$

Using the equations 2-47, 2-48, 2-49, 2-57 and 2-60, the homogeneous part of a mixed ionic electronic conductor can be expressed as

$$\Delta\varphi_{Hom_2} = \frac{1}{F}\left(\mu_{e_{SE,\,T+\Delta T}} - \mu_{e_{SE,\,T}}\right) + \frac{1}{F}\int_{\mu'_{Me,T}}^{\mu''_{Me,T+\Delta T}} \left[t_i \frac{d\mu_{Me}}{dx} + \left(t_i S_i^* - t_e S_{e_{SE}}^*\right)\frac{dT}{dx}\right] \qquad \text{Eq. 2-61}$$

where t_i, t_e represent the transference number of ions and electrons respectively.

2.4.3 Thermo voltage and thermoelectric power

The total potential difference developed across cell (A) can be written by incorporating Eq. 2-53, Eq. 2-58 and Eq. 2-63 into Eq. 2-46

$$U = -\frac{1}{F}\left\{\int_{\mu'_{Me,T}}^{\mu''_{Me,T+\Delta T}} t_i \frac{d\mu_{Me}}{dx} + \left[t_i S_i^* - t_e S_{e_{SE}}^* - S_{e_{Pt}}^*\right]\frac{dT}{dx}\right\}. \qquad \text{Eq. 2-62}$$

The chemical potential can be expressed as

$$\mu_{Me} = \mu_{Me}^o + RT\ln a_{Me} . \qquad \text{Eq. 2-63}$$

Hence, the total differential of μ can be written as [18, 78, 79]

$$\frac{d\mu_{Me}}{dT} = \frac{d\mu_{Me}^o}{dT} + R\ln a_{Me} + RT\frac{d\ln a_{Me}}{dT} . \qquad \text{Eq. 2-64}$$

Taking into consideration Eq. 2-64 the voltage of cell (A) can be modified as

$$U = \left\{ \int_{a'_{Me,T}}^{a''_{Me,T+\Delta T}} -\frac{R\,T}{F} t_i \, d\ln a_{Me} + \left[\frac{t_i}{z\,F} \left(\left(S^o_{Me} - R \ln a_{Me} \right) - S^*_i \right) - \frac{t_e}{F} S^*_{e_{SE}} - \frac{1}{F} S^*_{e_{Pt}} \right] dT \right\}.$$

Eq. 2-65

The thermoelectric power of the solid electrolyte (SE) employed in cell (A) can be defined as

$$\varepsilon = \lim_{\Delta T \to 0} \frac{U}{\Delta T} = \frac{dU}{dT}\,. \qquad \text{Eq. 2-66}$$

Using Eq. 2-66 and Eq. 2-65, the thermoelectric power of the solid electrolyte of cell (A) can be expressed as follows:

$$\varepsilon_{SE/Pt} = \frac{1}{F}\left[t_i \left(S^o_{Me} - R\ln a_{Me} - RT\frac{d\ln a_{Me}}{dT} - S^*_i + S^*_{e_{Pt}} \right) + t_e \left(S^*_{e_{SE}} + S^*_{e_{Pt}} \right) \right] \qquad \text{Eq. 2-67}$$

where $\varepsilon_{SE/Pt}$ represents the thermoelectric power of the electrolyte with reference to Pt. The absolute thermoelectric power for the solid electrolyte can be obtained by subtracting the thermoelectric power due to Pt leads.

Eq. 2-67 can be written in simplified form as

$$\varepsilon_{SE/Pt} = \frac{1}{F}\left[t_i \left(S^o_{Me} - R\ln a_{Me} - RT\frac{d\ln a_{Me}}{dT} - S^*_i \right) + t_e \left(S^*_{e_{SE}} \right) \right] + \frac{1}{F} S^*_{e_{Pt}} \qquad \text{Eq. 2-68}$$

The first term in Eq. 2-68 represents the absolute thermoelectric power of the solid electrolyte while the second term represents the thermoelectric power of the Pt leads.

Hence,

$\varepsilon_{SE/Pt} = \varepsilon_{SE} + \varepsilon_{Pt}$.

As the value of ε_{Pt} is very small [80] in comparison to the total thermoelectric power ($\varepsilon_{SE/Pt}$), it could be considered as negligible. Consequently, the thermoelectric power of the solid electrolyte exposed to a temperature gradient and of chemical potential gradient in cell (A) could be obtained from Eq. 2-68.

2.4.3.1 Data evaluation

The thermoelectric power of the solid electrolyte in cell (A) (Eq. 2-68) can be written in terms of the p-electronic conduction parameter ($a_\oplus$) by incorporating the expression for the transference number of the respective species i.e. Eq. 2-20 (cf. section 2.1.1.3) into Eq. 2-68 and under the assumption that

$a_\theta >> a_{Na} \approx a_\oplus$

it follows

$$\varepsilon = \frac{1}{F}\left\{\begin{array}{l}\left(1+\frac{a_{\oplus}}{a_{Me}}\right)^{-1}\left(S^{o}_{Me} - R\ln a_{Me} - RT\frac{d\ln a_{Me}}{dT} - S^{*}_{i}\right) + \\ \left[1-\left(1+\frac{a_{\oplus}}{a_{Me}}\right)^{-1}\right]\ S^{*}_{e_{S.E.}}\end{array}\right\} + \frac{1}{F}S^{*}_{e_{Pt}} \quad . \qquad \text{Eq. 2-69}$$

At constant temperature T, the quantities $S^{o}_{Me} - S^{*}_{i} + S^{*}_{e_{Pt}}$ and $S^{o}_{e} + \frac{Q^{*}_{e}}{T}$ can be approximated as constants i.e.,

$S^{o}_{Me} - S^{*}_{i} = C_1$

and

$S^{o}_{e} + \frac{Q^{*}_{e}}{T} = C_2$

Hence, Eq. 2-69 can be simplified in the following form:

$$\varepsilon = \frac{1}{F}\left[\left(1+\frac{a_{\oplus}}{a_{Na}}\right)^{-1}\left(C_1 - R\ln a_{Me} - RT\frac{d\ln a_{Me}}{dT}\right) + \left(1+\frac{a_{Me}}{a_{\oplus}}\right)^{-1}\left(-R\ln a_{Me} + C_2\right)\right]. \qquad \text{Eq. 2-70}$$

Eq. 2-70 can be exactly evaluated in terms of the p-electronic conduction parameter ($a_{\oplus}$) by means of a non-linear regression technique taking into account a field of experimental data $\varepsilon = f\left(T, a_{Me}\right)$ and the value for $\frac{d\ln a_{Me}}{dT}$ (cf. section 2.4.3.2), even though C_1 and C_2 are unknowns. The measurements enable us to verify the behaviour of the p-electronic conduction parameter under different levels of the chemical potential of the potential determining species thereby providing a deeper insight of the impact of the ambience over the behaviour of the p-electronic conduction parameter.

2.4.3.2 Calculation of $\frac{d\ln a_{Me}}{dT}$

For calculating the expression for $\frac{d\ln a_{Me}}{dT}$, one has to consider the general reaction occurring at the phase boundary between solid electrolyte and electrode:

$$\nu_a A \Leftrightarrow \ \nu_b B + \nu_m Me + \nu_o O_2 \qquad \text{Eq. 2-71}$$

where ν_j: stoichiometric numbers, positive for products and negative for reactants. O_2 is the oxygen gas in the atmosphere. A/B refers to the combination of the phase systems used in the present investigation to establish the chemical potential of the neutral species of the solid electrolyte as

A/B: $Na_2MoO_4/Na_2Mo_2O_7$

Me_2CO_3/CO_2

$MeSi_xO_{2x+0.5}/SiO_2$, (Me = Na, K).

From the basic principle of thermodynamics of chemical equilibrium and using Eq. 2-71, it follows

$$\ln a_{Me} = \frac{\nu_a \ \Delta_f G_A^\circ - \nu_b \ \Delta_f G_B^\circ}{\nu_m \ RT} - \frac{\nu_o}{\nu_m} \ln p_{O_2} + \frac{RT}{\nu_m} \ln \frac{a_A^{\nu_a}}{a_B^{\nu_b}} . \qquad \text{Eq. 2-72}$$

In Eq. 2-71, provided both the phases A and B remain as pure phases during the establishment of equilibrium, by definition in pure compounds the Raoultian activity is equal to unity.

On differentiating Eq. 2-72 with respect to temperature it follows

$$\frac{d \ln a_{Me}}{dT} = \frac{\nu_b \ \Delta_f G_B^\circ - \nu_a \ \Delta_f G_A^\circ}{\nu_m R T^2} . \qquad \text{Eq. 2-73}$$

By substituting the data on the standard Gibbs free energy of formation of the respective substances that are taken from the literature [23, 70-73], the value of $\frac{d \ln a_{Me}}{dT}$ can be obtained.

2.4.3.3 Polarity of the thermoelectric power

In the present work, the sign convention to be followed with respect to the polarity of the thermoelectric power is such that the cold end of the solid electrolyte is connected to the positive pole of the multimeter. The same sign convention has been used by Kröger [81] to define the polarity of the thermoelectric power of mixed ionic-electronic conductors.

2.5 Thermodynamic stability of NASICON

There is only one serious report in the literature [82] concerning the thermodynamic stability of NASICON. Moreover nothing is known about the existence of the phase equilibria prevailing in NASICON. With a view to gain insight about the phase stability of NASICON isothermal measurements were performed. The measuring principle is based on a galvanic cell that allows to reproducibly transform the sodium activity into an oxygen chemical potential and to measure that by means of an oxygen ion conducting solid electrolyte, i.e. e.g. yttria stabilized zirconia (YSZ).

Based on previous approaches with similar intention but aiming at different materials [83, 84, 85], the galvanic cell used for the thermodynamic stability measurements of sodium oxide activity in NASICON, is represented as follows

$$Pt|CO_2,O_2 \;|\; Na_2CO_3\ (Au) \;|\; NASICON\ (Au) \;|\; YSZ \;|\; O_2|Pt \qquad (VIII)$$

where YSZ is used as a solid electrolyte. The quantities p''_{O_2} and p'_{O_2} are the oxygen chemical potentials at the surfaces of YSZ; a'_{Na}, a''_{Na} and a'''_{Na} are the sodium activities established at the interfaces of the sodium ion conductors i.e. between Na_2CO_3 and the gas phase, between NASICON and YSZ, and between NASICON and Na_2CO_3, respectively.

The data obtained using the above cell configuration definitely precludes any effect due the electronic transference through the solid electrolyte [86].

The galvanic cell voltage can be evaluated according to the Nernst equation

$$U = \frac{RT}{4F} \ln\left(\frac{p''_{O_2}}{p'_{O_2}}\right). \qquad \text{Eq. 2-74}$$

The measuring electrode consists of a sintered NASICON pellet in contact with a densified disk of Na_2CO_3. Both of these compounds are electronically short-circuited using metallic Au wires thus maintaining the same sodium activity established at the CO_2, $O_2|Na_2CO_3$ interface to that of Na_2CO_3|NASICON. The sodium activity at the CO_2, $O_2|Na_2CO_3$ interface is established according to Eq. 2-24 (cf. section 2.2.1).

It is known from similar studies on other systems [15] that at constant temperature and pressure, the sodium oxide activity a_{Na_2O} in NASICON will be fixed by the phase equilibrium

$$Na_{1+x}Zr_2Si_xP_{3-x}O_{12} \rightleftarrows Na_{1+x-y}Zr_2Si_xP_{3-x}O_{12-y/2} + \frac{1}{2}\,y\,Na_2O\ (NASICON). \qquad \text{Eq. 2-75}$$

Eq. 2-75 relates the sodium oxide activity to the thermodynamic stabilities of $Na_{1+x}Zr_2Si_xP_{3-x}O_{12}\left(\Delta_f G^{\circ}_{Na_{1+x}Zr_2Si_xP_{3-x}O_{12}}\right)$ and $Na_{1+x-y}Zr_2Si_xP_{3-x}O_{12-y/2}\left(\Delta_f G^{\circ}_{Na_{1+x-y}Zr_2Si_xP_{3-x}O_{12-y/2}}\right)$.

$$\ln a_{Na_2O} = \frac{2\left(\Delta_f G^{\circ}_{Na_{1+x}Zr_2Si_xP_{3-x}O_{12}} - \Delta_f G^{\circ}_{Na_{1+x-y}Zr_2Si_xP_{3-x}O_{12-y/2}}\right)}{yRT} - \frac{\Delta_f G^{\circ}_{Na_2O}}{RT} + \frac{2}{y}\ln\frac{a_{Na_{1+x-y}Zr_2Si_xP_{3-x}O_{12-y/2}}}{a_{Na_{1+x}Zr_2Si_xP_{3-x}O_{12}}}$$

Eq. 2-76

where $a_{Na_{1+x}Zr_2Si_xP_{3-x}O_{12}}$ and $a_{Na_{1+x-y}Zr_2Si_xP_{3-x}O_{12-y/2}}$ are the Raoultian activities of

$Na_{1+x}Zr_2Si_xP_{3-x}O_{12}$ and $Na_{1+x-y}Zr_2Si_xP_{3-x}O_{12-y/2}$ respectively and $\Delta_f G^\circ_{Na_2O}$ is the standard Gibbs free energy of formation of K_2O.

According to

$$Na_2O \leftrightarrow 2Na + \frac{1}{2}O_2 \qquad \text{Eq. 2-77}$$

the activity of sodium oxide dissolved in NASICON determines the oxygen potential p''_{O_2} depending on the sodium activity a''_{Na}.

$$\ln p''_{O_2} = \frac{2\Delta_f G^\circ_{Na_2O}}{RT} + 2\ln a_{Na_2O} - 4\ln a''_{Na} \ . \qquad \text{Eq. 2-78}$$

The galvanic cell is a stacked pellet assembly in which both the reference and the measuring electrodes are exposed to the same gas atmosphere which is a $CO_2 + O_2$ mixture in this case. Whilst both of the gas components, i.e. CO_2 and O_2 act as the potential determining species at the measuring electrode, only O_2 is the potential determining one at the reference electrode. Hence, the equilibrium existing at the reference electrode may be written as

$$1/2O_2 + 2e^-(Pt) \leftrightarrow O^{2-}(YSZ) \ . \qquad \text{Eq. 2-79}$$

Taking equations 2-24, 2-78 and 2-79 into consideration, Eq. 2-74 can be rewritten in terms of sodium oxide activity as follows

$$\ln a_{Na_2O} = \frac{2FU}{RT} - \frac{\Delta_f G^\circ_{Na_2O} - \Delta_f G^\circ_{Na_2CO_3} + \Delta_f G^\circ_{CO_2}}{RT} - \ln p_{CO_2} \ . \qquad \text{Eq. 2-80}$$

Eq. 2-80 enables the determination of the sodium oxide activity and thus the thermodynamic stability of the NASICON by measuring the galvanic cell voltage at known CO_2 partial pressures of the gas atmosphere.

2.6 Fundamentals of impedance spectroscopy

Impedance spectroscopy (IS) is extensively used to characterise electrical properties of solid electrolytes and their interfaces with variously conducting electrodes. To evaluate the electrochemical behaviour of the electrolyte or/and electrode materials, electrical measurements are often performed on cells having two identical electrodes and the electrolyte in form of parallelepiped of circular or rectangular cross section. The most common and standard approach in IS is to measure the impedance in the frequency domain by applying an electrical perturbation namely voltage and recording the real and

imaginary parts of the measured complex resistance. The frequency dependence of the complex resistance is characteristic of the materials and electrodes being used.

A typical impedance spectrum for instance of a zirconia based O^{2-} conducting electrolyte with Pt/O_2 electrodes shown in Fig. 2-17a is characterised by two semicircles in the Z' and Z'' plane, the so called Nyquist plot [87]. The semicircles shown in Fig. 2-17b have been attributed by Bauerle [87] as the grain boundary (left semicircle), and the electrode reaction taking place at the interfaces of the solid electrolyte and electrodes (right semicircle) and the corresponding equivalent circuit is shown in Fig. 2-17b.

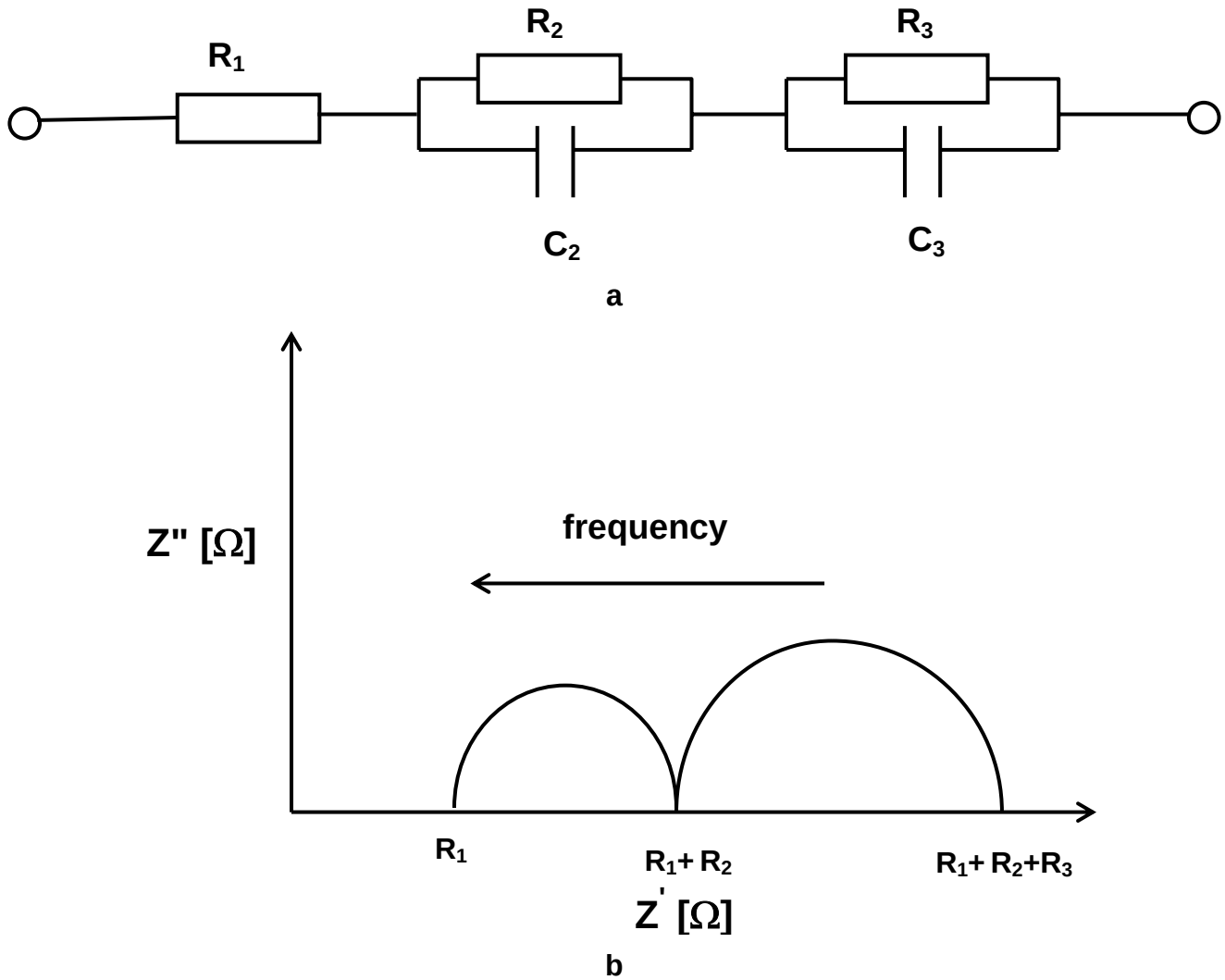

Fig. 2-17 A typical impedance spectrum (b) and corresponding equivalent circuit (a) [87]

The values of R_1, R_2 and R_3 depicted in Fig 2-17b respectively represent the resistance of grain, grain boundary and of the electrode reactions. This is the conventional way to assign the observed semicircles followed in most of the reports in the literature.

However, it is worth mentioning that Näfe [88] pointed out the unambiguous assignment of the semicircles is doubtful. Moreover, it is often not feasible to interpret the obtained impedance results in terms of the simplified electrical equivalent circuit [89].

In the present investigation, this technique was used to study the influence of the chemical potential of the neutral counterpart of the mobile species in the solid on the impedance of the cation conducting solid electrolyte in a single compartment galvanic cell (I). The present approach is different from the previous investigations insofar as only relative changes of the complex resistance of the material with the chemical activity have been taken into account at constant temperature in contrast to the conventional procedure where it is assumed apriori that a particular resistance represents the absolute value of the material's property. Thus, in the present procedure there is no need to assign the observed semicircles with a specific feature of the material.

Taking into account the geometrical aspects i.e. the thickness (t) and the surface area (A) of the solid electrolyte, the conductivity was calculated from the measured impedance spectrum according to the following formula:

$$\sigma = \frac{t}{AR} \qquad \text{Eq. 2-81}$$

where R represents the real part of the complex impedance measured for the solid electrolyte at constant temperature and the activity.

3. Experimental

3.1 Characterization Techniques

3.1.1 Chemical Analysis

The solid electrolytes (Na-beta-Al_2O_3, K-beta-Al_2O_3, NASICON) and the constituent of electrode materials (Na-silicate, K-silicate) used in the present investigation were analysed with respect to the content of potassium, sodium, aluminium and silicon by optical emission and optical absorption spectrometry with inductively coupled plasma excitation (OES-ICP, JY 70 Plus, Instruments S.A., France). A carrier hot gas extraction method was used in a resistance furnace at $T > 2500°$ C, (TC-436 DR, Leco, USA) to determine the oxygen content.

3.1.2 X-ray analysis

The phase composition of the materials was investigated at room temperature by X-ray diffractometry (XRD) (Siemens Diffractometer D5000/Kristalloflex) using Ni-filtered Cu-$K\alpha_1$ radiation (λ = 1.5418 Å) and a graphite monochromator in flat plane $\theta/2\theta$ geometry, in the 2θ = 10-80° range. The step size was 0.02° with a scan time of 2 s per step. The voltage and current used for the measurements were 40 kV and 30 mA respectively. X-ray patterns were identified by means of the JCPDS X-ray database [90] using the EVA 5.0 Diffract program.

3.1.3 Scanning electron microscopy (SEM)

The microstructure and composition of the phases of Na-beta-alumina and K-beta-alumina were investigated using a field emission microscope Zeiss DSM982 GEMINI coupled with energy dispersive X-ray system (Oxford- Instrument ISIS 300). The samples were given a $\sim$ 2 nm thick carbon coating before observation.

To probe the microstructure, a ceramographic preparation of the materials was done. The beta aluminates are extremely sensitive to water and even react with moisture in air. Hence the preparations of commercially available sodium and potassium beta alumina were done in complete absence of water and moisture. The polishing procedure of the commercial lapped beta-alumina specimens has been outlined in Table 3-1. For micro-structural analysis, the surfaces of Na-beta-alumina, K-beta-

alumina and NASICON samples were polished to a 1 μm finish and etched for 20 min at 1693 K.

Table 3-1 Ceramographic preparations of K and Na-beta-Al_2O_3 and NASICON

Step		Substrate	Diamond spray [μm]	Lubricant	Time [min]	Pressure [N/mm^2]	Speed U/min
1	Polishing	Texmet (Nylon cloth)	6	Butandiol	20-45	90	150
2		DP-Dac (Nylon cloth)	3	Butandiol	40-60	90	150
3		DP-Dac	1	Butandiol	30-60	90	150

3.2 Solid electrolytes

The ceramic materials employed as solid electrolyte in the present investigation are complied in Table 3-2.

Table 3-2 Solid electrolytes under investigation

Solid Electrolyte	Company	Form	Dimension
Na_2CO_3	Laboratory-prepared	Pellet	6 mm * 30 mm $^{++}$
NASICON	Laboratory-prepared	Pellet	10 mm * 3.0 mm $^{+}$
K-beta-alumina	Ionotec Inc. UK	Tube	16 mm * 1.5 mm $^{+}$ 20 mm $^{++}$
K_2CO_3	Laboratory-prepared	Pellet	11 mm * 20 mm $^{++}$
Na-beta-alumina	Asea Brown Boveri, Germany	Tube	25 mm * 0.2 mm $^{+}$ 20 mm $^{++}$
YSZ	Friatec AG, Germany	Pellet	10 mm * 1 mm $^{+}$

* Diameter $^{+}$ Thickness $^{++}$ Height

3.2.1 Na-beta-alumina

The commercial Na-beta-alumina (NBA) tube with one end closed as supplied by Asea Brown Boveri, Germany, with dimensions 25 mm outer diameter, 1.0 mm wall thickness having chemical composition of 9.14 wt% Na_2O, 3.32 wt% MgO and 87.48 wt% Al_2O_3

was cut to a length of 20 mm and 15 mm to be used as a solid electrolyte. The XRD pattern reveals the material consists of a phase mixture of β+β'' thus should be considered as Na-(β+β'')-alumina, with predominant β" phase as shown in Fig. 3-1. The micro-structural properties of the sintered material (average grain size, the porosity and the pore size) were evaluated using the Image C Statistic program.

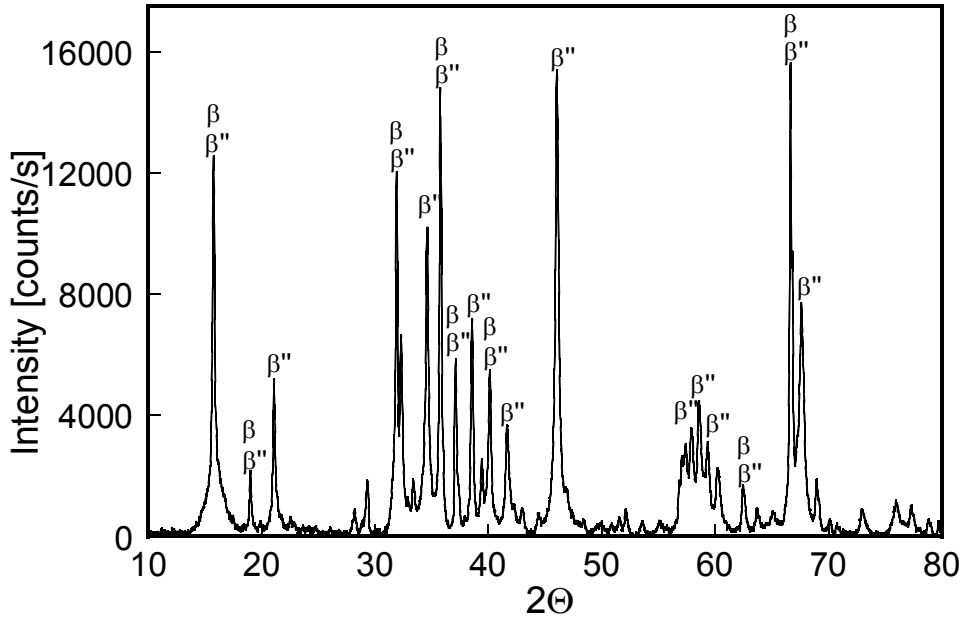

Fig. 3-1 XRD pattern of the commercial Na-beta-alumina tube

A micrograph of the material is shown in Fig. 3-2.

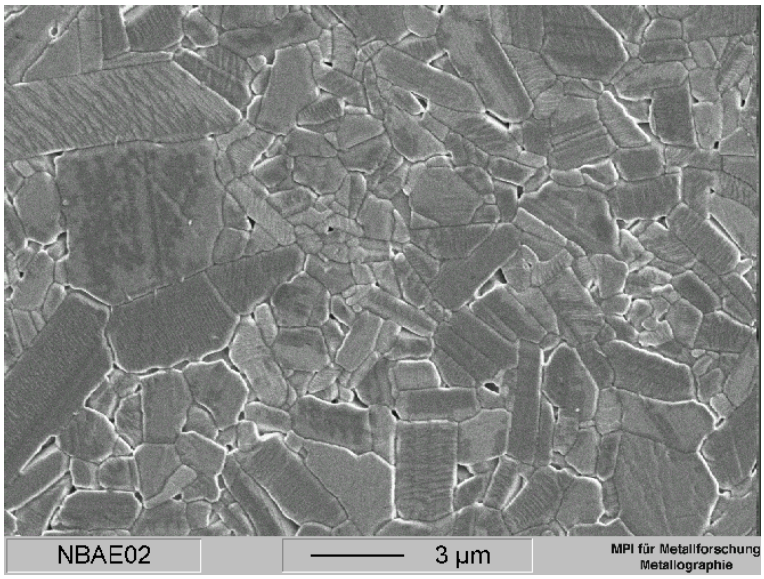

Fig. 3-2 SEM image of the commercial Na-beta-alumina tube

The microstructure is homogeneous, consists of plate-like grains of about 1-10 μm. As seen the pores are closed and total porosity amounts nearly 2%. The average grain size is 2 μm.

3.2.2 K-beta-alumina

The commercially available K-beta-alumina (KBA) supplied by Ionotec Inc., UK, with dimensions 16 mm outer diameter, 1.5 mm wall thickness, was cut into two pieces of length 18 and 20 mm. It has a chemical composition, corresponding to 11.58 wt% K_2O and 0.73 wt% Li_2O (rest Al_2O_3). The chemical analysis obtained from EDS spectra for the K-beta-Al_2O_3 sample as given in Table 3-3 is in agreement with that taken from OES-ICP.

Table 3-3 Elemental composition of K-beta-alumina

Element	Concentration, %	Intensity correction	Weight, %	Weight (sigma), %	Atomic %
O	63.55	1.9952	39.80	0.44	54.03
Al	38.97	0.9873	49.74	0.40	39.65
K	8.42	1.0093	10.41	0.19	5.78
Total			100.00		

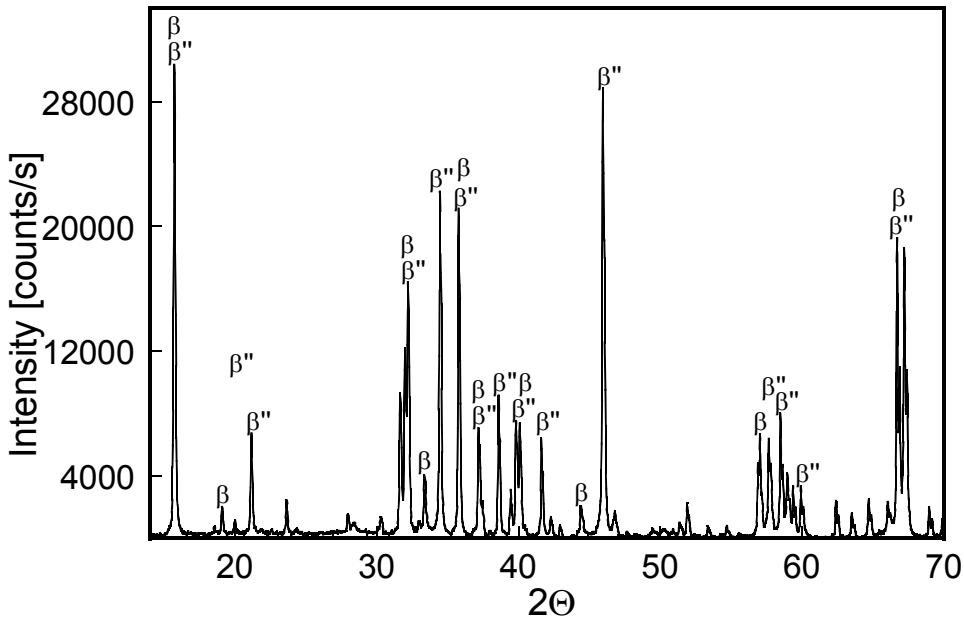

Fig. 3-3 XRD pattern of the commercial K-beta-alumina tube

The XRD pattern (Fig. 3-3) reveals that the material consists of a mixture of β+β″ phases thus should be considered as K-β+β″-alumina (K-beta-alumina). The content of β and β″are 5 and 95% respectively [91, 92].

3.2.3 NASICON

The material was synthesized by the solid-state reaction method as described in [15] in form of a pellet with dimensions 10 mm diameter and 3 mm thickness. The XRD pattern of the material is depicted in Fig. 3-4. The microstructure revealed that the material is homogeneous. The chemical composition of the NASICON was analysed by EDX technique and shown in Table 3-4. According to the analysis the material has the formula $Na_3Zr_2Si_2PO_{12}$.

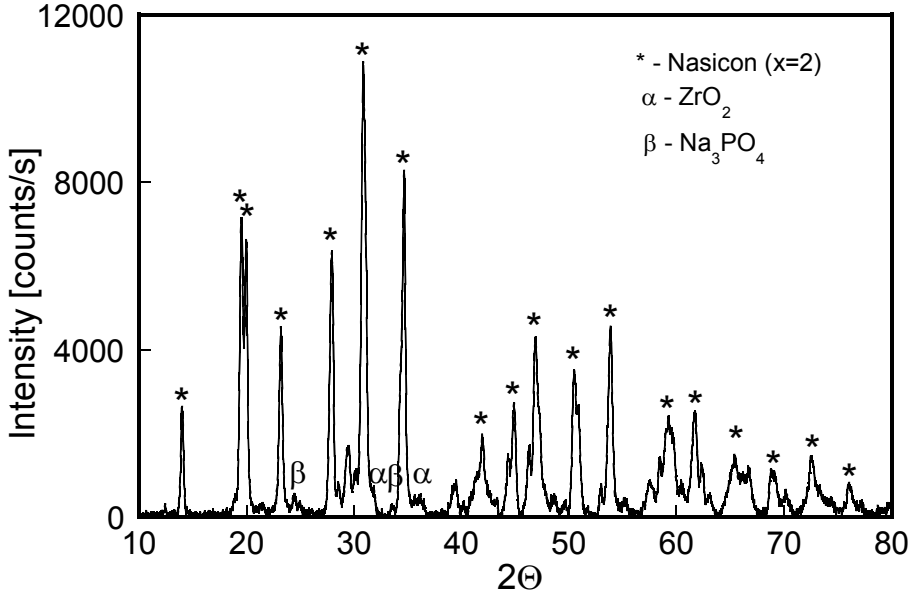

Fig. 3-4 XRD pattern of NASICON material

Table 3-4 Elemental composition of NASICON material

Element	Concentration, %	Intensity correction	Weight, %	Weight (sigma), %	Atomic %
O	39.09	1.5545	30.19	0.58	52.79
Na	12.60	0.9907	15.28	0.30	18.60
Si	9.84	0.9491	12.46	0.25	12.41
P	5.65	1.2256	5.54	0.32	5.00
Zr	22.63	0.7438	36.53	0.69	11.20
Total			100.00		

3.2.4 Na_2CO_3 and K_2CO_3

To fabricate carbonate pellets Na_2CO_3 and K_2CO_3 powders available commercially (Merck GmbH, Germany, 99.9%) were taken as the starting material. Initially the powders were fired at 573 K overnight for the removal of water and subsequently compressed into pellets using cold isostatic pressing (800 kN/mm^2, 1 min) of dimensions 30 mm, height 6 mm diameter (Na_2CO_3) and 20 mm height, 10 mm diameter (K_2CO_3). The pellets were then sintered at 1023 K for 10 h (Na_2CO_3) and 1073 K for 8 h (K_2CO_3) in air. The density of the sintered pellets was 96% of the theoretical value. The characterization of the sintered pellets by XRD reveals that the material consists of pure Na_2CO_3 (Fig. 3-5) and K_2CO_3.

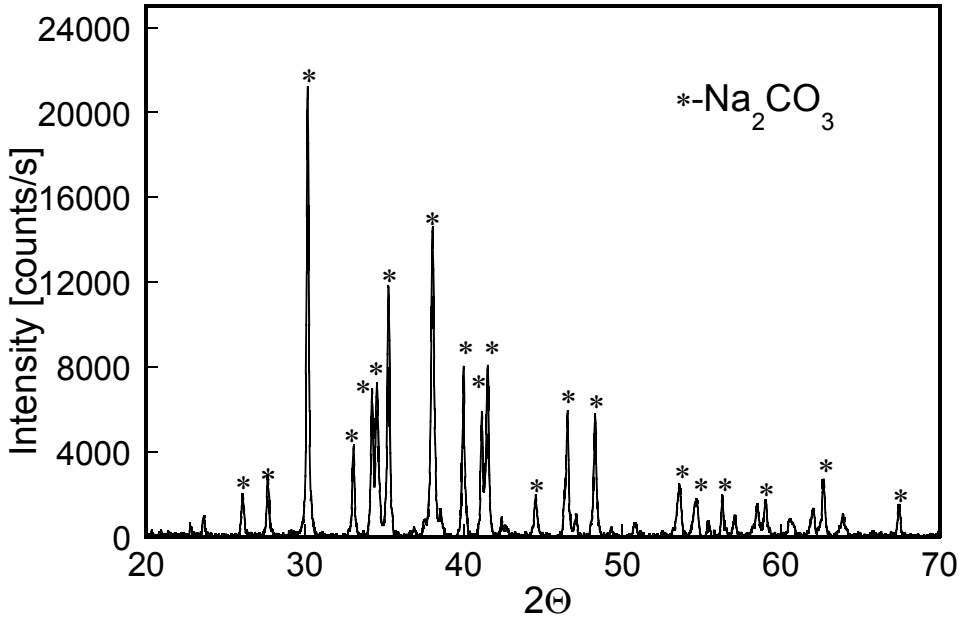

Fig.3-5 XRD pattern of Na_2CO_3

3.3 Electrodes

3.3.1 Carbonate/gas electrode

For preparation of the carbonate electrodes, the same procedure was employed as outlined in section 3.2.4. The only difference is that in the present case the pellets were electronically short circuited by statistically distributed gold wires (thickness 250 µm). The sintered pellets were cut and polished to flatness (diameter: 17 mm, 28 mm; thickness: 1-1.5 mm). The room temperature resistance of the samples was less than 1 Ω. The different metal activities were achieved by using various gas mixtures in

equilibrium with the carbonates. The gas mixture was established by successively diluting premixed O_2-CO_2 or CO_2-O_2-Ar gas mixtures with pure Ar (≤ 10 ppm impurities). For that purpose calibrated mass flow controllers (FC-2900; TYLAN General) were employed.

The premixed gases had the following compositions:

1. Ar with 200 ppm O_2 ($p_{O_2} = 2 \cdot 10^{-4}$ bar) and 200 ppm CO_2 ($p_{CO_2} = 2 \cdot 10^{-4}$ bar).
2. Ar with 10000 ppm O_2 ($p_{O_2} = 0.01$ bar) and 10000 ppm CO_2 ($p_{CO_2} = 0.01$ bar).
3. CO_2 with 85-vol% O_2 ($p_{CO_2} = 0.15$ bar, $p_{O_2} = 0.85$ bar).

This facilitates to cover a range of approximately 3–4 orders of magnitude in the metal activities. The total gas flow through the cell compartment was kept constant at a rate of 36 ml/min.

3.3.2 Silicate/SiO_2/O_2 electrode

The sodium silicate was prepared as water glass as described in the following. Initially the Na_2CO_3 and SiO_2 powders (Merck GmbH, Germany) were fired at 573 K overnight for removal of water and mixed homogeneously by using a ball mill grinder in the molar ratio of 1:3. The obtained mixture was dried at 573 K. The mixture was heated till 1023 K so that Na_2CO_3 melts down and reacts with SiO_2. At this temperature the mixture was kept for 30 minutes and finally heated till 1673 K to form sodium silicate glass. The preparation of the glass has been done in a Pt crucible. The Na-silicate glass so obtained was dissolved in pressurized water at 473 K for 20 h in an autoclave. The chemical analysis of the liquid by the OES technique reveals that the glass has the composition $NaSi_xO_{2x+0.5}$ with x = 1.5 that is supported by EDX on the dried solid material.

Table 3-5 Elemental composition of Na-silicate ($NaSi_xO_{2x+0.5}$) glass

Element	Concentration, %	Intensity correction	Weight, %	Weight (sigma), %	Atomic %
O	94.62	3.2031	49.27	0.31	61.20
Na	11.02	0.9918	18.55	0.21	16.03
Si	16.83	0.8729	32.18	0.25	22.77
Total			100.00		

The elemental composition is compiled in Table 3-5. A layer of water glass was deposited on both side of the electrolyte pellet by dropping the solution and dried by adding particles of SiO_2 powder simultaneously.

The gold net along with platinum wires placed on the sides of the sample served as a part of the electrode for electrical contacts as shown in Fig. 3-6.

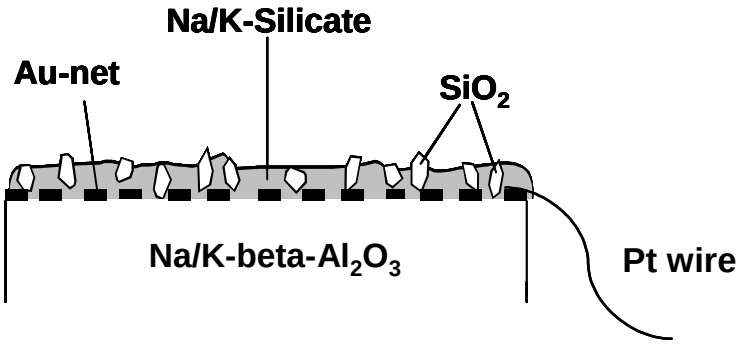

Fig. 3-6 Schematic set-up of thermo cells

In the similar fashion, the K-silicate glass was prepared and deposited on that part of solid electrolyte that serves as electrode. From the chemical analysis the composition of the glass was found to be $KSi_xO_{2x+0.5}$ with x=1.5 and the elemental composition is shown in Table 3-6.

Table 3-6 Elemental composition of K-silicate ($KSi_xO_{2x+0.5}$) glass

Element	Concentration, %	Intensity correction	Weight, %	Weight (sigma), %	Atomic %
O	38.08	1.3757	42.64	1.37	60.63
K	21.21	1.0527	31.06	0.88	18.07
Si	16.84	0.9870	26.30	0.75	21.30
Total			100.00		

To establish various alkaline metal (Na, K) chemical potential, a number of premixed O_2, O_2 + Ar gases were used. The oxygen containing gases had the following compositions:

1. Pure O_2 (p_{O_2} = 1 bar),
2. Ar with 10000 ppm O_2 (p_{O_2} = 0.01 bar),
3. Ar with 200 ppm O_2 ($p_{O_2} = 2 \cdot 10^{-4}$ bar).

To expand the interval of alkaline metal activities various gas mixtures comprising H_2 with H_2O and Ar were used. The gases were flown through a cryostat to achieve desired values of H_2O partial pressure before flushing the cell compartment so as to establish an oxygen partial pressure, which in turn defines a chemical potential of the species under consideration. The partial pressure of H_2O was varied by changing the cryostat temperature between 5–18 °C. The H_2 containing gases had the following compositions:

1. Pure H_2 (p_{H_2} = 1 bar),
2. Ar with 10000 ppm H_2 (p_{H_2} = 0.01 bar),
3. Ar with 1000 ppm H_2 (p_{H_2} = 0.001 bar).

This facilitates to cover a broad range of potassium or sodium activities of approximately 4–5 orders of magnitude. The total gas flow through the cell compartment was kept constant at 36 ml/min (section 3.3.1). The apparatus used to establish different partial pressures of the gases is schematically shown in Fig. 3-7.

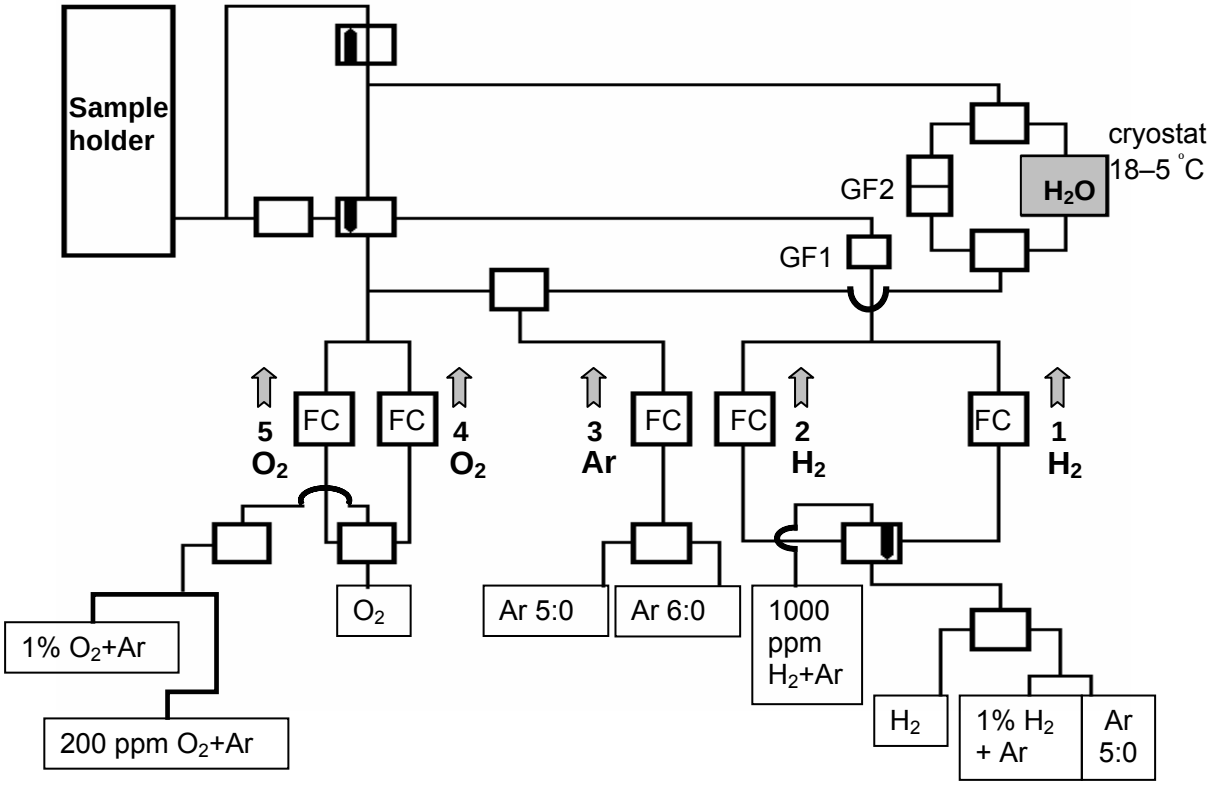

Fig. 3-7 Schematic sketch of experimental apparatus

3.3.3 Na-Mo-O/O_2 electrode

An eutectic mixture of Na_2MoO_4 + $Na_2Mo_2O_7$ was used as an electrode to establish as before a different range of sodium chemical potential. The phases Na_2MoO_4 and $Na_2Mo_2O_7$ constitute a eutectic mixture in the system MoO_3-Na_2MoO_4 [93] as shown in Fig. 3-8.

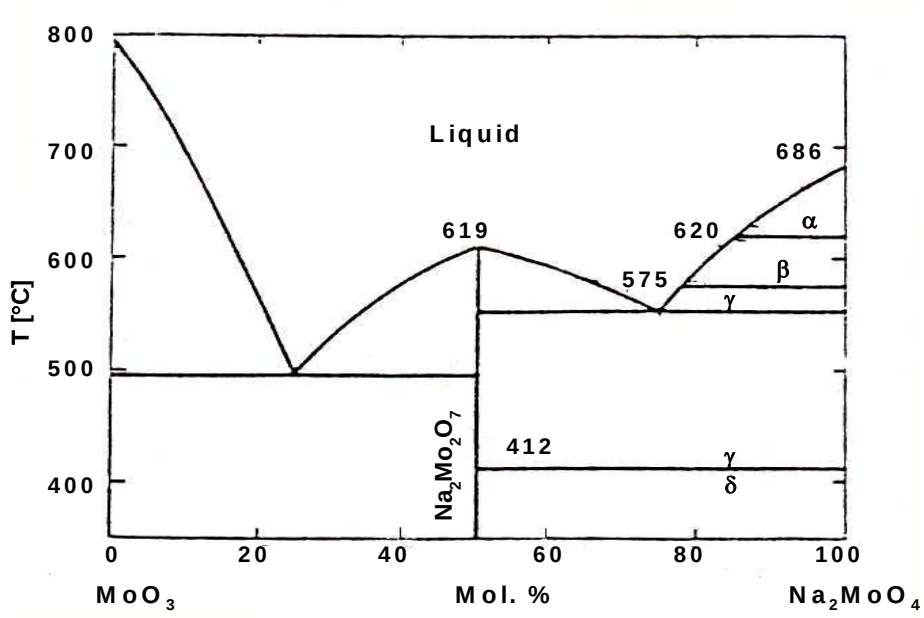

Fig. 3-8 Phase diagram of the MoO_3-Na_2MoO_4 system constitute an eutectic mixture of Na_2MoO_4+$Na_2Mo_2O_7$ [93]

The eutectic mixture was prepared by thoroughly mixing and melting 76 mol% Na_2MoO_4 (pure, ALDIC) and 24 mol% MoO_3 (Extra pure, Merck) powders at 973 K. The phase mixture was characterized by XRD (Fig. 3-9), DTA (Fig. 3-10) and the homogeneity of the mixture was checked by SEM. Two endothermic and three exothermic effects were observed in the DTA curve for the mixture. The first endothermic peak indicates the phase transition between β to α while the second is the melting peak. With regard to the exothermic effects, the 3rd and 4th peak indicate the phase transition from γ to β and β to α respectively. The 5th peak represents the solidification process.

The mixture was pelletized having dimensions, diameter: 27 mm, thickness: 1mm, with statistically distributed gold wires and fired at 773 K for 2 h.

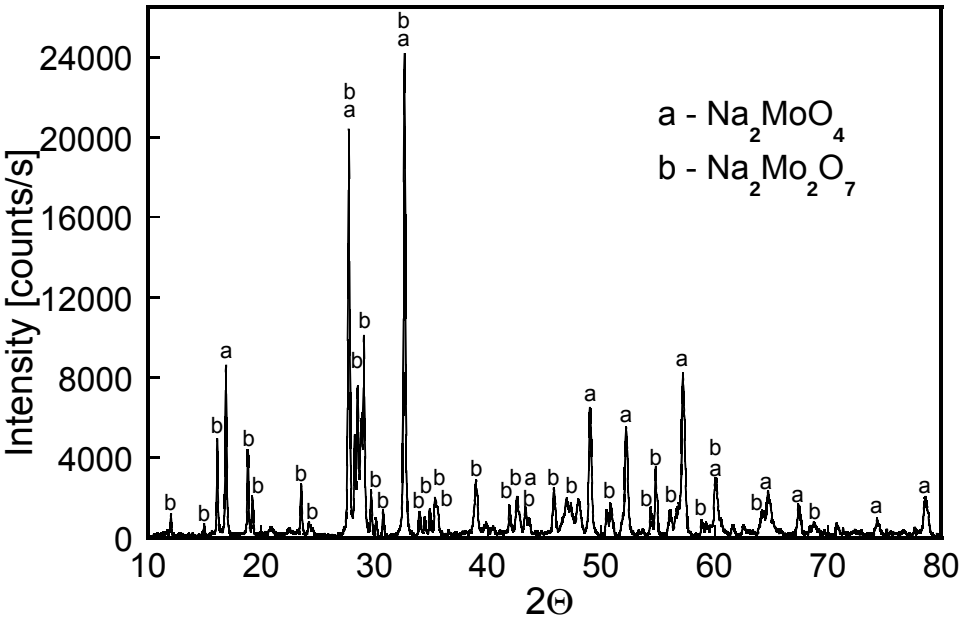

Fig. 3-9 XRD pattern of the eutectic phase mixture Na_2MoO_4+$Na_2Mo_2O_7$

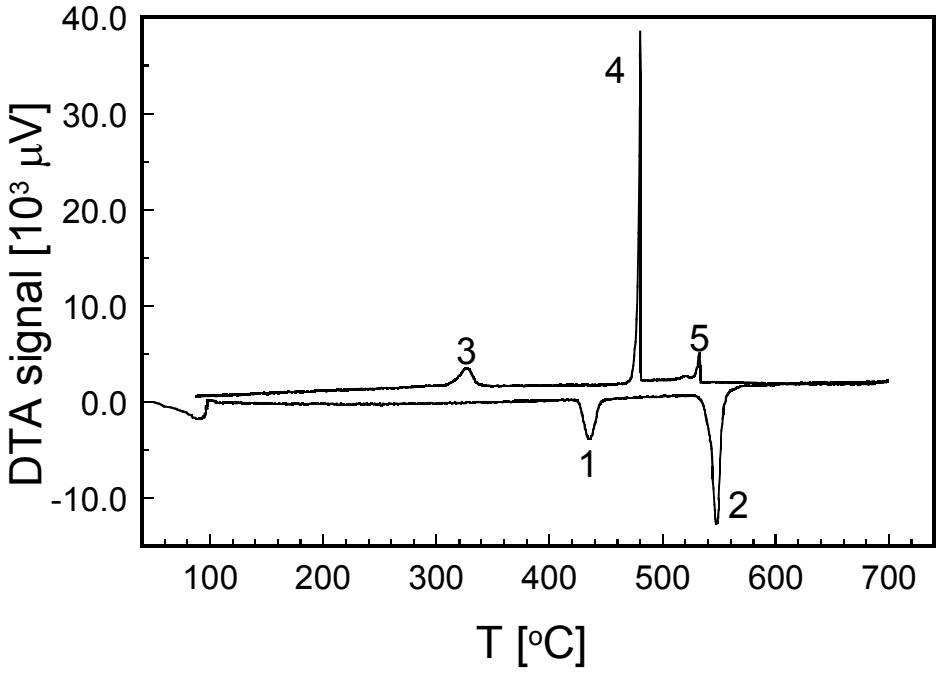

Fig. 3-10 DTA traces of the eutectic phase mixture Na_2MoO_4+$Na_2Mo_2O_7$. 1 and 2 are the endothermic while 3, 4 and 5 are the exothermic peaks

3.3.4 Sputtering method

In order to obtain an electronic short circuit through some of the solid bodies used as a part of electrode materials an Au layer of about 300 nm thickness was sputtered on to

the pelletized body. The sputtering layer is in the form of a ring as shown in Fig. 3-11. The sputtering method is described in Table 3-7.

Table 3-7 Sputtering conditions

Method	DC magnetron sputtering		
Target	Gold, 5 cm diameter		
Film thickness	300 nm		
Deposition conditions	0.02 Torr Ar	20 W	25 °C
Post annealing	1 h at 350 °C in air		

3.4 Galvanic cells

Various cells operated under isothermal and non-isothermal conditions were fabricated to study the thermodynamic stability and p-electronic conduction parameter of the ceramic materials under investigation.

3.4.1 Cells under isothermal condition

Fig. 3-11 illustrates schematically the experimental set-up of the isothermal galvanic cell used to evaluate the thermodynamic stability of NASICON.

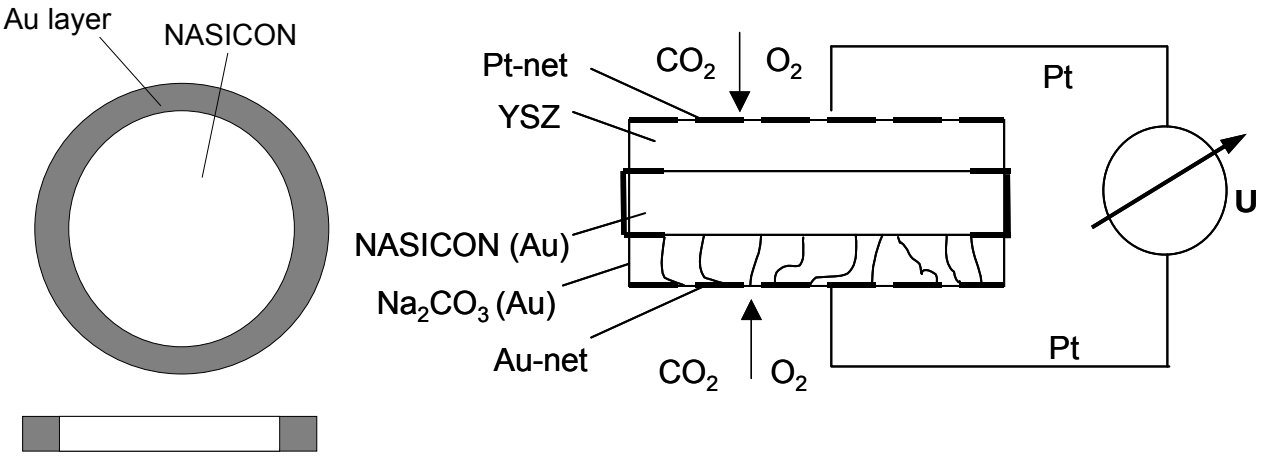

Fig. 3-11 Top and front view of the NASICON pellet sputtered with Au where the hatched area represents the Au layer together with schematic arrangement of the galvanic cell

An yttria-stabilized zirconia (YSZ) pellet having the composition $Zr_{0.91}Y_{0.09}O_{1.955}$ (Friatec AG, Germany) with 10 mm diameter, 1 mm thickness and relative density greater than 99% was used as the oxide-ion conducting solid electrolyte. One of the parallel surfaces

of the pellet was ground and polished in order to achieve a better contact with the NASICON pellet at the interface. The other surface of the YSZ pellet was painted with platinum paste (DEMETRON 308 A, Germany), which was fired in air at 1273 K to form an electrode reversible to O^{2-} ions. The short-circuit NASICON and Na_2CO_3 pellets formed a part of the measuring electrode. In order to electronically short-circuit the NASICON, the sputtering method was used (section 3.3.4). Hence the interface of YSZ that is in contact with the NASICON pellet is still reversible only to O^{2-} ions. The room temperature resistance of the electrode between the parallel surfaces was verified to be less than 1 Ω. Pt wires along with Au nets served as electrical leads at the electrodes.

The galvanic cell was spring loaded (Fig. 3-12) and positioned in the uniform temperature zone of an inductively heated furnace. The whole set-up was flushed with CO_2-O_2-(Ar) gas mixtures of known compositions as given in section 3.3.1. The partial pressures of the gases are changed in the ascending and descending direction alternately. The voltage was measured using a high impedance electrometer (KEITHLEY 617, USA) and was recorded continuously by a computer controlled programme. The final value of the voltage was registered after waiting for the steady state. This takes normally more than 24 h under the conditions in the present investigation. Details of experimental apparatus are depicted in Fig. 3-13.

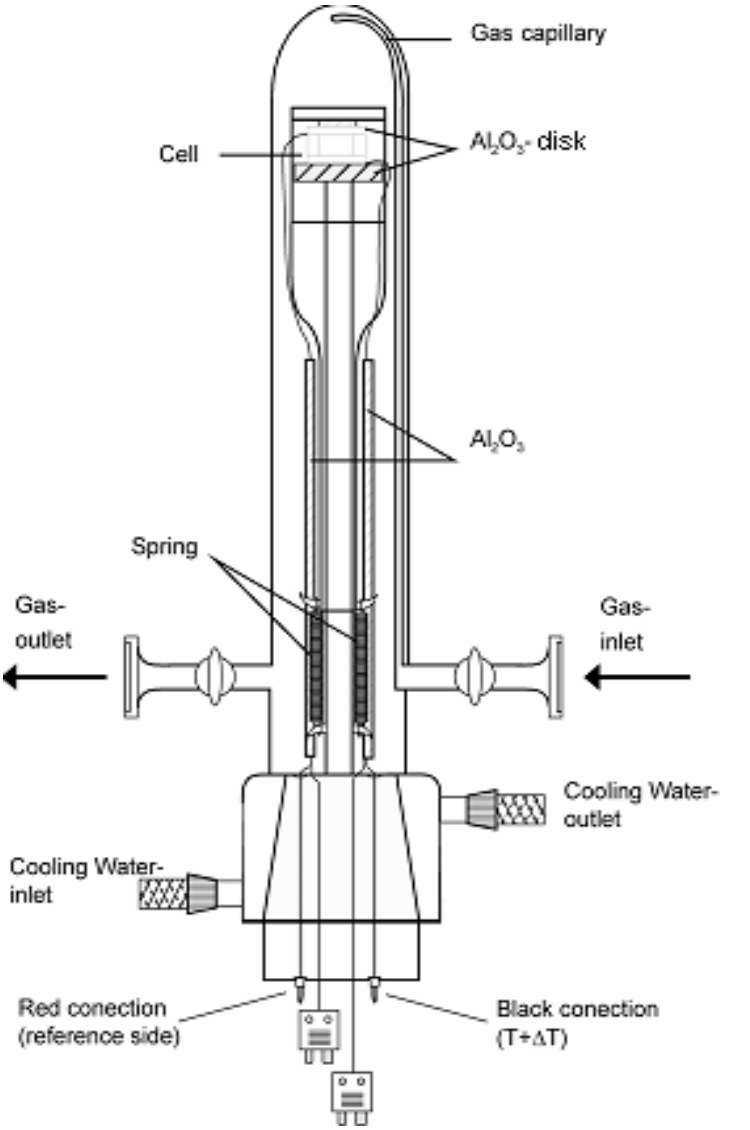

Fig. 3-12 Galvanic cell along with schematic sketch of the placement of cell in the non-uniform temperature zone of the furnace

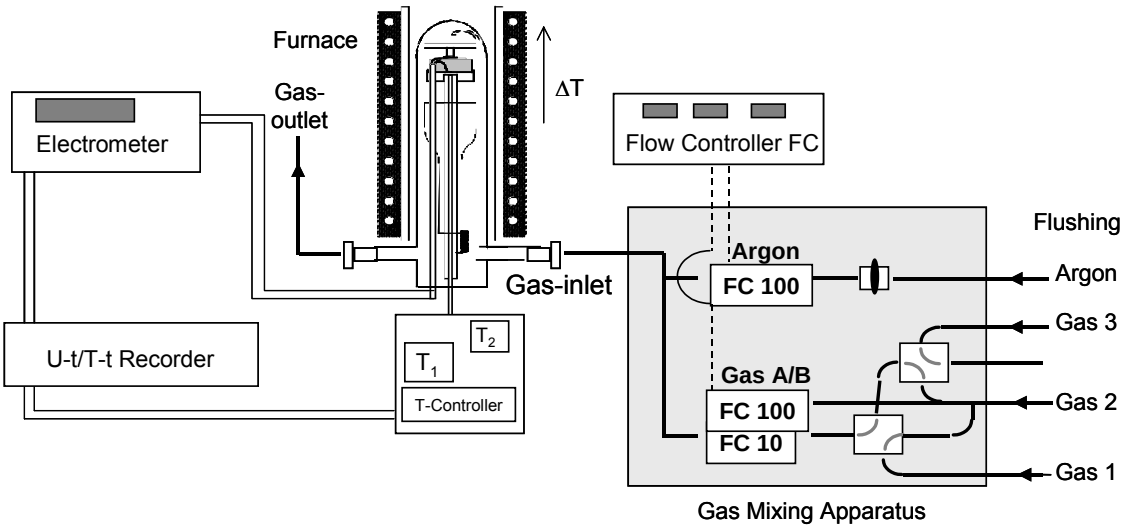

Fig. 3-13 Experimental apparatus

3.4.2 Cells under non-isothermal condition

To determine the p-electronic conduction parameter of various cation conducting solid electrolytes Na-beta-Al_2O_3, K-beta-Al_2O_3, Nasicon, Na_2CO_3 and K_2CO_3 by thermoelectric power technique, the following thermo-cells have been studied and are shown schematically in Fig. 3-14.

Pt | CO_2, O_2, Au | Na_2CO_3 | Au, O_2, CO_2 | Pt (I)

Pt | CO_2, O_2, Na_2CO_3 (Au) | NASICON | Na_2CO_3 (Au), O_2, CO_2 | Pt (II)

Pt | CO_2, O_2, K_2CO_3 (Au) | KBA | K_2CO_3 (Au), O_2, CO_2 | Pt (III)

Pt | CO_2, O_2, Au | K_2CO_3 | Au, O_2, CO_2 | Pt (IV)

Pt | O_2, $NaSi_yO_{2y+0.5}$, SiO_2 (Au) | NBA | $NaSi_yO_{2y+0.5}$, SiO_2 (Au), O_2 | Pt (V)

Pt | O_2, Na_2MoO_4, Na_2MoO_7 (Au) | NBA | Na_2MoO_4, Na_2MoO_7 (Au), O_2 | Pt (VI)

Pt | O_2, $KSi_yO_{2y+0.5}$, SiO_2 (Au) | KBA | $KSi_yO_{2y+0.5}$, SiO_2 (Au), O_2 | Pt (VII)

The cells were held in a position between two α-alumina blocks and the whole set-up was spring loaded as depicted in Fig. 3-12, thereby obtaining good contact between sample and electrode. The temperature was measured by means of two pre-calibrated Pt-10%Pt-Rh (type S) thermocouples placed at the two ends of the sample. The entire assembly was placed in a vertical furnace thus maintaining a temperature gradient across the two ends of the sample as shown in Fig. 3-15.

The temperature of one end of the cell was maintained constant by an electronic temperature controller with an accuracy of $\pm$0.5 K. The presence of an inherent temperature gradient ΔT inside a tube furnace was used to create a temperature difference between the two ends of the cell. Measurements were done at different temperature gradients with ΔT approximately equal to 1–20 K. The measurements were carried out at various temperatures and activities of the mobile species as shown in sections 3.3.1 and 3.3.2. The voltage was recorded after ascertaining the constancy of values ($\pm$0.1mV, t $\geq$ 12 h) by means of a high input impedance electrometer (Keithley 6517A). The reversible nature of the thermo voltage was tested by short-circuiting it and verifying that the voltage returns to its original value. The data were recorded as a function of time by means of a computer controlled programme. A detailed experimental arrangement is shown in Fig. 3-12.

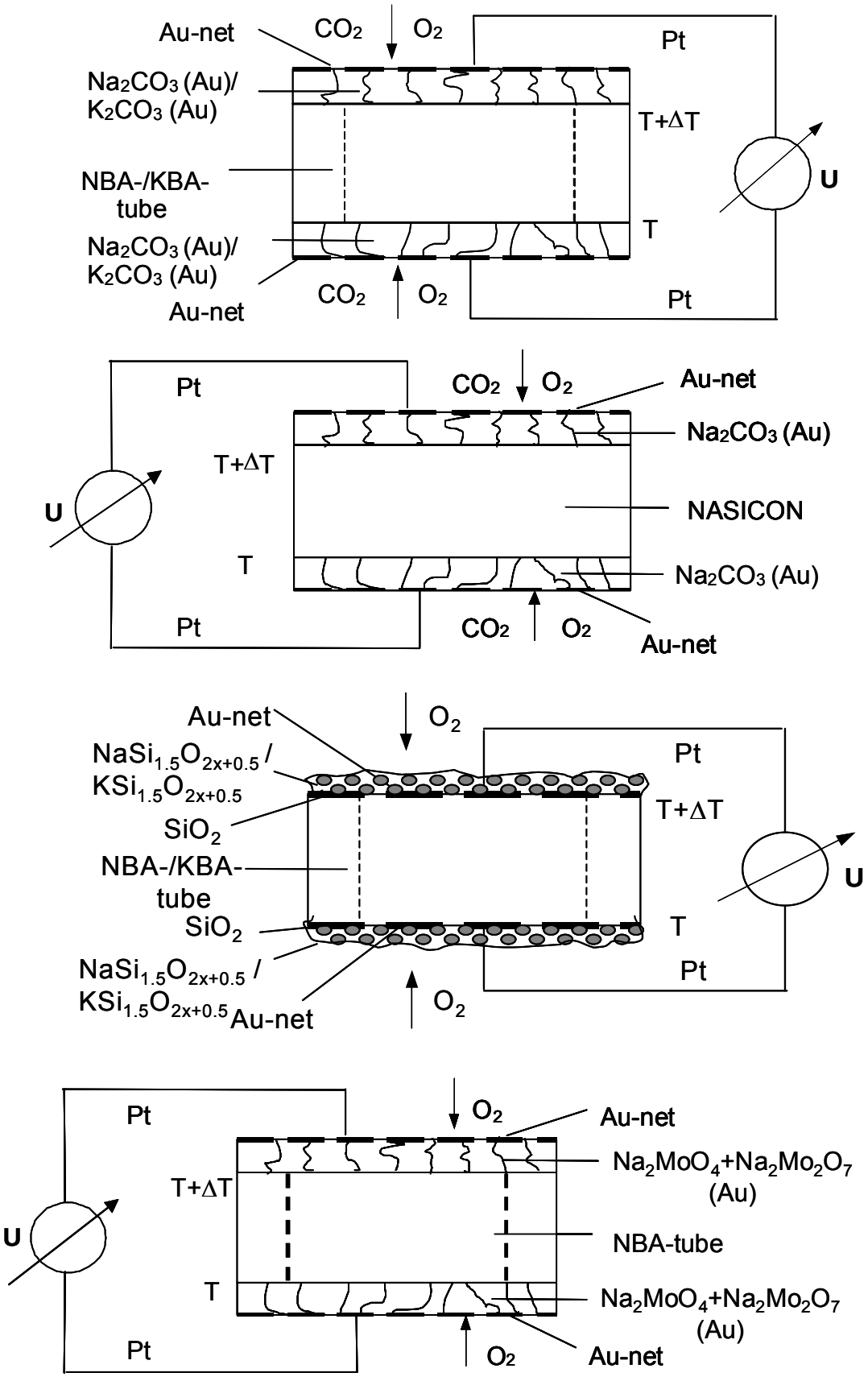

Fig. 3-14 Schematic set-up of thermo-cells

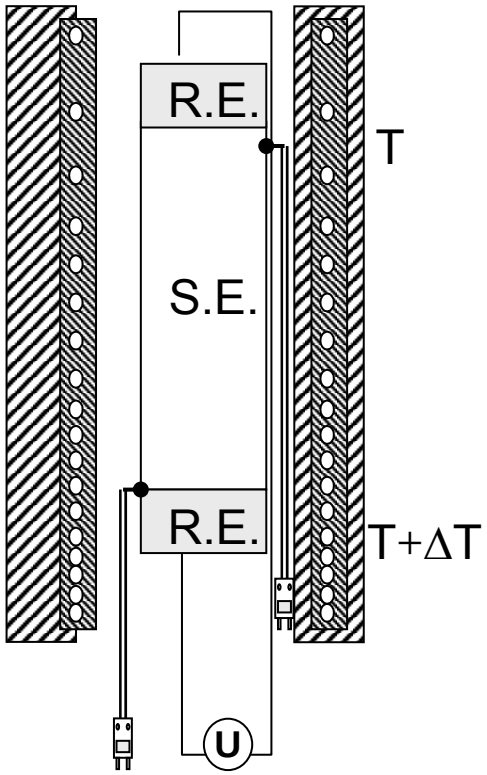

Fig. 3-15 Schematic sketch of the thermo-cell in the non-uniform temperature zone of the furnace. S.E. denotes solid electrolyte, R.E. is reversible electrode

3.4.3 Cells for impedance spectroscopy measurements

The total impedance of the solid electrolyte (Na_2CO_3) in the present investigation was measured by means of ac impedance spectroscopy using a Solartron 1255B system (BELLTEC Ing. Buero Glocke, Germany) in the frequency interval from $1 \cdot 10^{-2}$ to $1 \cdot 10^{6}$ Hz under various temperatures. The signal amplitude was 8 mV. All the experimental data obtained by the Potentiostat/ Galvanostat 273 A (EG & G Princeton Applied Research, USA) were imported to a personal computer. The experiment was controlled using a computer programme (Impedance Spectroscopy, EG & G Princeton Applied Research, USA). The measurements were performed under the same conditions as in case of thermo cells at various sodium activities.

4. Results and discussion

4.1 Thermodynamic stability of NASICON

According to Eq. 2-80, the voltage of the cell (VIII) is related to the chemical potential of sodium oxide dissolved (a_{Na_2O}) in NASICON as well as to the CO_2 partial pressure in the ambience. By making use of Eq. 2-80 to determine a_{Na_2O} which is a measure of the thermodynamic stability of NASICON and simultaneously provides information about the establishment and maintenance of the thermodynamic equilibrium. In Fig. 4-1, the potential difference between the poles of cell (VIII) is plotted against the temperature at a particular gas composition (p_{CO_2}= 19.4 · 10^{-6} bar and p_{O_2} = 19.7 · 10^{-6} bar).

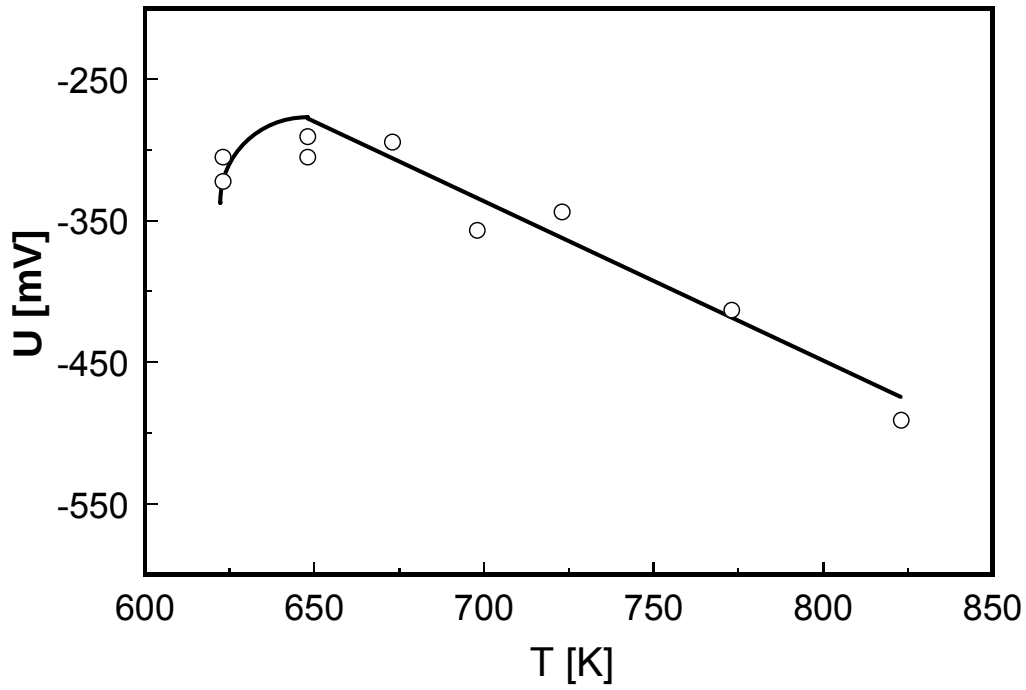

Fig. 4-1 Temperature dependence of voltage of the galvanic cell (VIII) at p_{CO_2} = 19.4 · 10^{-6} bar and p_{O_2} = 19.7 · 10^{-6} bar

The voltage varies linearly with temperature in the high temperature region while at lower temperatures i.e. below T = 375 °C, there is a deviation from the linear behaviour towards more negative values. For demonstrating the performance of the cell with respect to reversibility and reproducibility the isothermal voltage is plotted against time as depicted in Fig. 4-2 for T = 550 °C. It becomes evident that a steady state voltage is established within few minutes after changing the measuring conditions and remains constant as long as no further changes occur in these conditions.

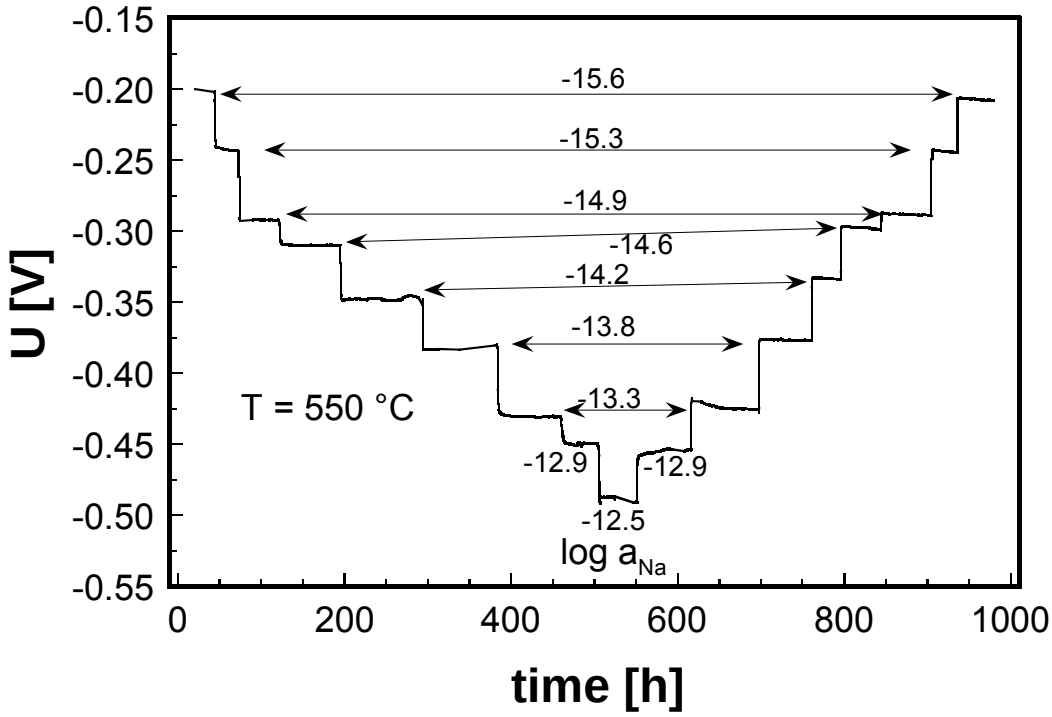

Fig. 4-2 Time dependence of the voltage of cell (VIII) at 550 °C for different sodium activities from one extreme to the other. The different values of logarithm of sodium activity established by experimental conditions are displayed

The voltage of the cell comes back to the same value under identical measuring conditions indicating explicitly reversibility and reproducibility. At low temperatures the time required to establish the steady state voltage is longer in comparison to high temperatures.

By inserting the experimental value of the voltage obtained along with those of p_{CO_2} and the thermodynamic data for Na_2CO_3, CO_2 which were taken from [70] in Eq. 2-80, the a_{Na_2O} for the NASICON phase mixture is computed under various sodium activities and temperatures. Fig. 4-3 demonstrates how under isothermal conditions the sodium oxide activity behaves as a function of the sodium activity during the first exposure of the material under the measuring conditions. The characterization of phase equilibrium in NASICON was done by changing stepwise the composition of NASICON with changing the sodium activity of the measuring electrode and detecting the response in terms of sodium oxide activity. As long as the sodium oxide activity is constant with changing the NASICON composition, the existence of the phase equilibrium given by Eq. 2-75 can be taken for sure. Depending on the sodium activity that is adjusted by CO_2 and O_2 content of the surrounding gas according to Eq. 2-24, the equilibrium represented by Eq. 2-75 may be shifted either to the left or right.

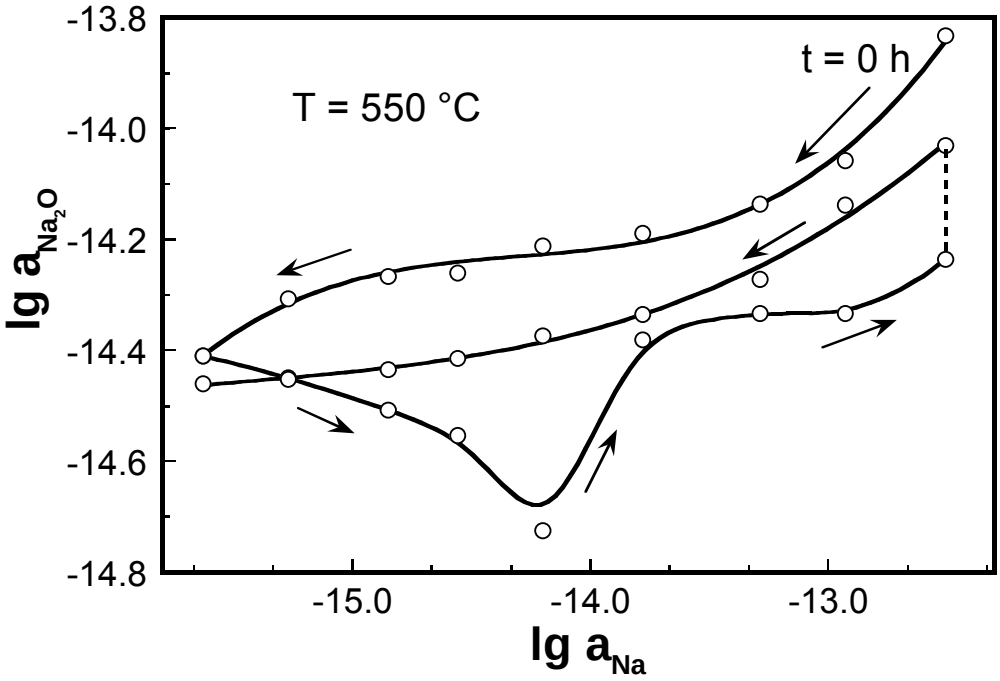

Fig. 4-3 Time dependent change of logarithm of sodium oxide activity as a function of logarithm of the sodium activity after heating up the cell and exposing it to the experimental conditions for the first time. (T = 550 °C, a_{Na} established according to Eq. 2-24 and adjusted by the gas composition. a_{Na_2O} evaluated according to Eq. 2-79)

Thus in this way the proportions in the NASICON phase composition can be changed with the sodium activity being the independent variable. As discernible from Fig. 4-3 the sodium oxide activity exhibits a plateau in the range of medium sodium activity after taking long time for equilibration. The sodium oxide activity increases at the right margin of the sodium activity interval and decreases at the left end indicating the equilibrium (Eq. 2-75) is stable only in a limited interval of sodium activity. It is evident from Fig. 4-3 that at the starting of the measurement the level of sodium oxide activity is high, then subsequently falls down with changes in sodium activity and time. It rises again and finally exhibits a plateau. It took more than 720 h until the material adapted to the conditions prevailing in cell (VIII). The enormous time required for the material to exhibit a plateau (Fig. 4-3) is a clear indication that the initial sodium oxide activity originating from the pre-treatment of the NASICON sample differs from the equilibrium state at the measuring conditions. It is worth mentioning that the X-ray diffraction analysis (cf. Fig. 3-4) reveals the presence of one single phase (section 3.2.3). However, the occurrence of the activity plateau demonstrates explicitly that two pure phases coexist or at least two phases with constant activity [94]. In this regard it should be mentioned that there might be presence of non-stoichiometric phases in the material that could not be

distinguished by the available diffraction pattern, which is why NASICON appears as X-ray single phase.

In a similar fashion as depicted in Fig. 4-3, log a_{Na_2O} versus log a_{Na} plots can be determined for the whole range of temperature and are depicted in Fig. 4-4.

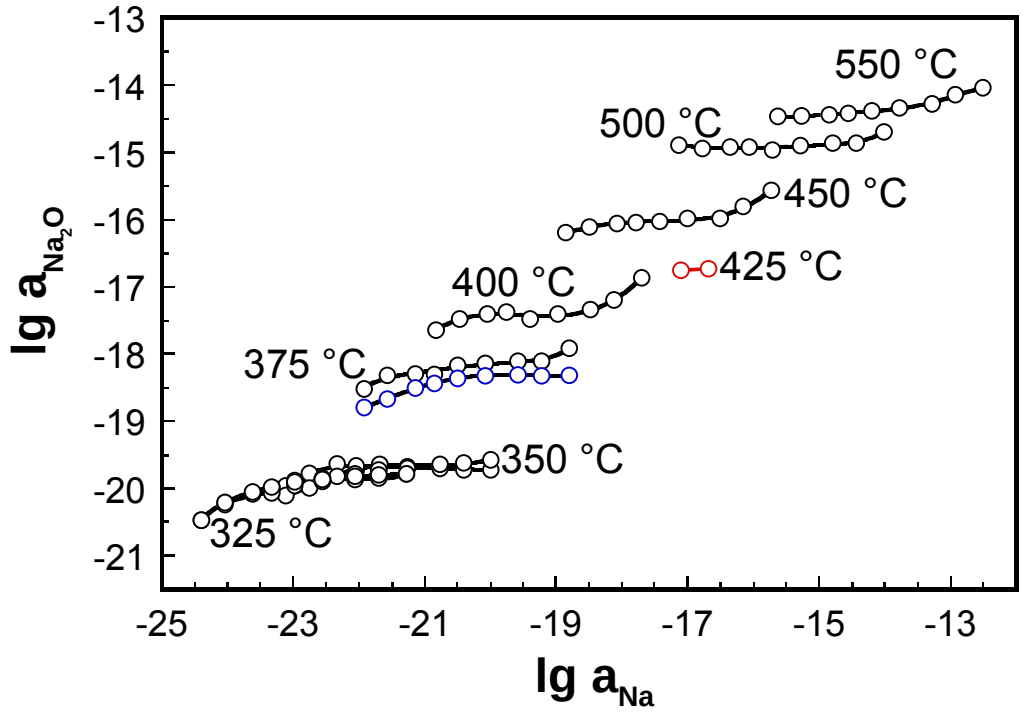

Fig. 4-4 Sodium oxide activities as a function of sodium chemical potential at various temperatures

Each of the plots is measured under isothermal conditions with stepwise decreasing and increasing the sodium activity alternately. As illustrated from Fig. 4-4 within the sodium activity window covered by the experimental conditions all the plots exhibit an activity plateau that demonstrates the existence of the phase equilibrium (Eq. 2-75) in NASICON as observed in previous investigations for Na-beta-Al_2O_3 and K-beta-Al_2O_3 [83, 84, 94]. As seen from Fig. 4-4 the width of the plateau changes with temperature. The plot mainly bent upwards towards the upper end of the temperature interval while at lower end of temperature they bent downward. At medium temperature i.e. T = 500 °C there is hardly any bending in the activity plateau resulting in maximum extension of the stability region of the phase equilibrium (Eq. 2-75). The occurrence of a plateau is a proof of the coexistence of a two-phase equilibrium with univariant behaviour indicating that the chemical potential of sodium oxide in NASICON is a function of temperature alone. Beyond the plateau region there is a gradual change in the sodium oxide activity implying that the material i.e. NASICON represents divariant behaviour and the

chemical potential of the sodium oxide becomes additionally a function of material composition in addition to temperature. Such behaviour is typical of nonstoichiometric phases. It is noteworthy that the voltage follows the linear behaviour with temperature at the highest sodium activity as shown in Fig. 4-1 even though the material does not exhibit the thermodynamic equilibrium in this activity.

By taking the ordinates of Fig. 4-4 that correspond to the plateau levels and plotting as a function of the inverse of temperature, plot 2 of Fig. 4-5 is obtained.

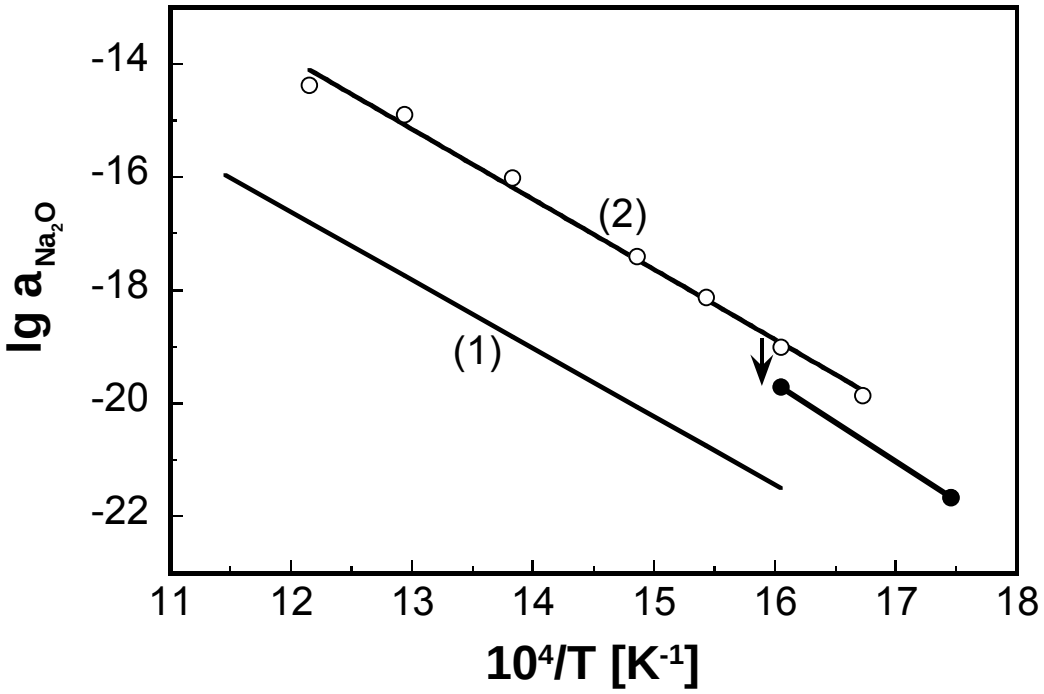

Fig. 4-5 Temperature dependence of the sodium oxide activity dissolved in NASICON ($Na_3Zr_2Si_2PO_{12}$) in comparison with literature data: (1) [82], (2) present study

A linear dependence of the logarithm of sodium oxide activity on the inverse temperature is obtained over a broad region of temperature which can be expressed by the following equation:

$$\log a_{Na_2O} = -\frac{11806.63 \pm 717.0}{T/K} + 0.18 \pm 0.99 \qquad (375 \le T \le 550\ °C). \qquad \text{Eq. 4-1}$$

At low temperatures due to the scarcity of the data it is not possible to quantify the behaviour. Deviating from the ideal situation depicted in Fig. 4-4 it happened after a certain period of time that the sodium oxide activity at 350 °C drifts away from the plateau level as depicted in Fig. 4-6.

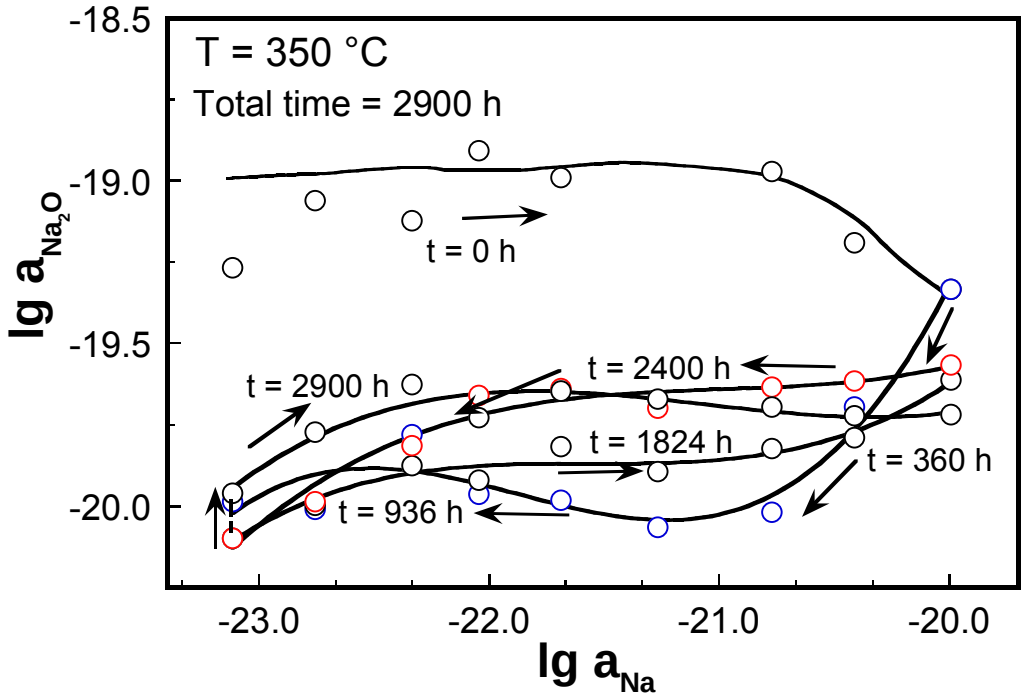

Fig. 4-6 Time dependent change of logarithm of sodium oxide activity as a function logarithm of sodium activity after stepwise cooling the cell from T = 550 °C to T = 350 °C

It initially shows a plateau, then subsequently shifts to the more negative direction with time and changes in sodium activity by nearly an order of magnitude and then scatters as shown in Fig. 4-6. It takes sufficiently long time i.e. more as 936 h for the sodium oxide activity to exhibit another plateau. The change in the sodium oxide activity plateau is reflected in the shift of the ordinates in Fig. 4-5. This indicates that during the course of measurement something has changed in the material.

It should be noted the different values of the sodium oxide activity at 350 °C in Fig. 4-5 correspond to the two different plateau levels of Fig. 4-6. As seen from Fig. 4-5 the sodium oxide activity due to the initial plateau level at 350 °C follows the behaviour of high temperature data whereas that corresponding to another level deviates. However, in view of the time-dependent trend of the data as illustrated in Fig. 4-6 the second plateau level is considered to be the more accurate and representative of the material rather than the initial one. To ascertain that no irreversible change occurred due to the step in the data at 350 °C as shown in Fig. 4-5 cell (VIII) was again heated up to 375 °C. No significant deviation from the prior value was observed indicating that the phase equilibrium established in NASICON is reversible and reproducible with respect to temperature. After this the cell was again stepwise cooled down first to 325 °C then 300 °C and the measurements were performed as illustrated in Fig. 4-5.

The only interpretation for the shifting of the data in the low temperature i.e. below 350 °C is that the phase equilibrium established at higher temperature is different from the low temperature interval.

The sodium oxide activity (plot 1 in Fig. 4-5) in NASICON ($Na_3Zr_2Si_2PO_{12}$) reported by Kale et al. [82] on the basis of the following solid state electrochemical cell

$$Pt|CO_2,\ O_2\,|Na_2CO_3\,|NASICON|(Y_2O_3)\ ZrO_2\,|\ In + In_2O_3|\ Ta,\ Pt \qquad (A)$$

is two orders of magnitude lower than the present data. The explanation of the discrepancy could be understood as follows:

In Kale's measurement there is no proof for the existence of the establishment of the phase equilibrium. Hence the results obtained need not necessarily be true equilibrium data. The electrochemical cell employed by Kale uses a different reference electrode. Besides there is no short-circuiting through the sintered pellets of the measuring electrode. Even though the short circuiting will not have an impact on the total cell voltage [86], it only ensures fast equilibration time. Hence, the time necessary to achieve steady state is comparatively faster with short circuit than without it. In view of this, the equilibration time period in Kale's measurement appears to be too small (10-20 minutes) compared with that in the present investigation (30-100 h) in order to reach steady state conditions.

In addition, the sodium activity established by the measuring electrode (Na_2CO_3, CO_2, O_2) in case of Kale's measurements is somewhat lower than that established under the present measuring conditions which necessarily must result in larger deviation from the equilibrium position and thus in the lower values of the sodium oxide activity. Both of the above reasons coupled together could explain the disagreement. Thus the findings indicate the importance of the check of the establishment of the phase equilibrium as this equilibrium only exists in a limited region of chemical potentials.

The observation of the plateaus of Fig. 4-4 is the prerequisite for the existence of the phase equilibrium (Eq. 2-75) and thus for the application of Eq. 2-76 with the view to determine the difference in the standard Gibbs energy of formation of the phases involved in equilibrium. By taking into account $\Delta_f G^o_{Na_2O}$ [70] and the sodium oxide activity according to Eq. 4-1, the difference $\Delta(\Delta_f G^\circ)$ of the standard Gibbs free energy of formation of the phases coexisting in NASICON can be evaluated and is displayed in Fig. 4-7 as a function of temperature.

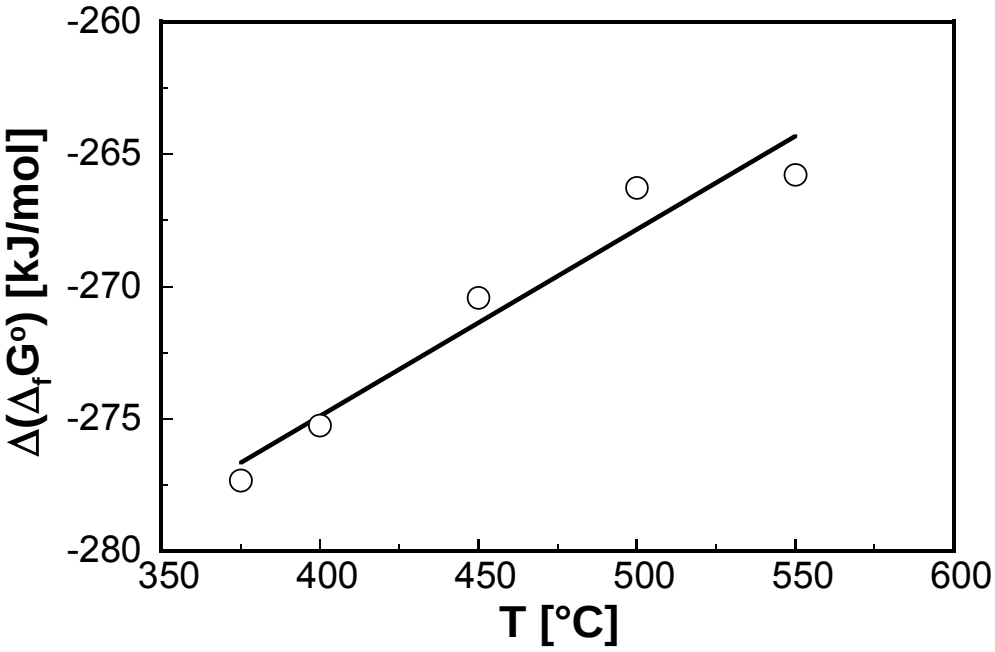

Fig. 4-7 Difference of the standard Gibbs free energy of formation of the phases coexisting in NASICON ($Na_3Zr_2Si_2PO_{12}$) as a function temperature

Owing to the complexity of the NASICON system there is no solid information regarding the phases that coexist in the phase equilibrium. The possible phases that could be involved in the equilibrium are put forth by means of the probable chemical reactions as follows:

$$Na_{1+x}Zr_2Si_xP_{3-x}O_{12} \rightleftarrows 2\,ZrO_2 + xSiO_2 + (x-1)\,Na_2O\ (NASICON) + \frac{3-x}{2}\,Na_2P_2O_6, \qquad (i)$$

$$Na_{1+x}Zr_2Si_xP_{3-x}O_{12} \rightleftarrows 2\,ZrSiO_4 + \frac{x-2}{2}\,Na_2Si_2O_5 + \frac{x}{2}\,Na_2O\ (NASICON) + \frac{3-x}{2}\,Na_2P_2O_6, \qquad (ii)$$

$$Na_{1+x}Zr_2Si_xP_{3-x}O_{12} \rightleftarrows \frac{3-x}{2}\,ZrP_2O_7 + \frac{x+3}{4}\,Na_2O\ (NASICON) + \frac{x-1}{4}\,Na_2Si_2O_5 + \frac{x+1}{2}\,ZrSiO_4 \qquad (iii)$$

$$Na_{1+x}Zr_2Si_xP_{3-x}O_{12} \rightleftarrows Na_{1+x-y}Zr_2Si_xP_{3-x}O_{12-y/2} + \frac{1}{2}\,y\,Na_2O\ (NASICON), \qquad (iv)$$

and

$$Na_{1+x}Zr_2Si_xP_{3-x}O_{12} \rightleftarrows Na_{1+x-y}Zr_2Si_xP_{3-x}O_{12-y/2} + Na_{1+x-z}Zr_2Si_xP_{3-x}O_{12-z/2} + \frac{z+y}{4}\,Na_2O\ (NASICON) \qquad (v)$$

It must be mentioned that the above reactions are used as examples to show which kinds of phases might coexist in the material and other equilibria could be proposed. However in the above equilibria as the number of phase increases the probability for the phases to coexist and exhibit equilibrium becomes unlikely. Moreover the log a_{Na_2O} is

very low for the material as depicted in Fig. 4-5; therefore the participating phases must have low sodium oxide chemical potential. Further study is needed for characterizing the phases present in NASICON.

4.2 Thermoelectric power of NASICON

4.2.1 Thermo voltage

The steady state non-isothermal voltage generated across cell (II) (section 3.4.2) is plotted against the temperature gradient ΔT for different sodium activities in Fig. 4-8 for T = 700 and 400 °C.

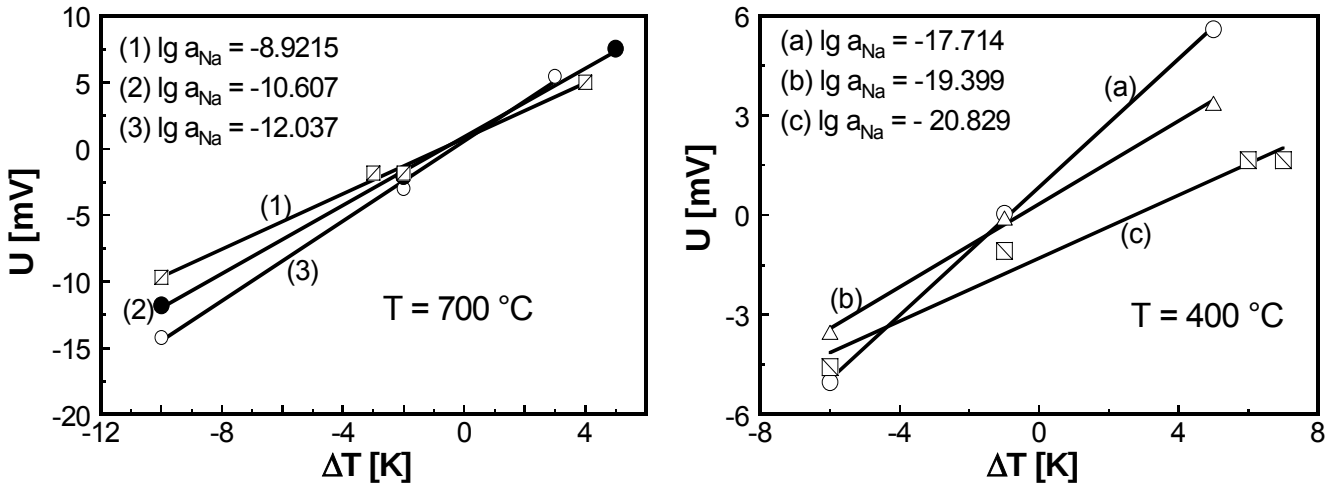

Fig. 4-8 Non isothermal voltage of cell (II) against ΔT at T = 700 and 400 ° C

The temperatures were chosen to demonstrate the behaviour of the thermo voltage at two extreme ends of the temperature interval covered. Irrespective of the temperature and sodium activity the thermo voltage was recorded for at least three different temperature gradients as shown in Fig. 4-8. As evident from Fig. 4-8, a linear thermo voltage versus temperature gradient dependence has been observed in the whole interval of sodium activity and temperature (400 °C $\leq$ T $\leq$ 700 °C) covered in the present investigation. It should be mentioned that the thermo voltage takes much longer time to reach a steady state value at low temperature as compared to high or moderate temperatures.

It is discernible from Fig. 4-8 that sometimes the thermo voltage at $\Delta T = 0$ does not or not completely vanish and approach zero as expected according to Eq. (2-65). This residual voltage is called an offset voltage U_0 which has a typical value of about 1.5 mV

at T = 550 °C as shown in Fig. 4-9. The variation of the offset voltage as a function of the sodium activity is depicted in Fig. 4-9 for T = 550 and 700 °C. The dependence of U_0 on sodium activity has no obvious trend as illustrated in Fig. 4-9.

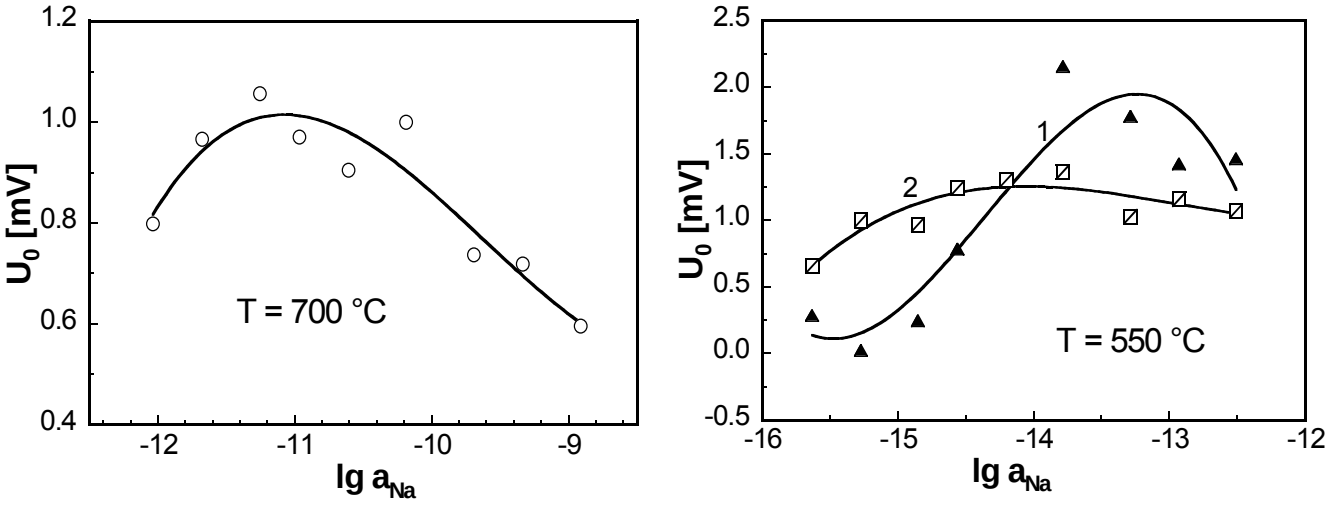

Fig. 4-9 Offset voltages (U_0) of cell (II) as a function of the sodium activity for T = 700 and 500 ° C (Curve 1: after heating up cell (II) and exposing the cell for the first time, curve 2: about 3600 h after curve 1)

In addition, the offset voltage depends on the pre-treatment of the material as it is shown in Fig. 4-9 for T = 550 °C. Curve 1 is obtained after heating up cell (II) and exposing the cell components for the first time to the measuring conditions while curve 2 is obtained 3600 h later and after the cell were operated under different temperatures.

4.2.2 Thermoelectric power

The thermoelectric power of NASICON as a function of the sodium chemical of the Na_2CO_3, CO_2, O_2 electrode is depicted in Fig. 4-10, 4-11 and 4-12. Throughout the measurements the sodium activity was adjusted by rising and decreasing the partial pressures of the CO_2, O_2 gas mixture. The ordinates in Fig. 4-10 represent the slope of the straight lines depicted in Fig. 4-8, i.e. the slope of the measured values of the thermo voltage versus temperature gradient. It can be clearly seen from Figs. 4-10, 4-11 and 4-12 that similar to previous findings on Na-beta-alumina under the same conditions [16], a non-linear dependence of the thermoelectric power on the sodium chemical potential is obtained.

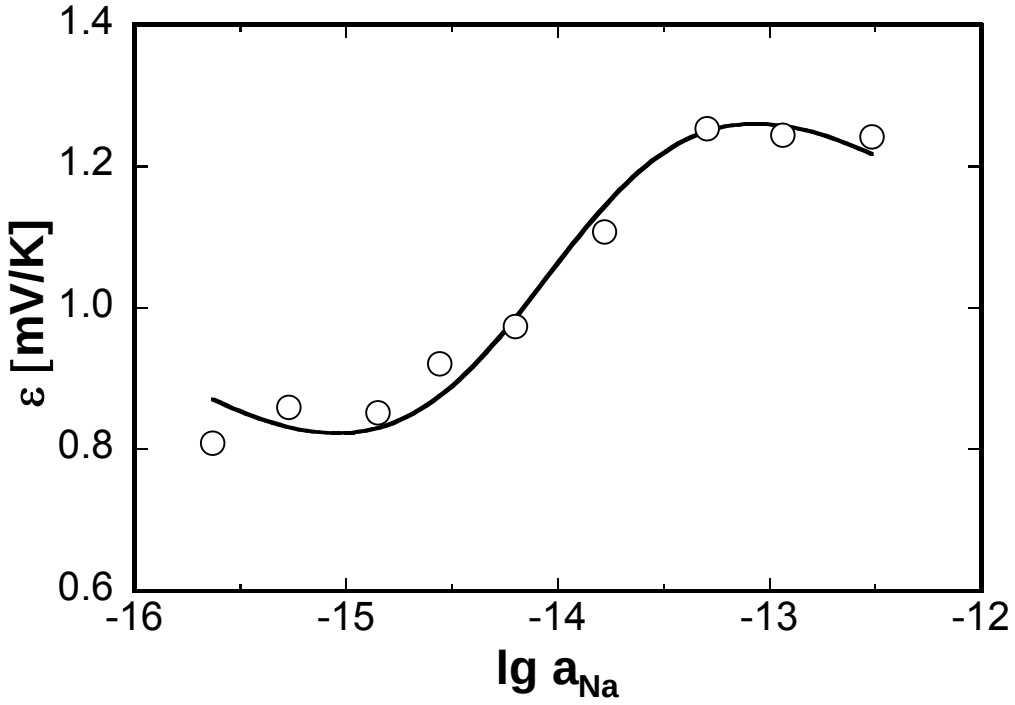

Fig. 4-10 Variation of the total thermoelectric power of NASICON with the sodium chemical potential at T = 550 °C

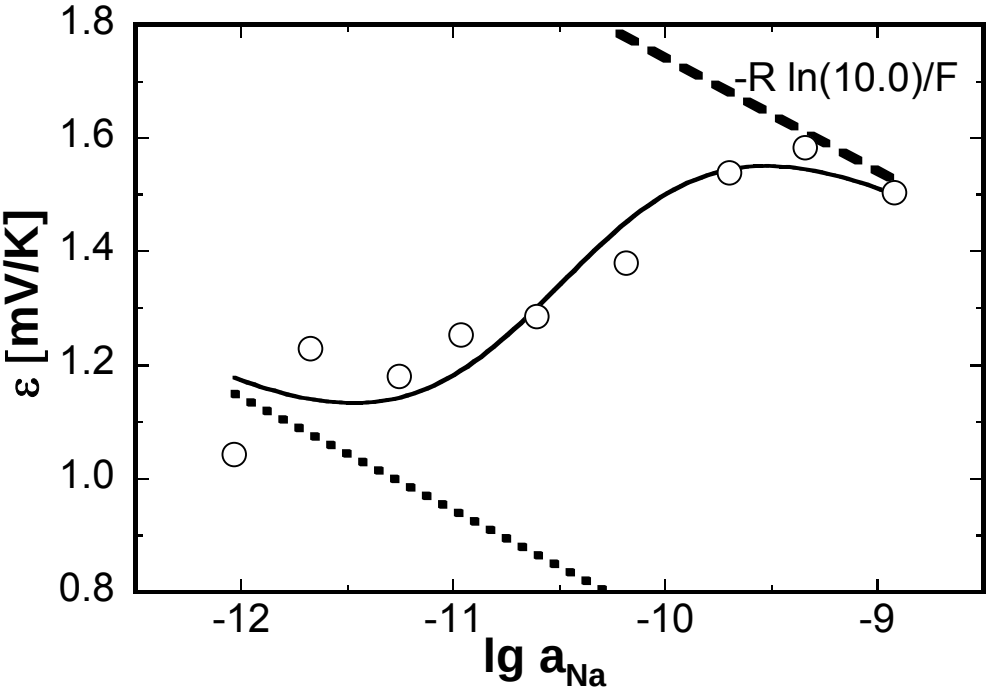

Fig. 4-11 Sodium chemical potential dependence of the thermoelectric power of NASICON at T= 700 °C (solid line curve fitting according to Eq. 2-70)

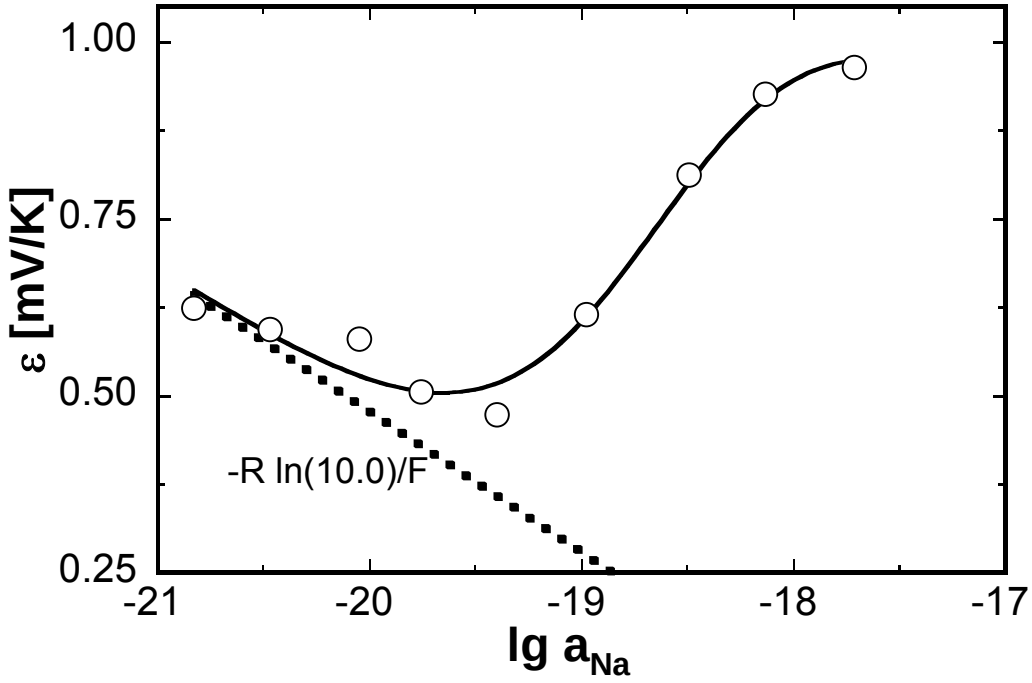

Fig. 4-12 Sodium chemical potential dependence of the thermoelectric power of NASICON at T= 400 °C (solid line curve fitting according to Eq. 2-70)

The same curve shape is observed in the whole temperature range (400-700 °C) for which Figs. 4-11 and 4-12 give evidence for the highest and lowest temperature respectively. In case of negligible electronic conductivity, the thermoelectric power versus sodium chemical potential relationship would represent a straight line with the slope –R ln(10.0)/F (cf. Eq. 2-70). Figs. 4-10, 4-11, 4-12 reveal that at high and low sodium chemical potential the total thermoelectric power of NASICON tends to approach the behaviour of a pure ionic conductor as depicted by the dashed line in Fig. 4-11. On decreasing the sodium activity further i.e. moving towards the right end of the x-axis (Figs. 4-11, 4-12) the influence of the electronic transference number on thermoelectric power increases. Hence a drop on thermoelectric power takes place and a new behaviour due to electron holes is established. Finally the plot of ε versus log a_{Na} becomes linear with slope –R ln(10.0)/F that represents the region dominated by electron holes at the low sodium chemical potential as depicted by dotted lines in Figs. 4-11, 4-12. On the other hand, if the sodium chemical potential increases, the ionic contribution on the thermoelectric power increases while that of electron holes decreases. Finally the electronic part becomes zero as illustrated by dotted lines in Fig. 4-13.

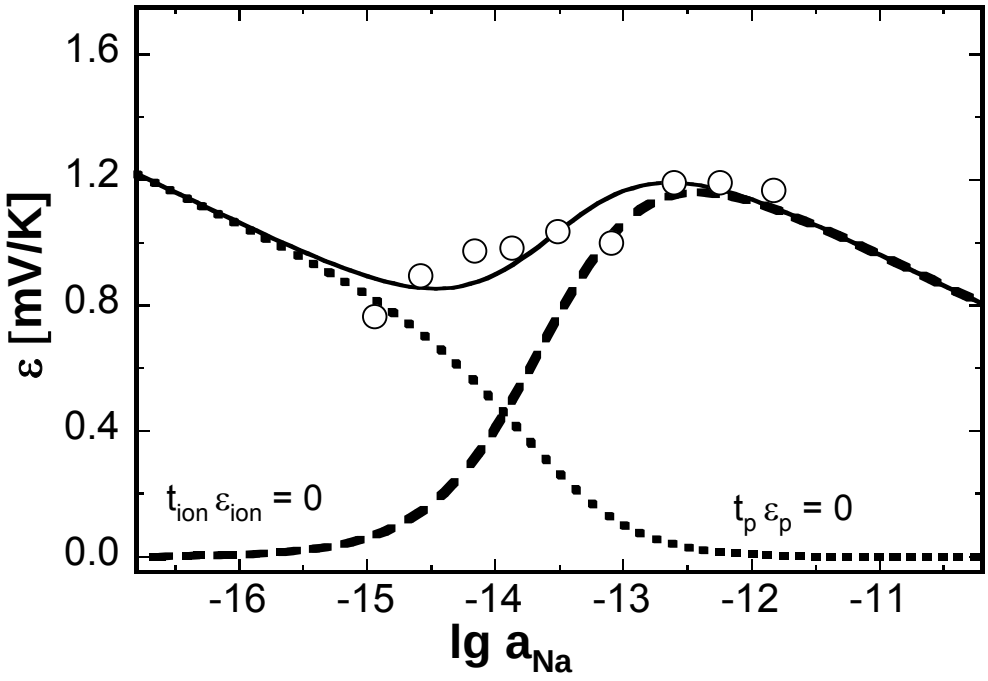

Fig. 4-13 Typical fitted results for the thermoelectric power illustrating contribution of partial thermoelectric power on total ($\varepsilon = t_{ion}\,\varepsilon_{ion} + t_p\,\varepsilon_p$) at T = 575 °C

The experimental data points of ε versus log a_{Na} plots are fitted fairly well according to Eq. 2-70 as depicted by the solid lines through these points illustrated in Figs. 4-10, 4-11, 4-12. The fitting of the results at T = 575 °C shown in Fig. 4-13 depicts the contribution of partial thermoelectric power of respective species i.e. ionic (ε_{ion}) and electron holes (ε_p). The measured values of the thermoelectric power under different sodium activity showed disagreement with the behaviour when the material is considered as predominant ionic conductor (dashed line in Fig. 4-11) thereby indicating that the obtained values are in a mixed ionic-electronic conduction domain.

By evaluating a field of experimental data $\varepsilon = f(a_{Na}, T)$, the p-electronic conduction parameter ($a_{\oplus}$) can be obtained by means of a non-linear curve fit regression procedure based on Eq. 2-70 as described in section 2.4.3.

4.2.3 Temperature dependence of $a_{\oplus}$

The p-electronic conduction parameter $a_{\oplus}$ determined according to the above procedure is plotted as a function of inverse of temperature shown in Fig. 4-14. As illustrated in Fig. 4-14 the log $a_{\oplus}$ versus 1/T dependence is a linear curve within the covered interval of temperature ($450 \leq T \leq 700$ °C) in accordance with previous experiences on Na-beta-

alumina [14, 16]. As shown in Fig. 4-14 the data points are compared with $a_{\oplus}$ values obtained for NASICON by the potentiometric technique [15].

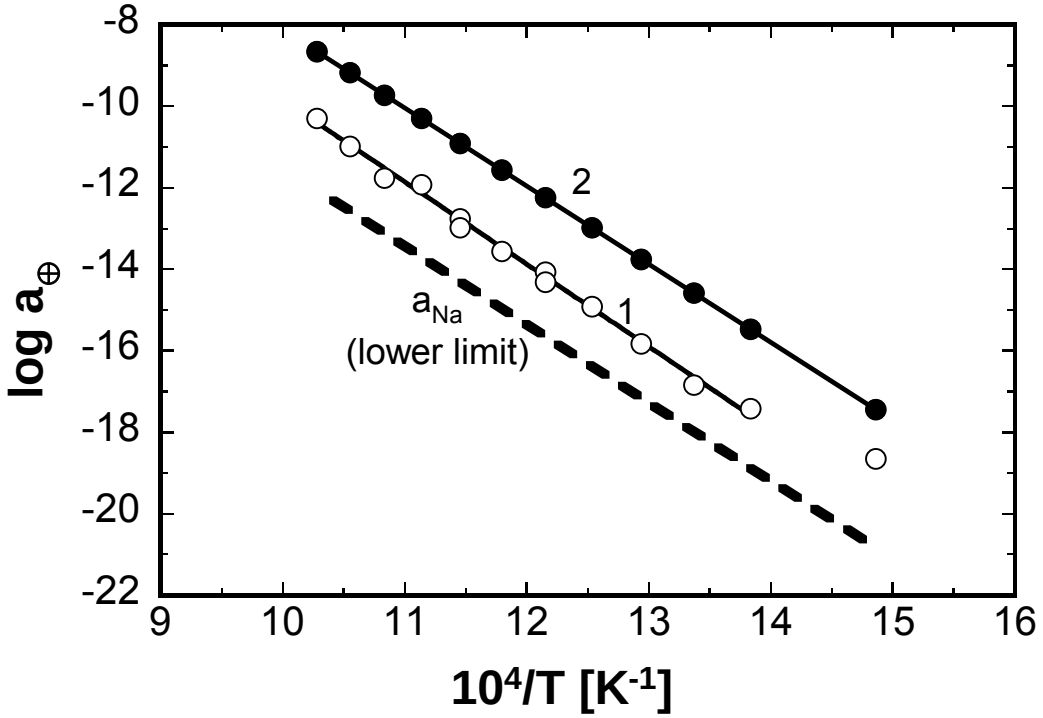

Fig. 4-14 Temperature dependence of p-electronic conduction parameter of NASICON evaluated by thermoelectric power measurements (curve 1) compared with that obtained by potentiometric measurements (curve 2 [15]) (dashed line: lower limit of the sodium activity of the sodium carbonate electrode)

Likewise, the lower limit of sodium activity of the carbonate electrode is given for the sake of comparison.

The data plot represents a straight line that can be quantified as,

$$\lg a_{\oplus} = 10.39 - \frac{20218.79}{T/K} \qquad (450 \le T \le 700\ ^{\circ}C) \qquad \text{Eq. 4-2}$$

In the low temperature interval i.e. T < 450 °C the data deviate from the linear behaviour. The deviation in this regime of temperature could be due to the sluggishness of the establishment of the steady state level. The slow electrode kinetics could be one of the factors responsible for that. It must be considered that during the measurement a permanent flux of charge carriers has to be maintained by the electrodes, which results in polarization effects. Hence in the low temperature regime the shape of the curve is determined by additional phenomena that are superimposed on the effect of partial electronic conduction. Thus the data in this region are not taken into consideration while quantifying $a_{\oplus}$.

As illustrated by Fig. 4-14, the data points run parallel to the temperature dependence of the sodium activity interval of the Na_2CO_3, CO_2, O_2 electrode. This is in agreement with the previous observations on Na-beta-alumina [9-14, 16] and NASICON [15]. As known from these investigations, the chemical surroundings, in this case the sodium activity established by the carbonate electrode dictates the magnitude of the p-electronic conduction parameter.

The present data of the p-electronic conduction parameter are an order of magnitude less than those obtained from the potentiometric measurements [15] implying that this parameter may adapt to the surrounding conditions [10, 11, 14]. The present investigation gives another indication for mixed ionic-electronic conduction in NASICON under the condition of measurements, in apparent contradiction to many reports stated in literature on using it as a pure ionic conductor for sensors [95-105] and thermodynamic investigations [106, 107].

4.3 Thermoelectric power of Na_2CO_3 and K_2CO_3

4.3.1 Thermo voltage

In Fig. 4-15 the thermo voltage of cells (II) and (IV) with Na_2CO_3 and K_2CO_3 as a solid electrolyte and simultaneously as a part of the electrodes (section 3.4.2) is plotted against the temperature gradient for different sodium and potassium activities respectively. Each of the points in Fig. 4-15 was obtained by keeping ΔT constant and waiting for 5-15 h until the non-isothermal voltage reaches a steady state value with longer time being necessary at the low temperature interval. The dependence of the voltage on ΔT can be described satisfactorily by a linear curve in the entire range of the measured temperature interval (400-800 °C). Fig. 4-15 demonstrates exemplarily the behaviour of the thermo voltage at the high and low end of the covered temperature regime.

It becomes evident from Fig. 4-15 that as found previously for NASICON (section 4.2.1), an offset voltage (U_0) is observed for both the sodium and potassium carbonates in the complete range of the temperature and activity interval. The offset voltage changes with the level of the chemical potential of Na or K and temperature. The magnitude of U_0 is small at the high and medium temperatures while in the lower end of the temperature interval it is higher as evident from Fig. 4-15.

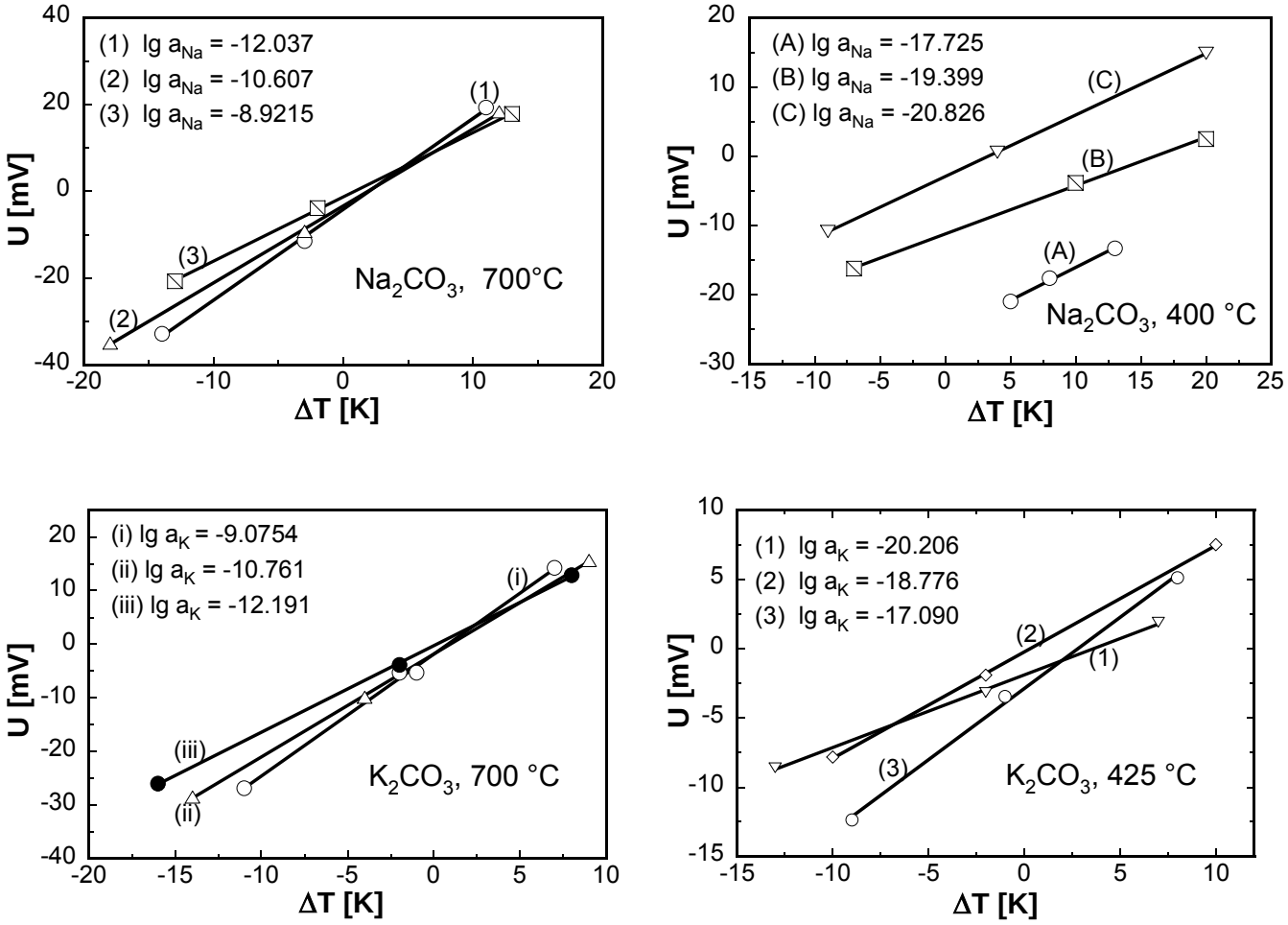

Fig. 4-15 Thermo voltage vs ΔT (Na_2CO_3, T = 700, 400 °C and K_2CO_3 T = 625, 425 °C)

The value of U_0 remains constant under different temperature gradients as the plot of thermo voltage versus ΔT remains linear in the whole interval of chemical potential and temperature. Hence the offset voltage U_0 does not appear to have an impact on the thermoelectric power of the materials.

4.3.2 Thermoelectric power

The behaviour of the thermoelectric power as a function of the chemical potential of Na or K is illustrated in Fig. 4-16 and Fig. 4-17 for Na_2CO_3 at 625 °C and K_2CO_3 at 525 °C respectively. The metal activity a_{Na} and a_K was changed either in increasing or decreasing order throughout the measurements and adjusted by altering the partial pressures of the CO_2, O_2 gas in equilibrium with the respective carbonates.

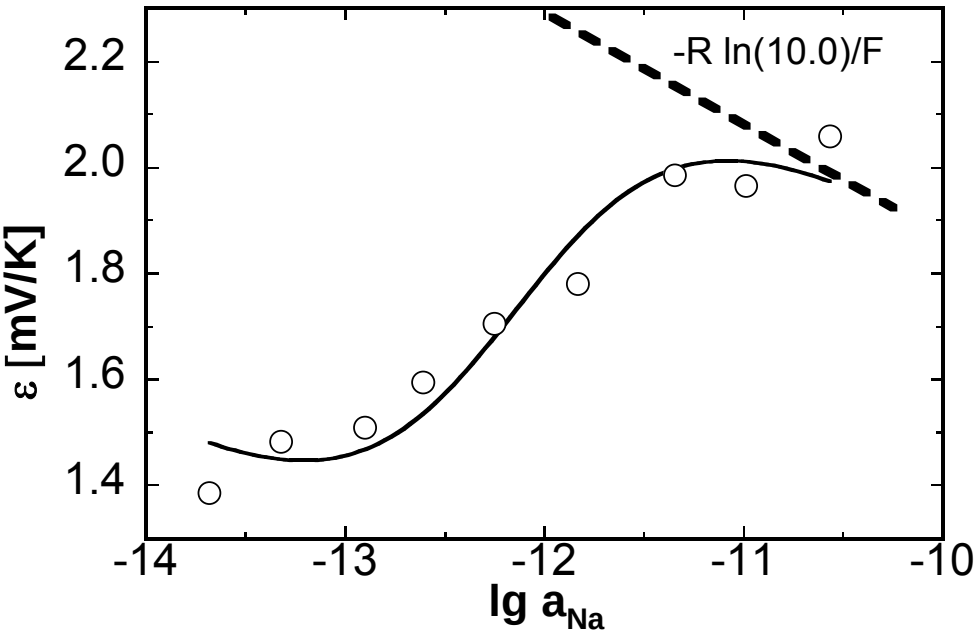

Fig. 4-16 Sodium chemical potential dependence of the thermoelectric power of Na_2CO_3 at T= 625 °C (solid line curve fitting according to Eq. 2-70)

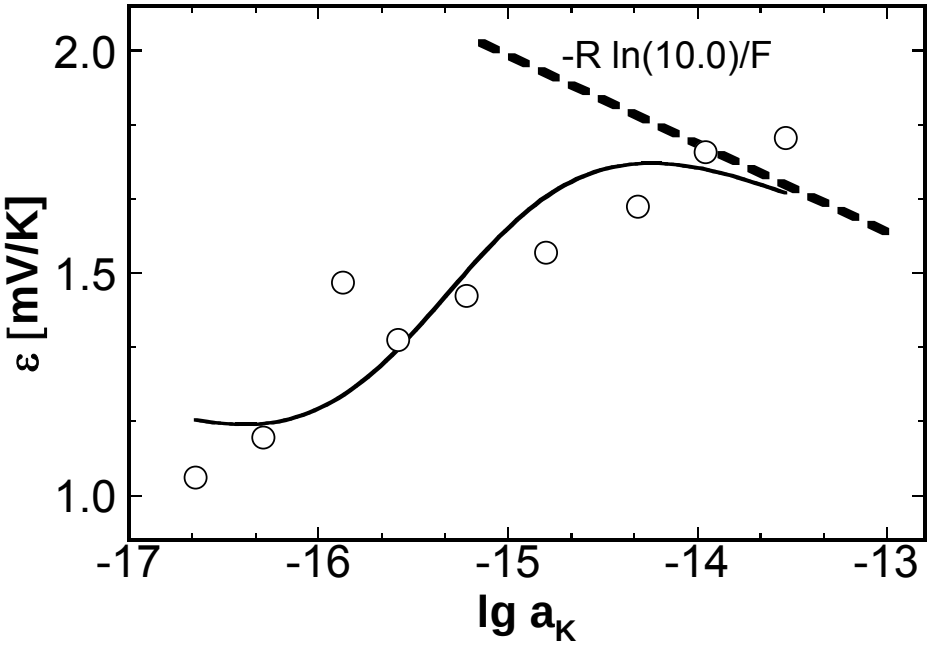

Fig. 4-17 Potassium chemical potential dependence of the thermoelectric power of K_2CO_3 at T= 525 °C (solid line curve fitting according to Eq. 2-70)

Figs. 4-16 and 4-17 make evident that similar to previous observations on NASICON (section 4.2.2), in the entire range of the temperature interval (400-800 °C) a non-linear dependence of the thermoelectric power on the metal chemical potential is obtained.

Considering the trend, at high chemical potential of Na or K, the total thermoelectric power increases with decrease in the chemical potential of the respective neutral species qualitatively according to Eq. 2-70. Both Na_2CO_3 and K_2CO_3 tend to approach to predominant ionic conductors and the profile of total thermoelectric power versus metal activity becomes increasingly linear with slope equal to –R ln(10.0)/F as discernible from Figs. 4-16 and 4-17. On decreasing the metal chemical potential, the data points deviate from the linear curve. The deviation is comparatively small in the region of high metal activities; it becomes much higher with decreasing metal activities due to the prevalent influence of the electronic conductivity in the material. Consequently a new behaviour due to electron hole is established in the low activity region.

In Fig. 4-16 the data points were measured by moving from left to right i.e. by increasing the sodium activity while Fig. 4-17 is obtained by changing the potassium activity from right to left. Below 450 °C there is an apparent influence of the direction of activity variation on the thermoelectric power of both carbonates as exemplarily demonstrated in Fig. 4-18 for Na_2CO_3.

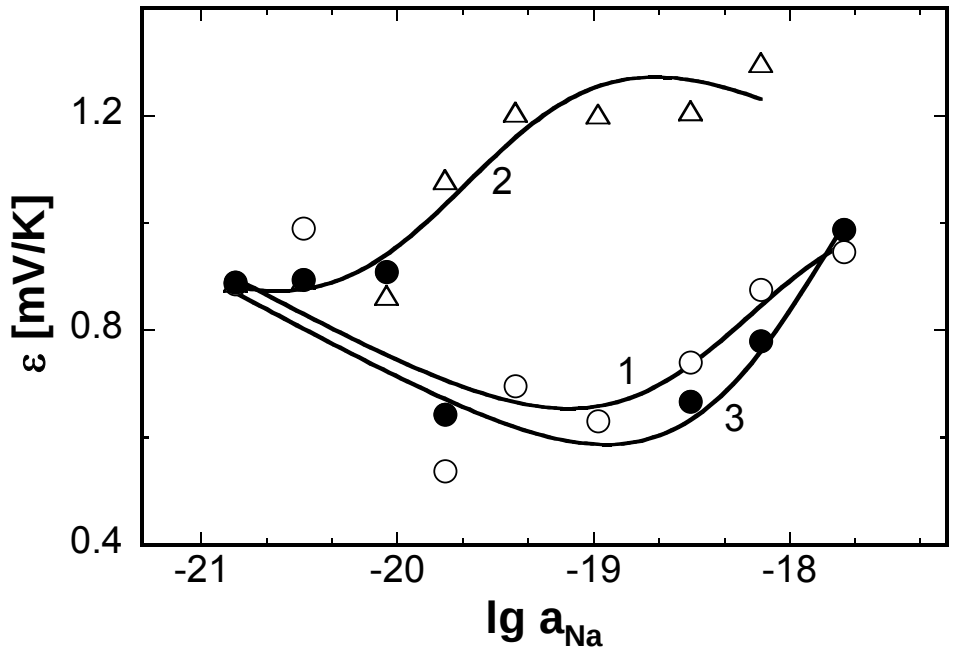

Fig. 4-18 Sodium chemical potential dependence of the thermoelectric power at T= 400 °C for Na_2CO_3 (solid line curve fitting according to Eq. 2-70. Curves 1, 3 are obtained after stepwise increasing the sodium activity, curve 2 is due to decreasing the sodium activity stepwise)

Curves 1, 3 are obtained by stepwise increasing the sodium activity whereas curve 2 occurs upon stepwise decreasing the activity i.e., moving from right to left of x-axis. Above 475 °C the direction in which the activity is changed does not play any role and the data on thermoelectric power are within the normal scattering

Taking into account Eq. 2-70, $a_{\oplus}$ can be quantitatively determined by the non-linear curve fit procedure. The experimental data points of ε versus log a_{Me} (Me = Na, K) can be satisfactorily described by means of the numerical values of $a_{\oplus}$ obtained from regression analysis as demonstrated by solid lines through these points in Figs. 4-16 and 4-17.

4.3.3 Temperature dependence of $a_{\oplus}$

The obtained $a_{\oplus}$ values at each temperature are plotted as a function of inverse temperature for Na_2CO_3 and K_2CO_3 depicted in Figs. 4-19 and 4-20 respectively. Following the previous observations on NASICON (cf. section 4.2.3), the log $a_{\oplus}$ vs. 1/T dependence is a linear curve within the temperature interval under investigation.

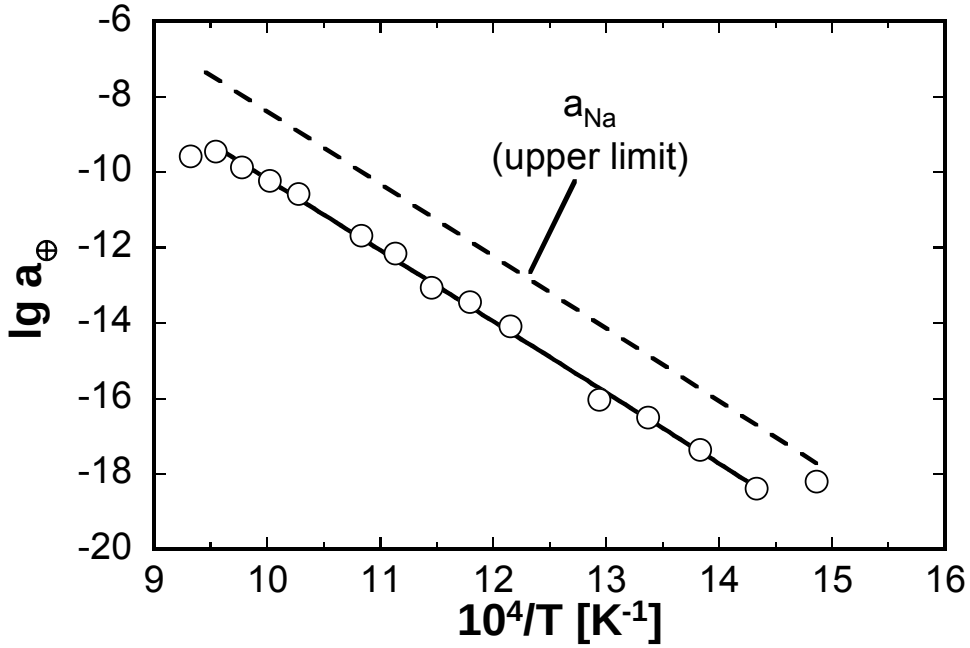

Fig. 4-19 Temperature dependence of p-electronic conduction parameter for Na_2CO_3 (dashed line: upper limit of the sodium activity covered by the sodium carbonate electrode)

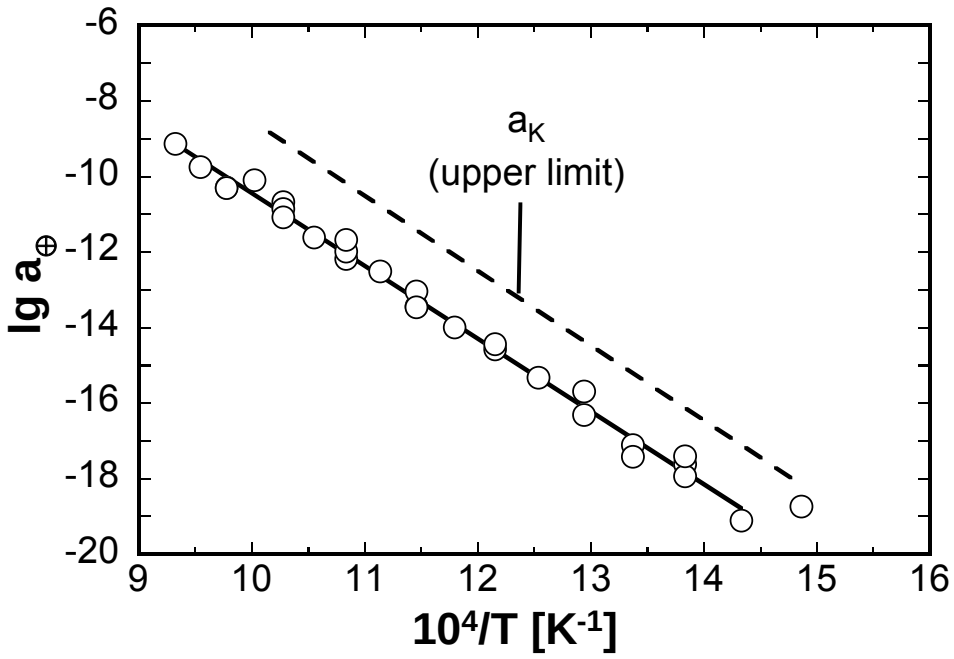

Fig. 4-20 Temperature dependence of p-electronic conduction parameter for K_2CO_3 (dashed line: upper limit of the potassium activity covered by the potassium carbonate electrode)

Quantitatively, the temperature dependence can be expressed as follows:

$$\lg a_{\oplus} = 8.69 - \frac{18872.27}{T/K} \qquad (425\ °C \le T \le 775\ °C) \qquad (Na_2CO_3) \qquad \text{Eq. 4-3}$$

$$\lg a_{\oplus} = 9.27 - \frac{19597.42}{T/K} \qquad (425\ °C \le T \le 750\ °C) \qquad (K_2CO_3) \qquad \text{Eq. 4-4}$$

At temperatures above T = 750 °C the data for $a_{\oplus}$ slightly deviate from the linear behaviour as observed for Na_2CO_3. The deviation could be interpreted as the starting of the decomposition of Na_2CO_3 under the prevailing measuring conditions. The decomposition temperature is 773 °C [43].

There is also a deviation from the linear behaviour for both Na_2CO_3 and K_2CO_3 in the low temperature region. This could be understood as resulting from a slow establishment of the steady state of the non-isothermal voltage. This is in agreement with the observation that, as mentioned above with decreasing temperature the ε versus log a_{Me} plots differ from each other depending on whether the metal activity is increased or decreased as depicted in Fig. 4-18. Another problem that could influence the low temperature behaviour is structural transformation of both carbonates. There is lot of confusion in the literature with respect to this [43, 63-65,116-118] which is why the exact

cause for the observed behaviour in the low temperature region can not be stated unambiguously.

In Figs. 4-19 and 4-20 the upper limit of the metal activity covered by the metal carbonates during measurements are given for the sake of comparison. The obtained data on $a_{\oplus}$ run parallel to the temperature dependence of the metal activity established by Me_2CO_3-CO_2-O_2 as illustrated by the dashed line in Figs. 4-19 and 4-20. This is in accordance with the previous studies on Na-beta-alumina [15, 16], NASICON (section 4.2.3), which again underline the dominating role of the chemical surroundings on the magnitude of the electronic conduction parameter.

Thus the present investigation indicates both Na_2CO_3 and K_2CO_3 behave as mixed conductors contrary to what is reported in literature regarding their use as solid electrolyte for sensor applications [43, 108].

4.4 Thermoelectric power of NBA

4.4.1 System NBA/Na-silicate/O_2

4.4.1.1 Thermo voltage

Fig. 4-21 shows the dependence of the steady state thermo voltage of cell (V) as a function of the temperature gradient for various sodium activities.

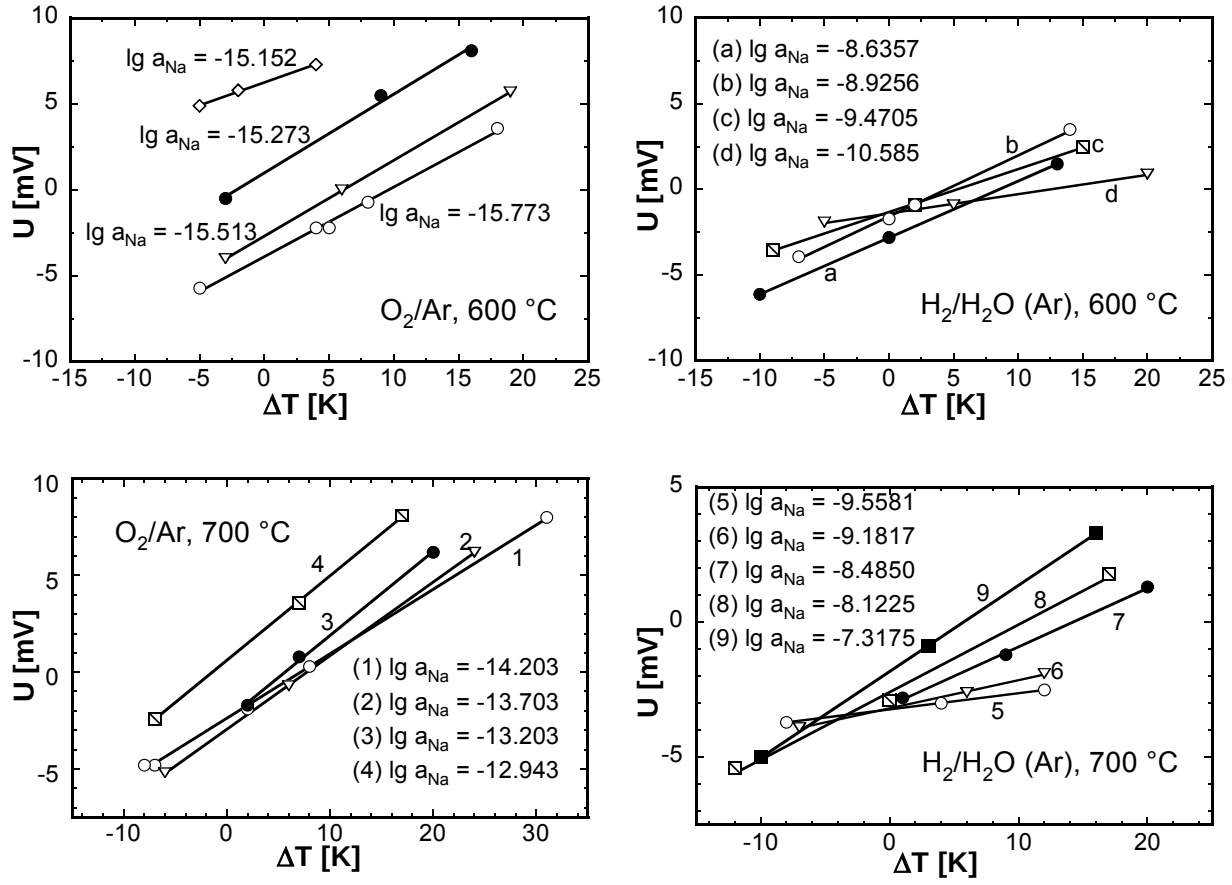

Fig. 4-21 Non isothermal voltage of cell (V) dependence on ΔT at T = 600 and 700 °C

The sodium activity was obtained by altering the oxygen partial pressure either by O_2/Ar or H_2/H_2O/Ar gas mixtures. Hence the sodium activity interval was adjusted within an order of magnitude in case of O_2/Ar and 3 orders of magnitude in case of H_2/H_2O/Ar.

The non-isothermal voltage reached a steady state level within 5-10 h after changing the temperature gradient depending on the level of the sodium chemical potential. There was no apparent influence of the direction of the activity variation on the thermo voltage of the cell. The minimum elapsed time between two experimental curves i.e. the straight lines in Fig. 4-21 was 36-48 h. In the entire range of the covered temperature

interval (600 °C ≤ T ≤ 700 °C) and activities, a linear variation of the thermo voltage with ΔT can be seen as illustrated in Fig. 4-21. Under zero temperature gradient i.e., $\Delta T = 0$ the thermo voltage should be zero under this condition according to Eq. 2-63. It is evident from Fig. 4-22 that an offset voltage (U_0) of about 1-2 mV is observed at T = 650 °C. The voltage U_0 changes both with respect to the temperature and activity (Fig. 4-22).

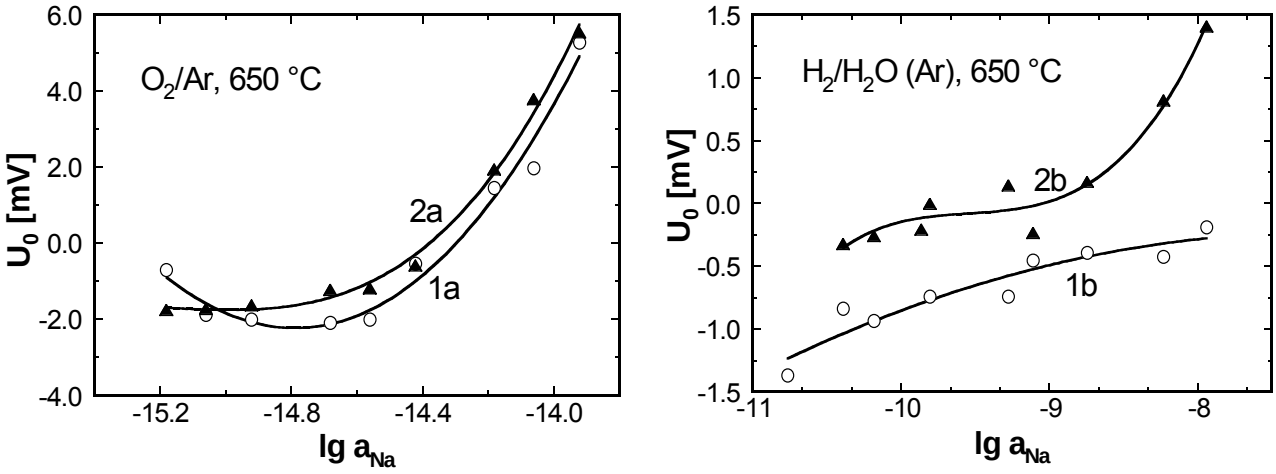

Fig. 4-22 Offset voltages (U_0) of cell (V) as a function of the sodium activity of the $NaSi_xO_{2x+0.5}/SiO_2/O_2$ (curves 1a, 2a) and $NaSi_xO_{2x+0.5}/SiO_2/H_2/H_2O$ (curves 1b, 2b) electrodes at T = 650 °C (Curve1 is obtained after stepwise increasing the chemical potential and curve 2 is due to decreasing the sodium activity stepwise)

In Fig. 4-22 curves 1, 2 represent the variation of U_0 by stepwise increasing and decreasing the sodium activity respectively: Curves 1a and 2a were obtained using $NaSi_xO_{2x+0.5}/SiO_2/O_2$ electrode and 1b as well as 2b by $NaSi_xO_{2x+0.5}/SiO_2/H_2/H_2O$ electrode. The measuring run done in the rising direction of the sodium activity comprised of curve 1a followed by 1b whereas in the falling direction of the activity curve 2b was obtained before curve 2a.

As evident from Fig. 4-22 the voltage drops down to a minimum value with decreasing sodium activity at least qualitatively. The voltage U_0 shifts to more positive values while moving towards to the left end of the x-axis only in case of H_2/H_2O gas mixtures as seen in Fig. 4-22.

Fig. 4-23 depicts the schematic sketch of the sodium chemical potential profile inside the solid electrolyte under the conditions established in cell (V).

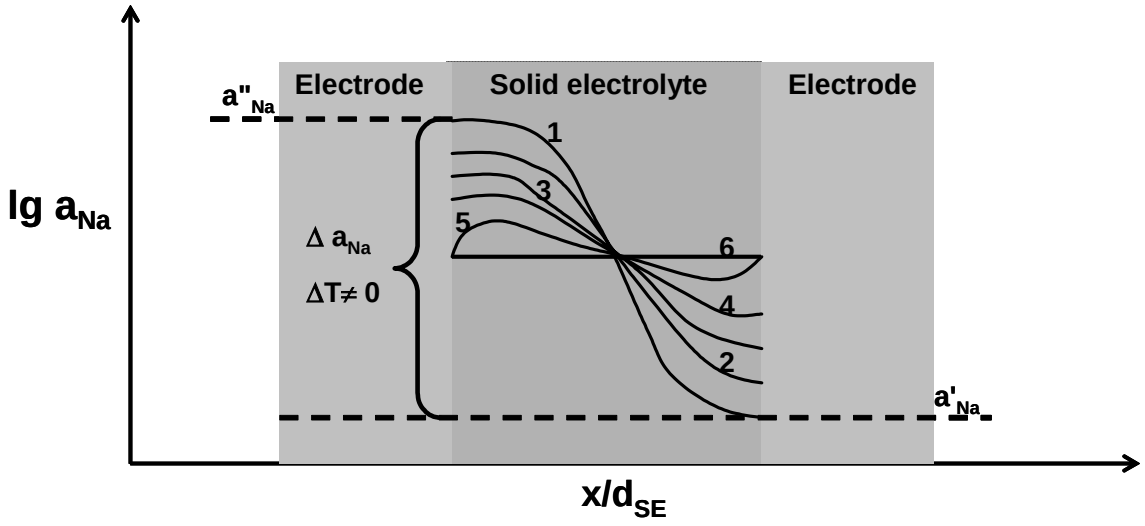

Fig. 4-23 Schematic sketch of the sodium chemical potential profile inside the solid electrolyte (Na-beta-alumina) under the conditions of cell (V)

The ordinates denote the sodium activity with which the solid electrolyte layer at position x is equilibrated. Curve 1 shows the sodium potential distribution under a finite temperature gradient ($\Delta T \neq 0$). This results in the potential difference across the solid electrolyte. When the temperature gradient is made zero, ideally curve 6 in Fig. 4-23 should be obtained which requires infinite amount of time. However, the potential distribution slowly approaches to the ideal behaviour while passing through curves 2, 3 and 4. Curve 5 represents the situation closer to ideal condition even though the sodium potential distribution is not completely levelled out which means a flux of charge carriers is still flowing through the electrolyte. This flux coupled with the electrode polarization which has not been taken into consideration in Fig. 4-23 gives rise to the offset voltage. Thus the generation of the offset voltage could be understood as resulting from a non-balance of the ions and electrons inside the solid electrolyte due to the incomplete equilibration with the surroundings [119]. As a consequence, a finite chemical gradient across the solid electrolyte is established even at $\Delta T = 0$.

4.4.1.2 Thermoelectric power

Figs. 4-24 and 4-25 show how the thermoelectric power of Na-beta-alumina (NBA) changes with the sodium activity of the $NaSi_xO_{2x+0.5}/SiO_2/O_2$ and $NaSi_xO_{2x+0.5}/SiO_2/H_2,H_2O$ electrodes correspondingly.

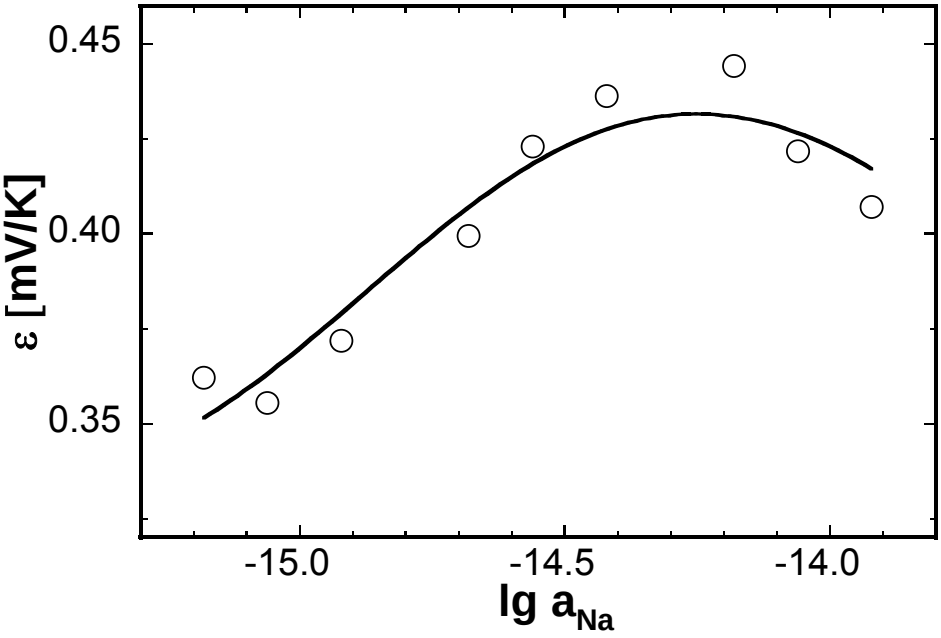

Fig. 4-24 Sodium chemical potential dependence of the thermoelectric power of Na-beta-alumina at T= 650 °C with $NaSi_xO_{2x+0.5}/SiO_2/O_2$ electrode (solid line curve fitting according to Eq. 2-70)

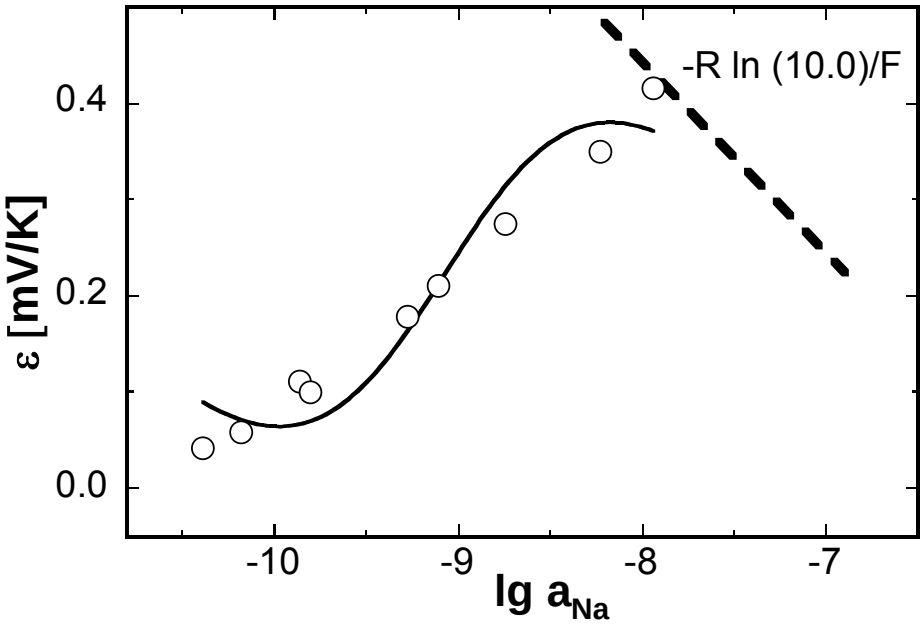

Fig. 4-25 Sodium chemical potential dependence of the thermoelectric power of Na-beta-alumina at T= 650 °C with $NaSi_xO_{2x+0.5}/SiO_2/H_2/H_2O$ electrode (solid line curve fitting according to Eq. 2-70)

The ordinates in Figs. 4-24 and 4-25 represent the slope of the measured values of the thermo voltage versus temperature gradient (cf. Fig. 4-21).

It is evident from Fig. 4-24 and Fig. 4-25 that a non-linear behaviour of thermo power with sodium chemical potential is obtained similar to previous observations on NASICON (cf. section 4.2.2), Na-beta-alumina [16] in the complete range of the temperature interval (600 °C ≤ T ≤ 700 °C). The experimental data points of the ε versus log a_{Na} plots can be described satisfactorily using Eq. 2-70 which is demonstrated by solid lines through these points as shown in Fig. 4-24 and Fig. 4-25.

As discussed in the preceding sections (cf. sections 4.2, 4.3) for ionic conduction the plot of ε vs. log a_{Na} in Figs. 4-24, 4-25 would represent a straight line with slope –R ln(10.0)/F in accordance with Eq. 2-70 (dashed line in Fig. 4-25). Examining the behaviour of the curve, at high sodium activity there is a small deviation of the thermoelectric power from the linear curve (dashed line in Fig. 4-25), since $a_{\oplus}$ though not negligible, is still very small compared to a_{Na}. However, moving further to the left of the abscissa in Fig. 4-25 the data points deviate strongly from the linear behaviour. This is because a_{Na} decreases exponentially and $a_{\oplus}$ prevails more and more over a_{Na} in Eq. 2-70 and the thermoelectric power breaks down due to the increasing influence of the electronic short circuiting through the solid electrolyte. Eventually the linear behaviour dominated by electron holes is observed.

4.4.1.3 Temperature dependence of $a_{\oplus}$

The $a_{\oplus}$ values obtained at each temperature using Eq. 2-70 and the field of data points ε = f (log a_{Na}, T) result in the log $a_{\oplus}$ versus 1/T dependence depicted in Fig. 4-26 and Fig. 4-27. The log $a_{\oplus}$ vs. 1/T dependence is a linear curve for both Na-silicate-SiO_2-O_2 and Na-silicate-SiO_2-H_2/H_2O electrodes as depicted in Figs. 4-26, 4-27.

Both the curves in Figs. 4-26 and 4-27 are parallel to the temperature dependence of the sodium activity of the corresponding electrodes which is in accordance with previous observations obtained on NBA [9, 12]; NASICON (section 4.2.3) and the carbonates (section 4.3.3). As known from these investigations, the findings indicate the dominating role of the chemical surroundings i.e. the sodium activity of the measuring electrode, on the magnitude of the p-electronic conduction parameter.

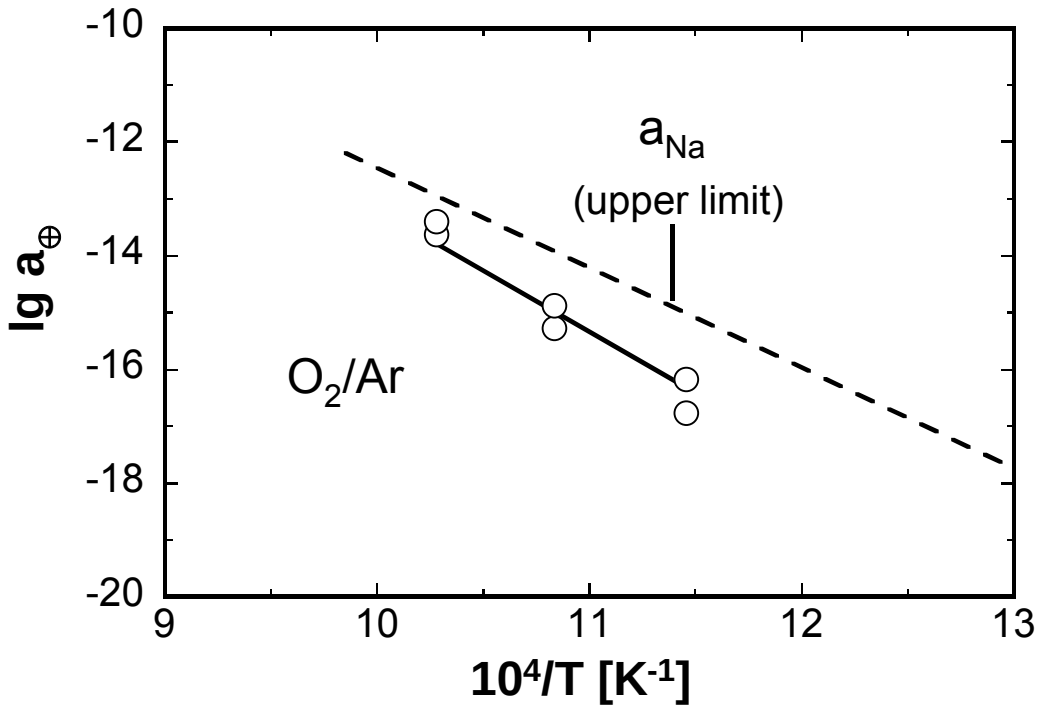

Fig. 4-26 Temperature dependence of p-electronic conduction parameter for Na-beta-alumina with $NaSi_xO_{2x+0.5}/SiO_2/O_2$ electrode (dashed line: upper limit of the sodium activity covered by the electrode)

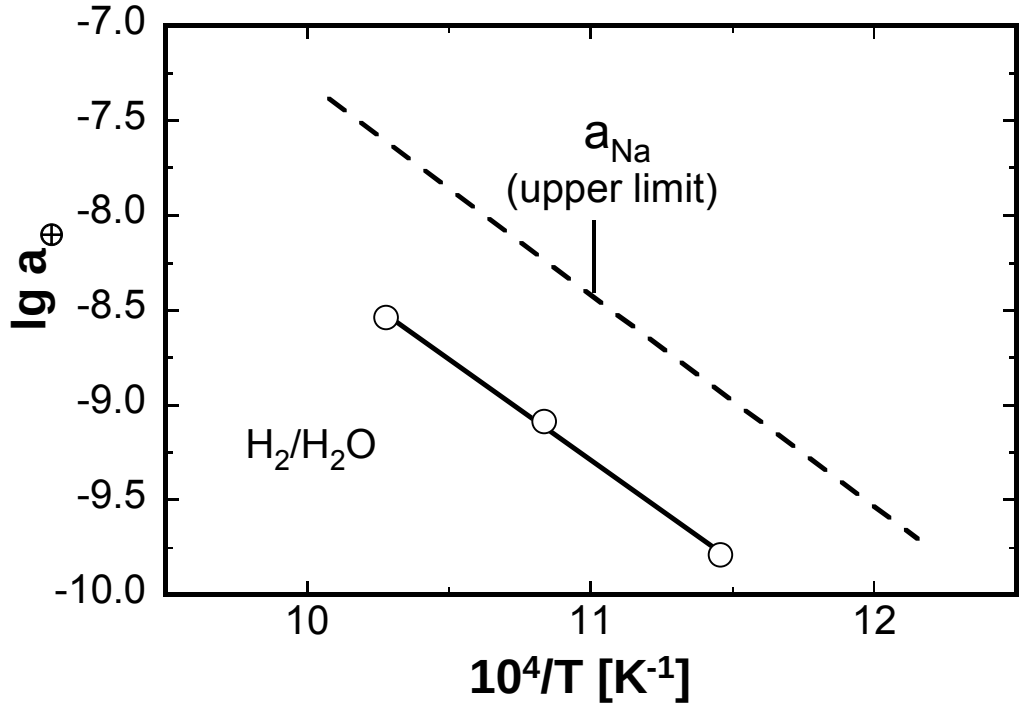

Fig. 4-27 Temperature dependence of p-electronic conduction parameter for Na-beta-alumina with $NaSi_xO_{2x+0.5}/SiO_2/H_2/H_2O$ electrode (dashed line: upper limit of the sodium activity covered by the electrode)

The temperature dependence of $a_{\oplus}$ can be expressed quantitatively by Eqs. 4-3a and 4-3b respectively as follows:

$$\lg a_{\oplus} = 8.28 - \frac{21463.88}{T/K} \qquad (600 \le T \le 700°C) \quad (NBA, Na_xSiO_{2x+0.5}/SiO_2/O_2)$$

Eq. 4-3a

$$\lg a_{\oplus} = 2.43 - \frac{10653.46}{T/K} \qquad (600 \le T \le 700°C) \quad (NBA, Na_xSiO_{2x+0.5}/SiO_2/H_2/H_2O)$$

Eq. 4-3b

The present results on $a_{\oplus}$ lies within the sodium activity interval covered by the electrodes of cell (V) as depicted in Figs. 4-26, 4-27. This means the chemical potential of the electrode lies outside the ionic conduction domain of the solid electrolyte Na-beta-alumina. In other words, Na-beta-alumina behaves as a mixed ionic-electronic conductor under the conditions of measurements. Thus the observation reveals that employing Na-beta-alumina as a pure ionic conductor in any solid state potentiometric measurement can be erroneous even though the reports in the literature points otherwise [109-113].

4.4.2 System NBA/Na-Molybdate/O_2

4.4.2.1 Thermo voltage

Fig. 4-28 shows how the steady state non-isothermal voltage of the cell (VI) (section 3.4.2) changes with the temperature gradient for different sodium activities at 500 °C. The thermo voltage varies linearly with the temperature gradient (ΔT) in the complete interval of the sodium activity covered in the present investigation.

The thermo voltage requires much longer time (app. 10-36 h) to achieve a steady state value in the relatively high activity than that in the low activity region (about 5-10 h). At the low and the medium activity there was no apparent influence of the direction of the thermal gradient variation on the thermo voltage. However at high sodium activity this observation remains no more valid.

Fig. 4-29 makes evident the evolution of the functional dependence of the thermo voltage on the temperature gradient at high sodium activity with time and variation of the thermal gradient. Curves a, b and c in Fig. 4-29 illustrates the consecutive measuring runs at a particular sodium activity. It took app. 10-15 days for the tendency to phase out depending on the level of the activity and the dependence to become time invariant.

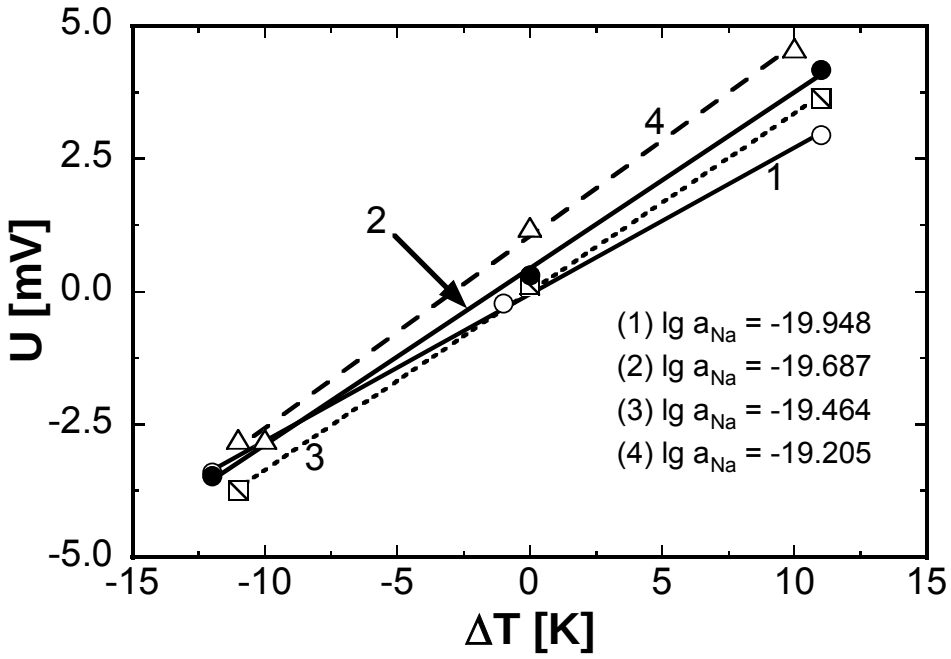

Fig. 4-28 Non isothermal voltage of cell (VI) as a function of ∆T at T = 500 °C under various sodium activity

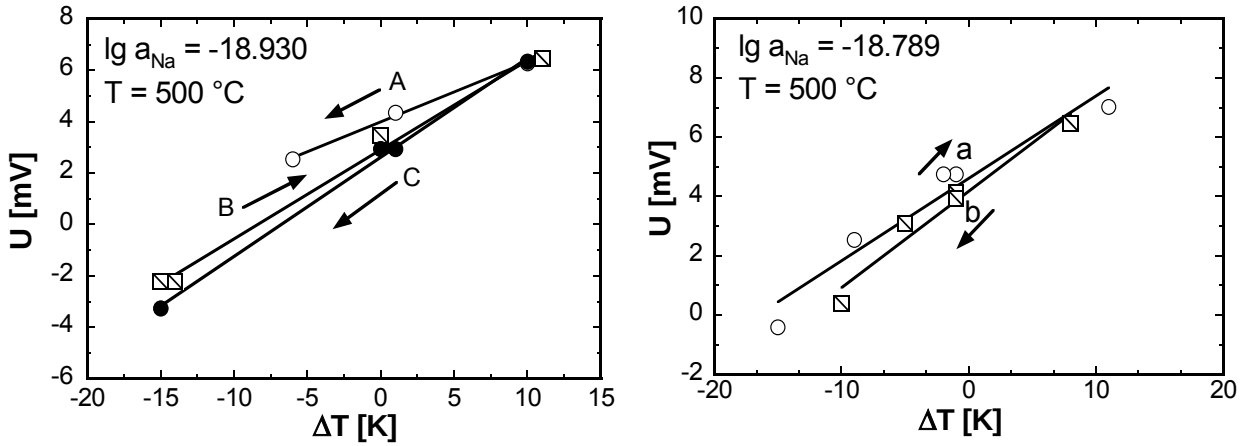

Fig. 4-29 Non isothermal voltage of cell (VI) as a function of ∆T at T = 500 °C under different sodium chemical potential

This peculiar phenomenon has not been observed with other systems considered in the present study. Nevertheless, the thermo voltage varies linearly with temperature gradient even in this region of the sodium activity. An offset voltage (U_0) of 2-4 mV was observed as previously found for NASICON (section 4.2.1), Na-beta-alumina (section 4.4.1.1) and alkali metal carbonates (section 4.3.1). The voltage U_0 changes with the level of the sodium chemical potential.

4.4.2.2 Thermoelectric power

The functional dependence of the thermoelectric power of Na-beta-alumina on the sodium activity of the $Na_2MoO_4/Na_2Mo_2O_7/O_2$ electrode is illustrated in Fig. 4-30 for T = 500 °C.

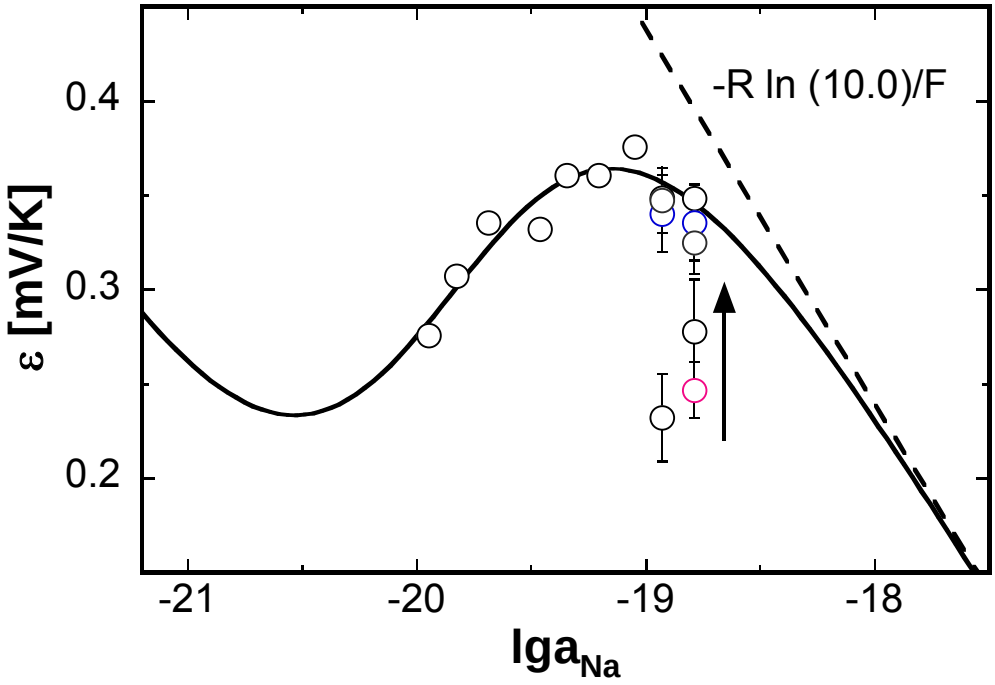

Fig. 4-30 Sodium chemical potential dependence of the thermoelectric power of Na-beta-alumina T= 500 °C (solid line curve fitting according to Eq. 2-70, dashed line represents pure ionic conduction slope)

The sodium activity was adjusted by alternately ascending and descending the partial pressure of the O_2 gas mixture throughout the measurements. The ordinates in Fig. 4-30 represent the slope of the straight lines depicted in Figs. 4-28, 4-29.

As seen from Fig. 4-30 the non-linear dependence of the thermoelectric power on the sodium activity is obtained in accordance with Eq. 2-70 and in agreement with the expectation from the previous findings on NASICON and alkali metal carbonates (section 4.2.2, section 4.3.2).

The data points in the high activity region as illustrated in Fig. 4-30 shift towards more positive values, which expresses the fact that the thermo voltage versus ΔT curve becomes steeper by alternately increasing and decreasing the thermal gradient as discussed in the preceding section. One of the possible reasons for this behaviour could be that the buffer capacity of the $Na_2MoO_4/Na_2Mo_2O_7$ system is hampered due to the extremely low O_2 partial pressure in this region of the activity. However the findings of a

previous study [73] on the thermodynamic investigations of this electrode system indicate that the system is stable under the conditions of present investigation. Thus, it is not possible to unambiguously state the exact cause for the particular behaviour of the thermoelectric power in the high activity region. Further work is required to understand the interplay of various phenomena resulting in such anomalous behaviour.

Fig. 4-30 depicts that the measured values of the thermoelectric power under various sodium activities do not follow the ionic conduction behaviour. As discussed before (cf. sections 4.2, 4.3 and 4.4) the deviation from the ionic conduction is due to the increasing impact of the electronic conductivity through the solid electrolyte, i.e. Na-beta-alumina.

By evaluating a field of experimental data $\varepsilon = f(a_{Na}, T)$, the p-electronic conduction parameter ($a_{\oplus}$) can be obtained by means of the non-linear curve fit procedure based on Eq. 2-70 as described in section 2.4.3.1.

4.4.2.3 Temperature dependence of $a_{\oplus}$

The p-electronic conduction parameter determined according to the above procedure is plotted as a function of the inverse of the temperature shown in Fig. 4-31. In accordance with the previous observations on NASICON (section 4.2.3), alkali metal carbonates (section 4.3.3), the log $a_{\oplus}$ versus 1/T dependence follows a linear curve within the covered temperature interval (425 °C ≤ T ≤ 500 °C).

The temperature dependence can be expressed as follows:

$$\lg a_{\oplus} = 2.42 - \frac{(17241.21 \pm 1833.09)\ \mathrm{K}}{T} \qquad (425 \le T \le 500°C) \qquad \text{Eq. 4-4}$$

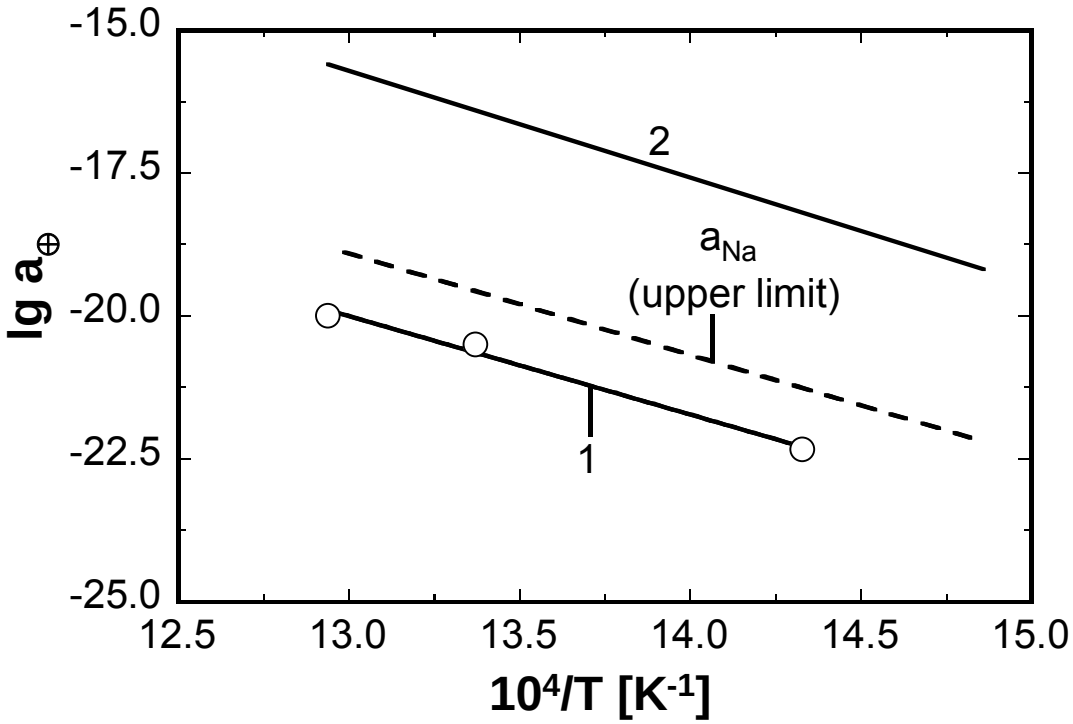

Fig. 4-31 Temperature dependence of p-electronic conduction parameter for Na-beta-alumina with $Na_2Mo_2O_7/Na_2MoO_4/O_2$ electrode (curve1) compared with that of Na-beta-alumina with $Na_2CO_3/CO_2/O_2$ electrode (curve 2 [16]) (dashed line: upper limit of the sodium activity region covered by the electrode of cell (VI))

As depicted in Fig. 4-31 the present findings are compared with $a_{\oplus}$ obtained for Na-beta-alumina under $Na_2CO_3/CO_2/O_2$ electrode using the thermo electric power technique [16]. Similarly, the upper limit of the sodium activity range covered by the electrode of cell (VI) during the measurement is given for the sake of comparison. The $a_{\oplus}$ values lie close to the upper limit of the sodium activity. In addition, the present data (curve 1) for the p-electronic conduction parameter of Na-beta-alumina are nearly 4 orders of magnitude lower than that obtained by [16] (curve 2 in Fig. 4-31). This underlines once again how the chemical surroundings dictate the magnitude and behaviour of the electronic conduction parameter as known from previous studies [9, 14, 15].

4.4.3 Sodium chemical potential dependence of $a_{\oplus}$

Fig. 4-32 depicts the variation of the p-electronic conduction parameter of Na-beta-alumina with the sodium chemical potential at T = 500 °C obtained using different electrodes and two different techniques i.e., thermoelectric power and solid state potentiometric measurements. The values of the abscissa have been achieved by

utilising $Na_2CO_3/CO_2/O_2$ and $Na_2MoO_4/Na_2Mo_2O_7/O_2$ as electrodes materials (cf. section 2.5.3) as shown in Fig. 4-32. The conditions in both cases are totally different with respect to the interval of the sodium chemical potential.

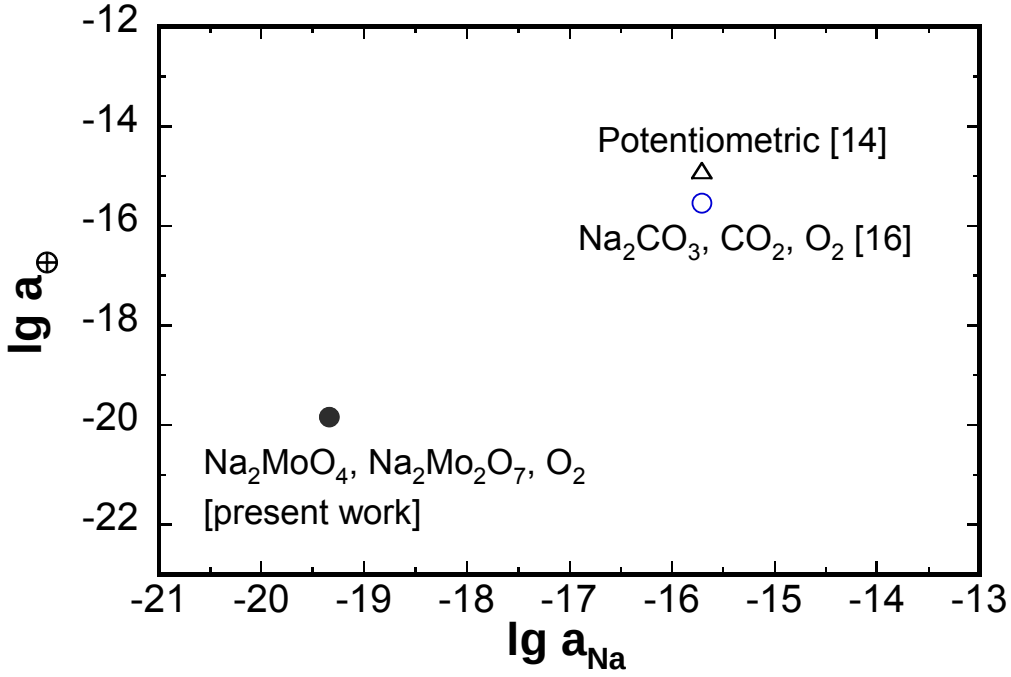

Fig. 4-32 Sodium chemical dependence of p-electronic conduction parameter for Na-beta-alumina with different electrodes

The constancy of p-electronic conduction ($a_\oplus$) of a solid electrolyte with respect to the chemical potential of the neutral species is a consequence of the classical defect chemical consideration. However as discernible from Fig. 4-32 $a_\oplus$ is not constant but changes with the chemical potential of the neutral sodium species in the surroundings of the solid electrolyte i.e. Na-beta-alumina.

As a possible interpretation the non-constancy of $a_\oplus$ could be understood as the consequence of minor changes in the composition of the electrolyte material under the impact of different levels of the chemical potential of the alkali metal in the surroundings. This is an expression of a kind of non-stiochiometry of the electrolyte due to which its nature as a solvent of all defects changes. Hence the equilibria constants determining the relevant defect equilibria changes (section 2.1.1.2). Therefore, $a_\oplus$ changes as well since it is related to these equilibria constants.

The present observation is in assent with the previous findings on Na-beta-alumina [9, 12, 14], NASICON (cf. section 4.2, [15]) and alkali metal carbonates (section 4.3) thereby substantiating the previous experimental findings [9, 14] that the p-electronic conduction parameter of solid electrolyte is not constant but a function of chemical potential of the neutral species in the surroundings in addition to temperature.

4.5 Thermoelectric power of KBA

4.5.1 System KBA/K_2CO_3/CO_2/O_2

4.5.1.1 Thermo voltage

Fig. 4-33 illustrates the dependence of the steady state non-isothermal voltage of cell (III) on the temperature gradient for two different temperatures i.e. for 400 and 600 °C and various potassium activities.

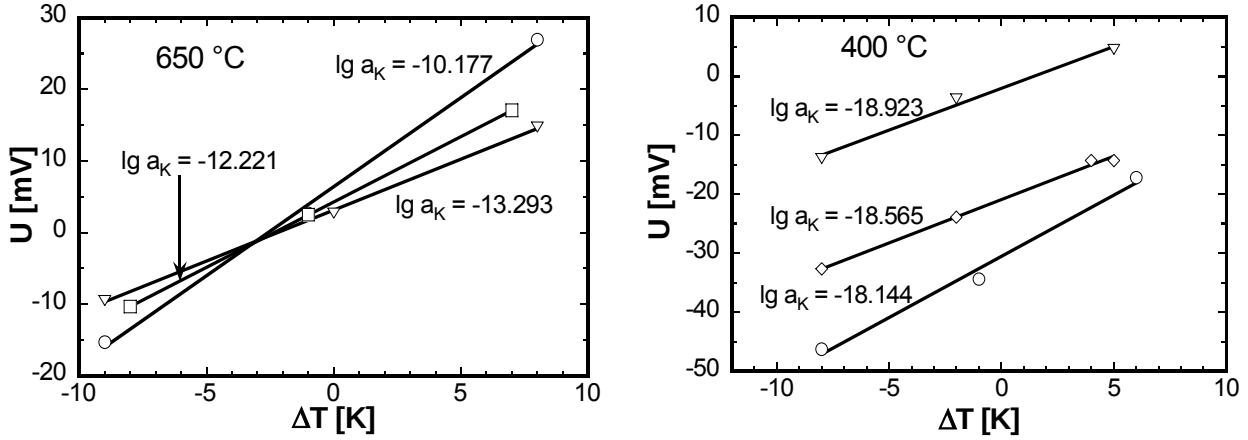

Fig. 4-33 Non isothermal voltage of cell (III) dependence on ΔT at T = 650 & 400 °C

It took about 5-15 h for the voltage to reach the steady state value with longer time being necessary for the lower temperature (T ≤ 450 °C). In the whole range of measured temperature and activity region, the thermo voltage varies linearly with temperature gradient. As previously described (sections 4.2, 4.3, 4.4), a non-negligible offset voltage occurs in the whole interval of the potassium activity and temperature covered during the measurement. There is however no obvious trend in the data.

4.5.1.2 Thermoelectric power

In similar fashion, as previously done (cf. sections 4.2, 4.4,), the thermoelectric power of K-beta-alumina was determined as a function of the potassium activity. Fig. 4-34 and Fig. 4-35 show three examples that illustrate how the thermoelectric power of K-beta-alumina changes with the potassium activity of the K_2CO_3/CO_2/O_2 electrode. The three different temperatures were chosen to illustrate the situation at the upper, medium and lower end of the temperature range under investigation. The values of the abscissa (cf. Fig. 4-34 and Fig. 4-35) were adjusted by alternately increasing and decreasing the composition of the CO_2-O_2-Ar gas atmosphere according to Eq. 2-21.

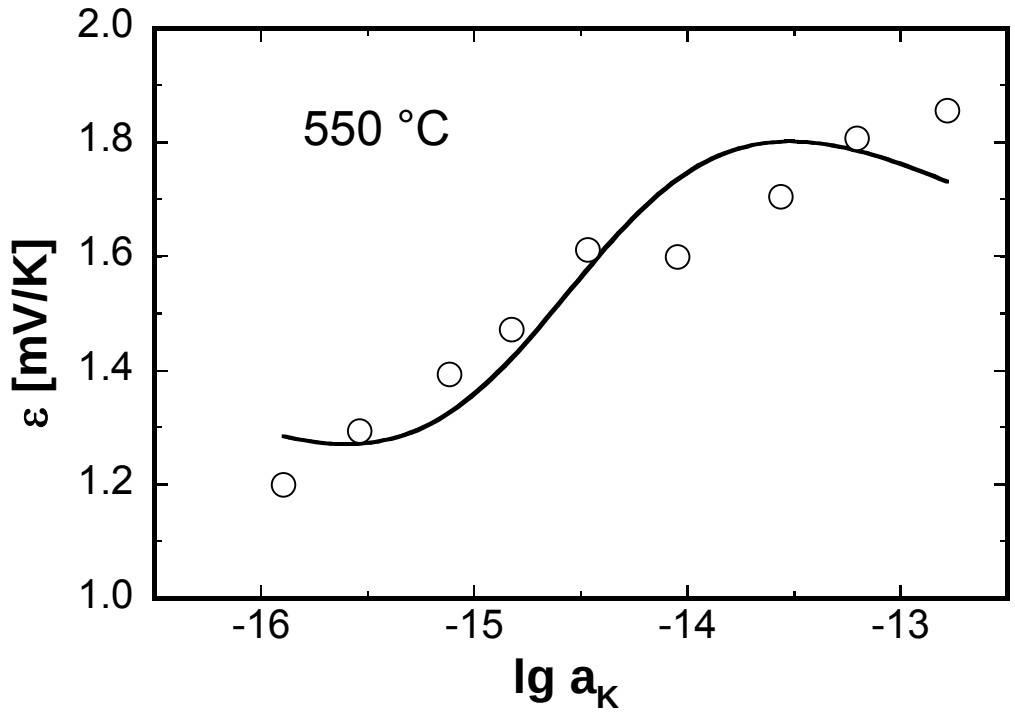

Fig. 4-34 Potassium chemical potential dependence of the thermoelectric power of cell (III) at T = 550°C (curve fitting according to Eq. 2-70 demonstrated by solid lines)

Figs. 4-34 and 4-35 illustrate that a non-linear dependence of the thermoelectric on the potassium activity is obtained. As previously described (section 4.2, 4.4) at high chemical potential of the species in the present case potassium, the ε versus lg a_K plot would represent a straight line with slope –R ln(10.0)/F (dotted line in Fig. 4-35).

The deviation from linear behaviour becomes more evident on moving toward the left end of the x-axis due to the increasing electronic short circuiting through the solid electrolyte. As clearly visible in Fig. 4-35 the data fall in between the pure ionic (dotted line) and the electronic conduction region (dashed line) thereby indicating that the material behaves as a mixed ionic-electronic conductor under the condition of measurement.

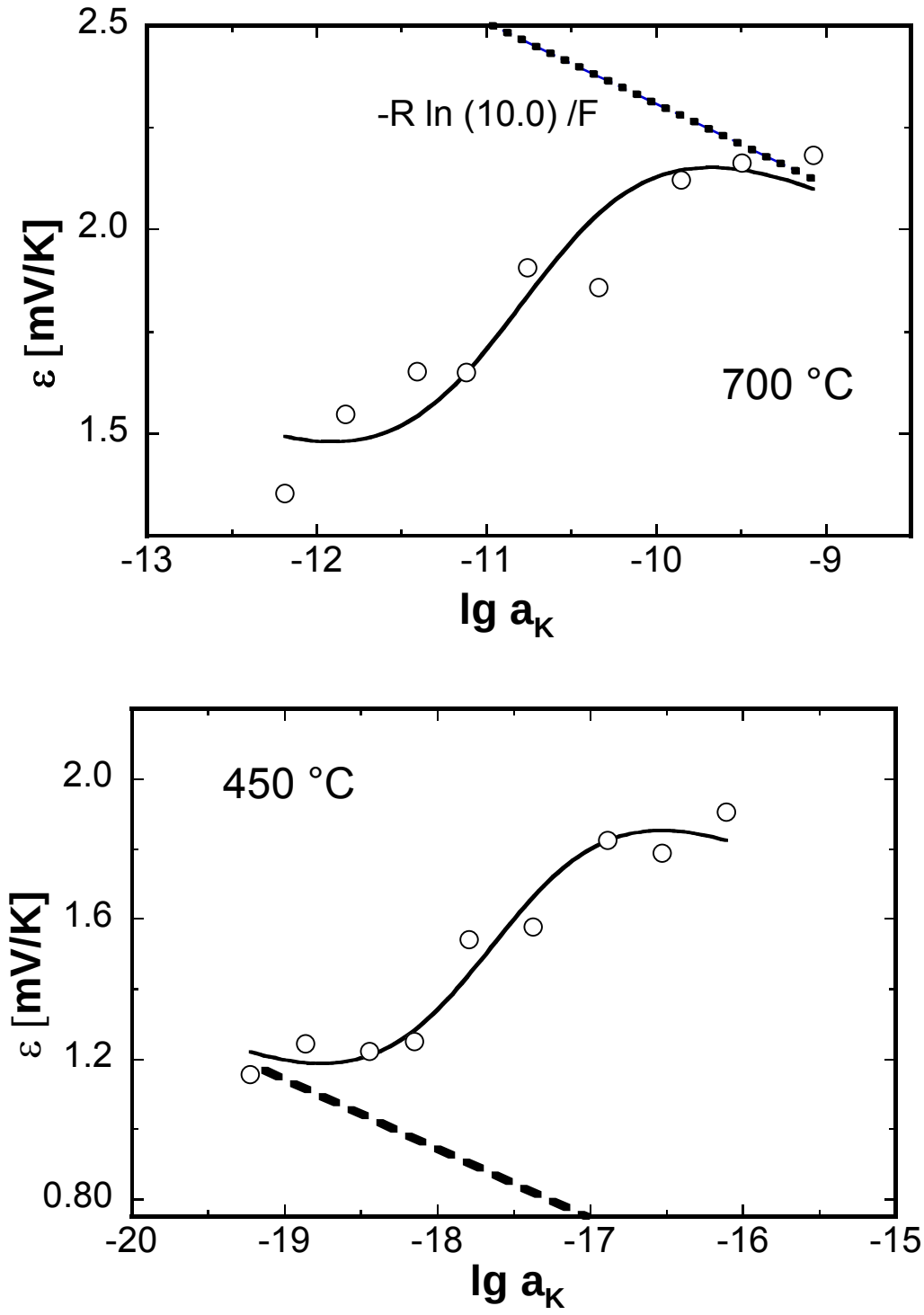

Fig. 4-35 Potassium chemical potential dependence of the thermoelectric power of cell (III) at T = 700 and 450 °C (curve fitting according to Eq.2-70 demonstrated by solid lines)

4.5.1.3 Temperature dependence of $a_{\oplus}$

The $a_{\oplus}$ values obtained by applying the non linear regression method (section 2.4.3.1) to all sets of ε versus log a_K plots and depicted in Fig. 4-36.

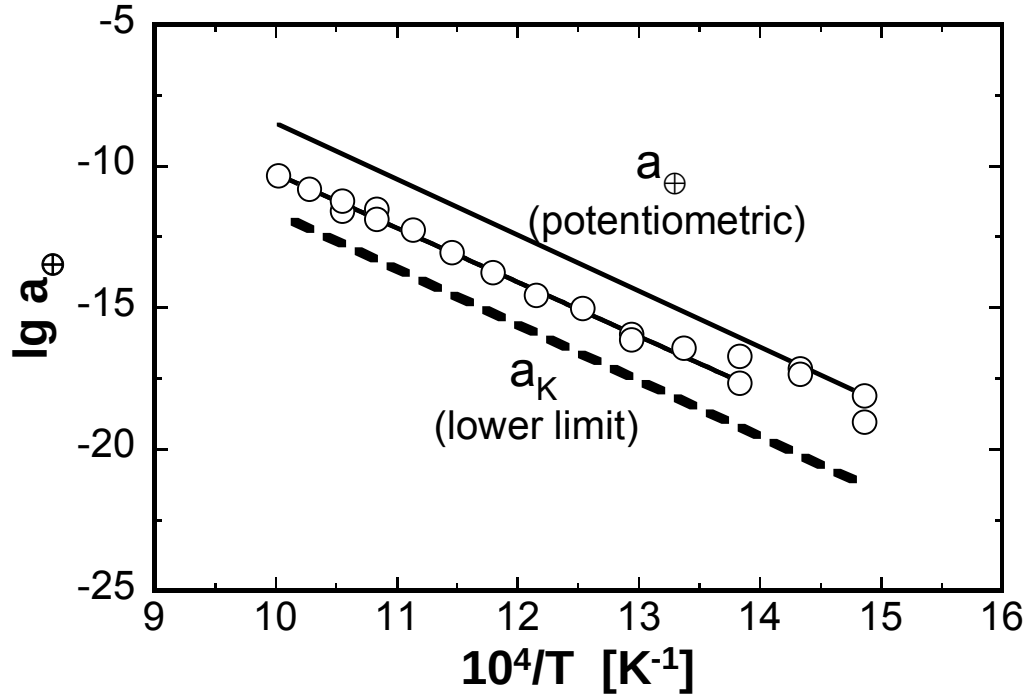

Fig. 4-36 Temperature dependence of p-electronic conduction parameter for K-beta-alumina with K_2CO_3, CO_2, O_2 electrode compared with that obtained from potentiometric measurement [23]

In accordance with expectation, the log $a_{\oplus}$ versus 1/T dependence is a linear curve in the temperature range 450 °C ≤ T ≤ 725 °C. The present findings are compared with $a_{\oplus}$ obtained from potentiometric measurement on K-beta-alumina [23]. As revealed from Fig. 4-36 the data on $a_{\oplus}$ at least between 450 °C and 725 °C run parallel to the temperature dependence of the potassium activity of the K_2CO_3, CO_2, O_2 electrode depicted by a dashed line.

Quantitatively, the temperature dependence of the logarithm of $a_{\oplus}$ can be expressed as follows:

$$\log a_{\oplus} = 8.895 - \frac{19153.918}{T/K} \qquad (450 \le T \le 725\ °C) \qquad \text{Eq. 4-4}$$

In the low temperature region the data slightly deviate from linearity. Obviously in this region the shape of the curve is determined by slow establishment of the steady state level of the thermo voltage that is not reached completely during the normal measuring run. Therefore, the data were not taken into account for evaluation of the temperature dependence of $a_{\oplus}$.

As discernible from Fig. 4-36 the present findings on $a_{\oplus}$ are an order of magnitude lower than obtained by potentiometric measurement. This is not a contradiction or falsification of previous studies but an expression for the fact that $a_{\oplus}$ is not constant but adapts to the chemical potential of the neutral charge species in the surroundings of the solid electrolyte. The present findings fit well in accordance with previous findings done on Na-beta-alumina, NASICON, alkali carbonates with regard to the non-conventional behaviour of $a_{\oplus}$.

4.5.2 System KBA/K-Silicate/O_2

4.5.2.1 Thermo voltage

The non-isothermal voltage generated across the cell (VII) plotted against temperature gradient (ΔT) for different potassium activities of the $KSi_xO_{2x+0.5}/SiO_2/O_2$ and $KSi_xO_{2x+0.5}/SiO_2/H_2/H_2O$ electrodes at 650 °C is depicted in Fig. 4-37.

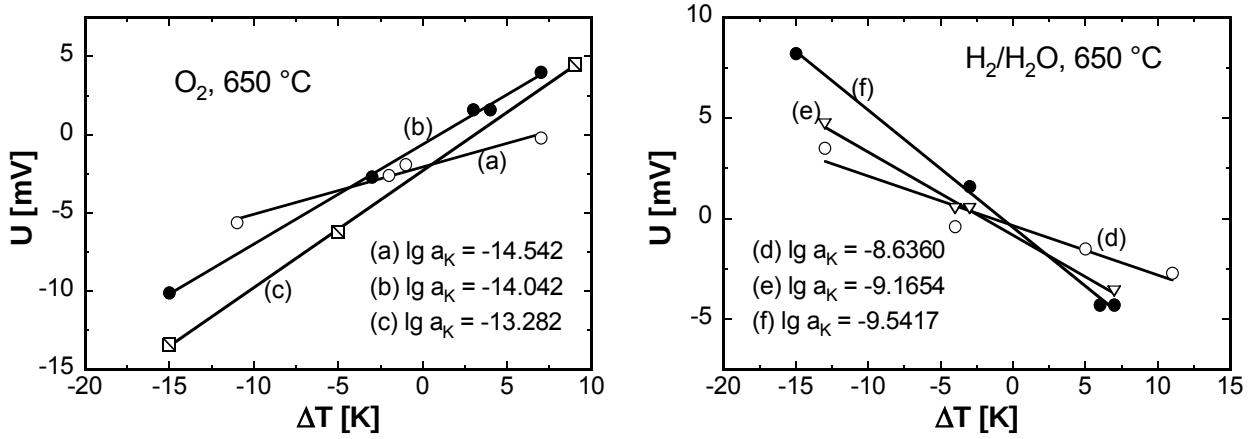

Fig. 4-37 Non isothermal voltage dependence on ΔT of cell (VII) under O_2 (Ar) and H_2/H_2O (Ar) atmosphere at T = 650 °C

The U versus ΔT plots can be satisfactorily be described by a linear curve at each temperature and chemical potential covered during the investigation. The occurrence of an offset voltage is observed as found in earlier studies (section 4.2, 4.4.1.1). The absolute magnitude of the offset voltage is rather small as compared with K-beta-alumina with $K_2CO_3/CO_2/O_2$ electrode and amounts to 0.5-1 mV at T = 650 °C.

4.5.2.2 Thermoelectric power

The functional dependence of thermoelectric power of K-beta-alumina on the potassium activity is illustrated in Fig. 4-38.

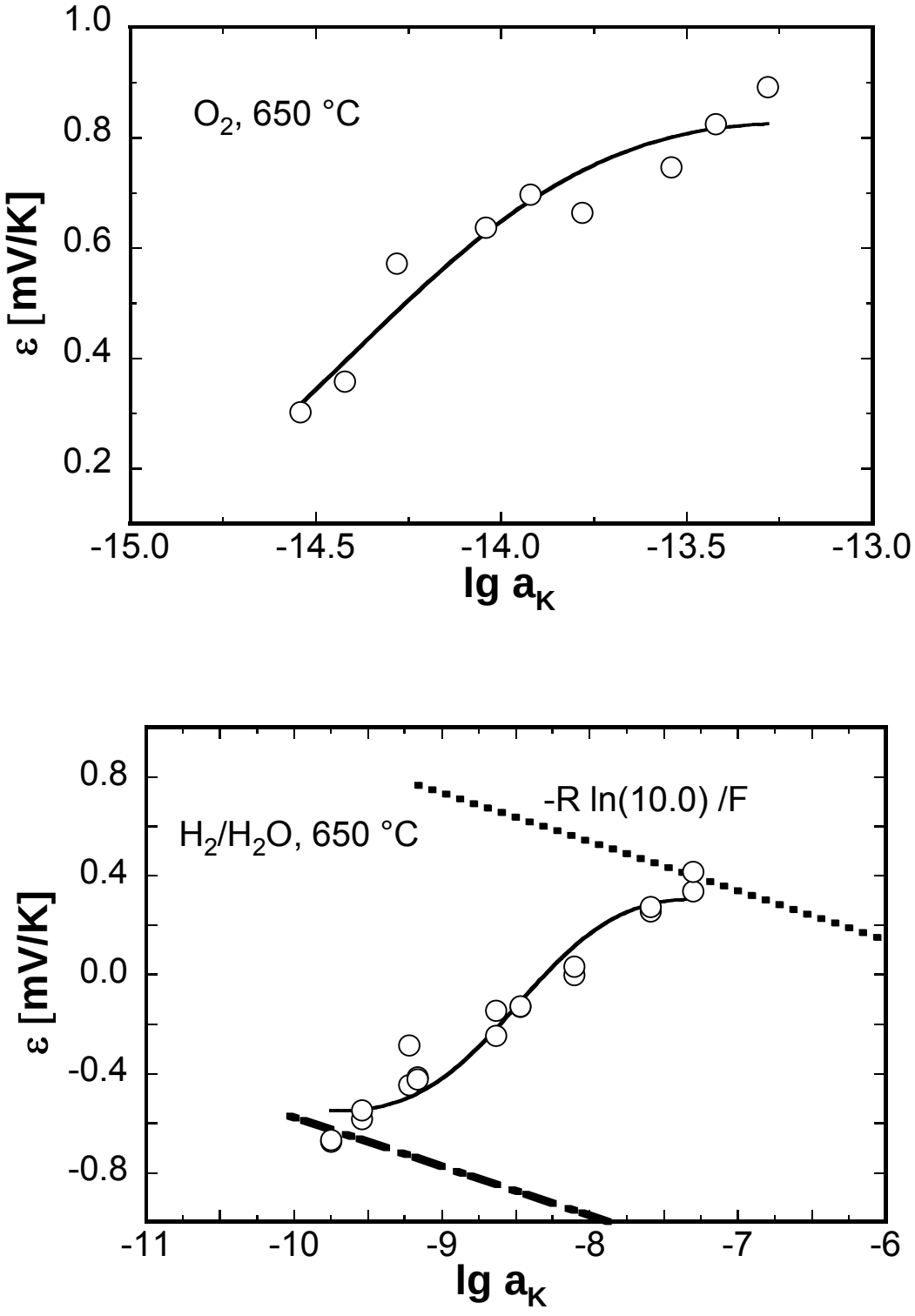

Fig. 4-38 Potassium chemical potential dependence of the thermoelectric power of cell (VII) at T = 650 °C (solid lines demonstrate the fitting according to Eq. 2-70)

The activity was adjusted within an interval of one order of magnitude in case of O_2 while 3 orders in case of H_2/H_2O gas atmosphere by stepwise rising and decreasing the compositions of the gases as shown in Fig. 4-38. The direction of activity variation has no apparent influence on the behaviour of thermoelectric power of the cell at least for 650 °C and the data lies within the normal scattering. The elapsed time between two successive points in Fig. 4-38 was 36-48 hours. It becomes evident from Fig. 4-38 that similar to previous observations on Na-beta-alumina under similar conditions (cf. section 4.4.1.2), a non-linear dependence of thermoelectric power on the potassium chemical potential is obtained.

It is discernible from Fig. 4-38 that at high potassium activity exemplified by the right end of the abscissa, the thermoelectric power varies linearly with the chemical potential (dotted line) with slope –R ln(10.0)/F in accordance with Eq. 2-70. With decrease in the activity the data deviate from the linear curve which becomes more pronounce at the low chemical potential region. This is due to the fact that a_K decreases exponentially on moving from right to left of the x axis and $a_\oplus$ prevails more and more over a_K in Eq. 2-70. Finally a new linear dependence of the thermoelectric on the activity dominated by electron holes is observed.

The reasonable fitting curves are achieved by simulating the experimental data according to Eq. 2-70 as demonstrated by the solid lines passing through the data points in Fig. 4-38.

4.5.2.3 Temperature dependence of $a_\oplus$

The logarithm of $a_\oplus$ that was obtained using the above procedure is plotted as a function of inverse of the temperature depicted in Fig. 4-39 for both K-silicate/SiO_2/O_2 and K-silicate-SiO_2/H_2/H_2O electrodes.

Both the curves in Fig. 4-39 are parallel to the temperature dependence of the potassium chemical potential of the corresponding electrodes. As clearly seen in Fig. 4-39 the obtained $a_\oplus$ data lies close to the potassium activity of the electrodes of cell (VII). It means the chemical potential of the electrode lies outside the conduction domain of the solid electrolyte K-beta-alumina.

Thus $a_\oplus$ appears to adapt to the chemical potential of the neutral species in the surroundings of the solid electrolyte confirming the previous findings [11-15] on the unconventional property of $a_\oplus$.

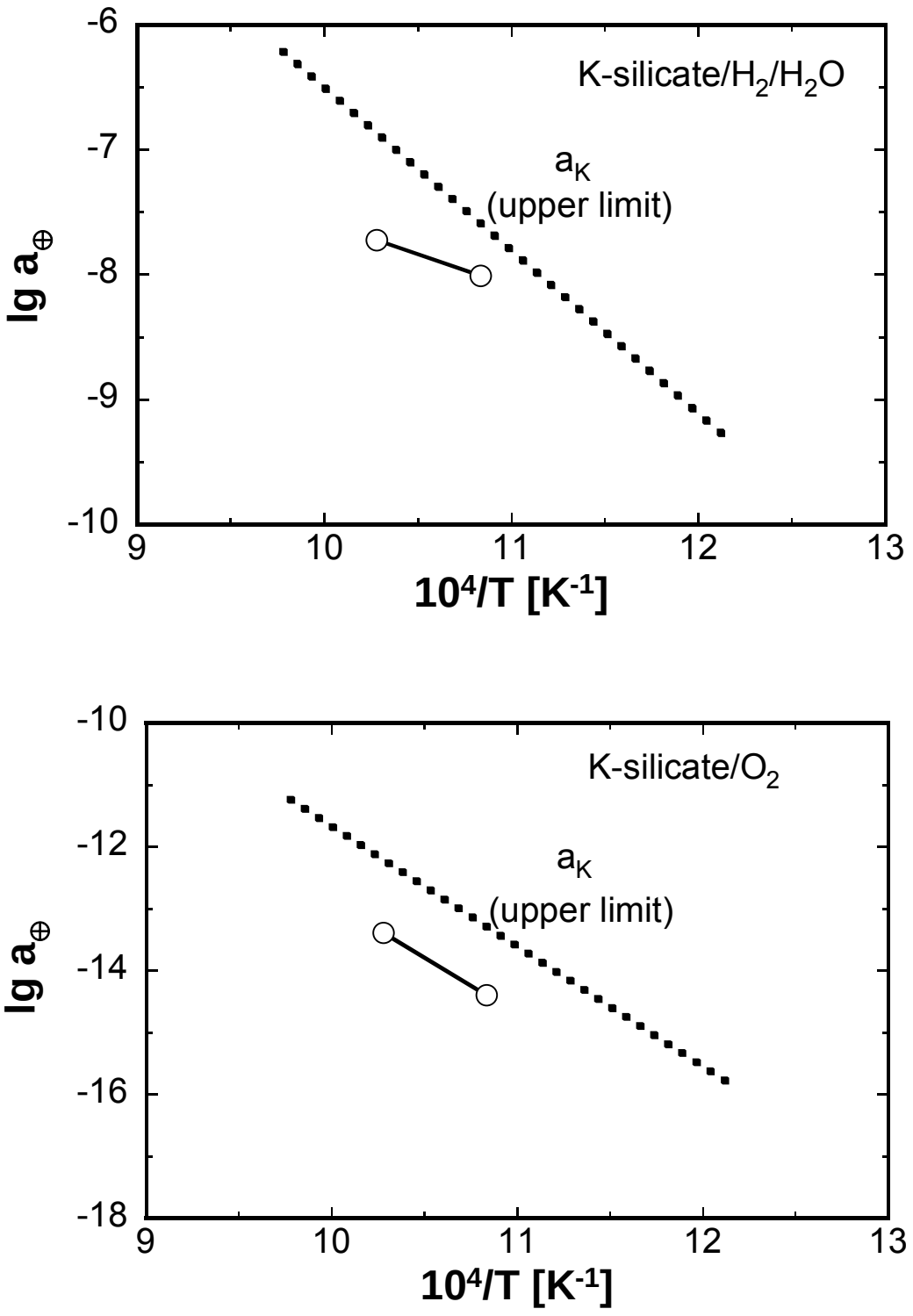

Fig. 4-39 Temperature dependence of p-electronic conduction parameter for K-beta-alumina with $KSi_xO_{2x+0.5}$, SiO_2, H_2/H_2O and $KSi_xO_{2x+0.5}$, SiO_2, O_2 electrodes

4.5.3 Potassium chemical potential dependence of $a_{\oplus}$

Fig. 4-40 illustrates the potassium chemical dependence of the logarithm of $a_{\oplus}$ for K-beta-alumina obtained by using different electrodes and two different techniques i.e. thermoelectric power and solid state potentiometric measurements.

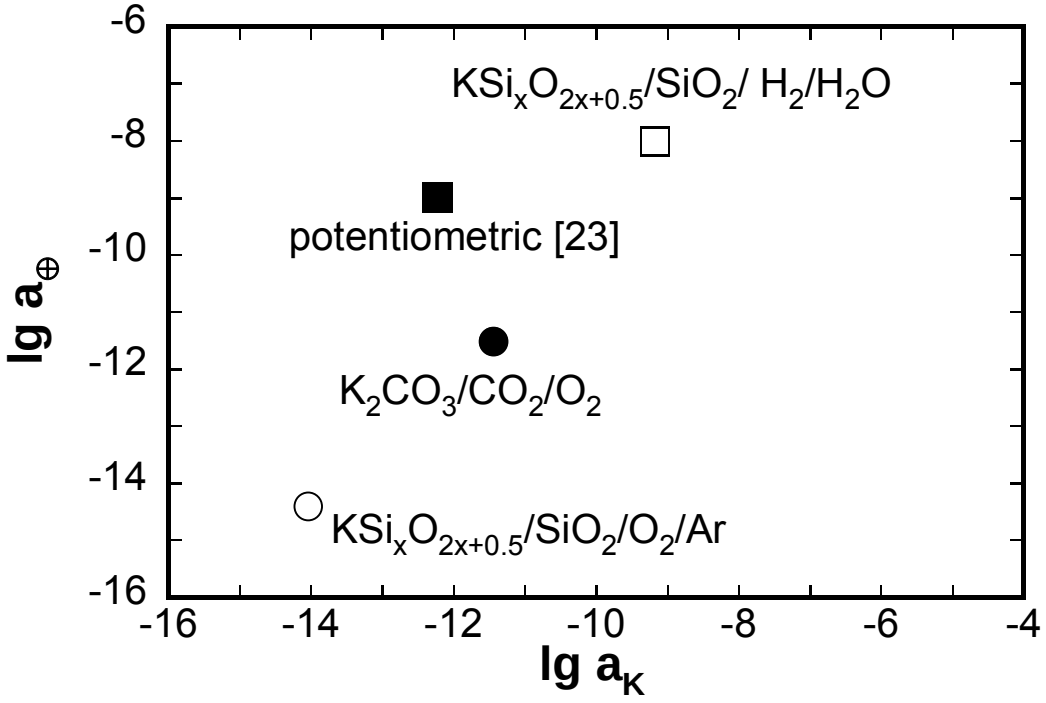

Fig. 4-40 Potassium dependence of p-electronic conduction parameter for K-beta-alumina with different electrodes at 650 °C

The values of the abscissa have been achieved by utilising $KSi_xO_{2x+0.5}/SiO_2/O_2$, $K_2CO_3/CO_2/O_2$ and $KSi_xO_{2x+0.5}/SiO_2/H_2/H_2O$ as electrode materials by means of which a spectrum of 6-7 orders of magnitude of the activity was covered.

As a consequence of the classical defect chemical consideration $a_{\oplus}$ is constant with change in the chemical potential of the neutral species. However as shown in Fig. 4-40 $a_{\oplus}$ varies with the potassium chemical potential in the surroundings of the solid electrolyte i.e. K-beta-alumina in contradiction to the defect chemical consideration. Interpreting similarly as in the case of Na-beta-alumina (section 4.4), the non-constancy of $a_{\oplus}$ could be understood as resulting from the minor changes in the composition of the electrolyte material under different levels of the chemical potential. The present observation agrees well with the previous findings on Na-beta-alumina ([9, 11, 14], section 4.4), NASICON (cf. section 4.2) that the electronic conduction parameter of solid electrolyte adapts to the chemical surroundings in addition to the temperature. Thus, the general relevance of the phenomenon is again underlined.

4.6 Impedance spectroscopy measurement on Na_2CO_3

Fig. 4-41a depicts the impedance spectrum of Na_2CO_3 obtained at T = 650 °C for a particular sodium activity in the form of a Nyquist plot. It is evident from Fig. 4-41a that three depressed semicircles in the impedance spectrum were observed.

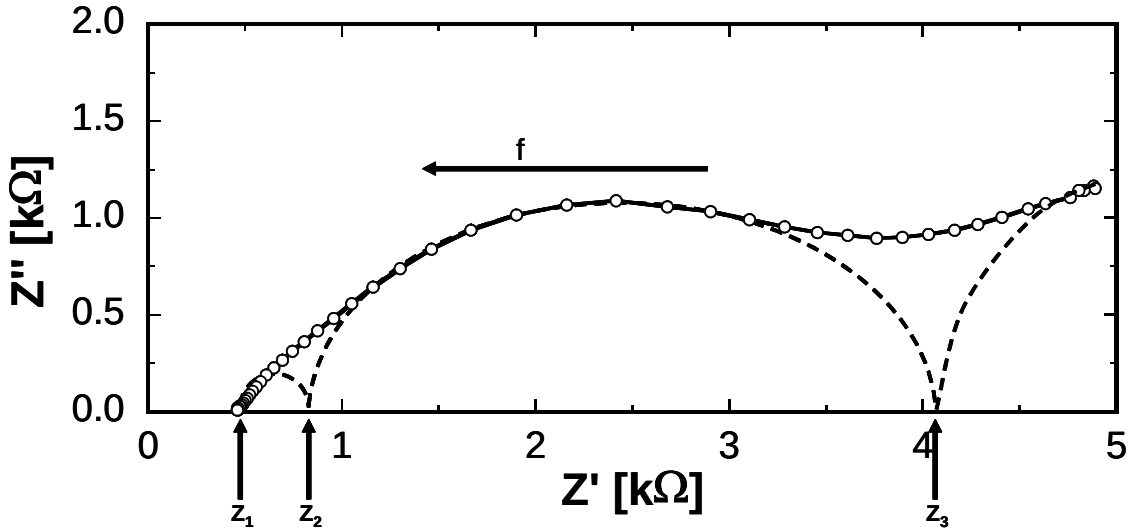

(a)

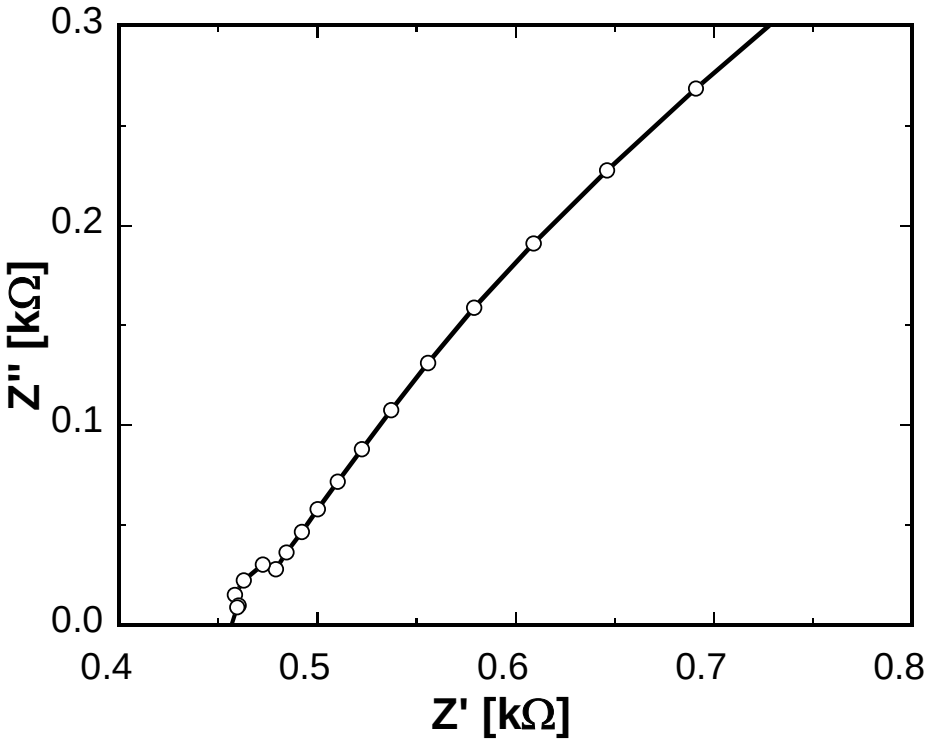

(b)

Fig. 4-41 (a) Impedance spectrum of Na_2CO_3 at lg a_{Na} = -13.105, T = 650 °C
(b) An enlarged view of high frequency semicircle Z_1Z_2

Fig. 4-42 depicts how the impedance spectrum of Na_2CO_3 changes as a function of the sodium chemical potential at 650 °C. The sodium activities were adjusted by alternately increasing and decreasing the O_2 and CO_2 partial pressures of the gas mixtures under isothermal conditions. Irrespective of the temperature, all the impedance spectra were recorded only after equilibrating Na_2CO_3 with corresponding gases for a minimum time period of 24 h. As illustrated in Fig. 4-42 the shape of the impedance spectrum plot changes with a_{Na}. The number of observed semicircles varies both with the sodium activity as well as the temperature.

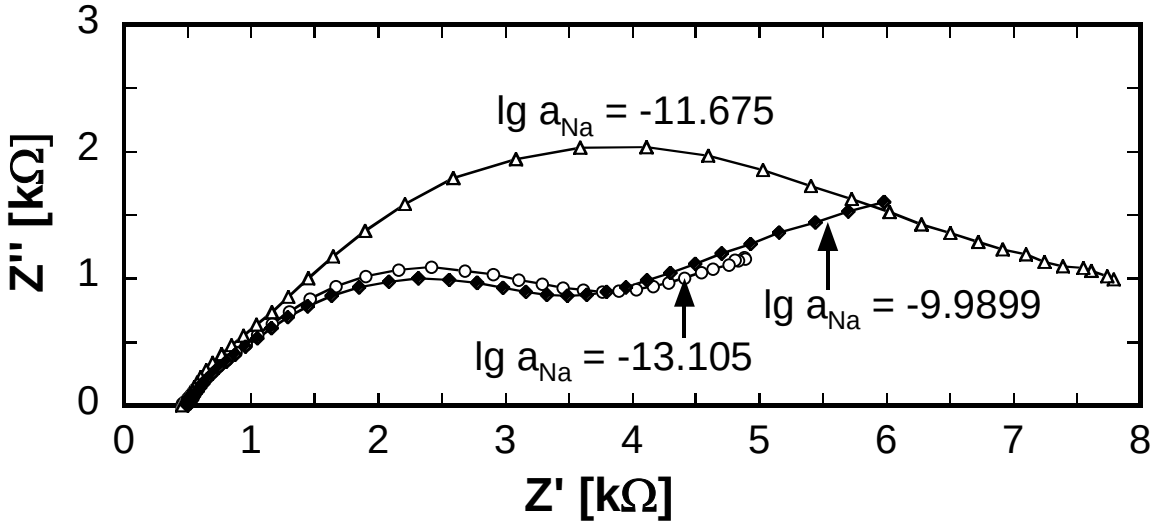

Fig. 4-42 Variation of the impedance spectra of Na_2CO_3 under various sodium activities at T = 650 °C

The magnitude of the intermediate semicircle is greatly influenced by changes in the sodium activity. However it does not follow any particular trend with the variation of sodium activities. This behaviour is characteristic of the entire temperature region covered in the present investigation (450 °C ≤ T ≤ 750 °C). As shown in Fig. 4-41b the high frequency semicircle at the extreme left end of the abscissa is very small in comparison with the middle and low frequency semicircles. This has been observed in the whole interval of covered sodium activity and temperature. The semicircles in the low frequency interval are relatively more depressed than that at high frequency end.

As seen from Figs. 4-41a, 4-42 the semicircles are not well separated from each other. An overlapping occurs and the necks between the semicircles cover large parts of the diagram. When one of the semicircles is much smaller than others, its unambiguous characterisation is difficult. The extremities can be obtained by extrapolation using the well defined part of the other semicircle as demonstrated in Fig. 4-41a. The intercepts of the semicircles with the real axis are represented by Z_n with n = 1, 2, 3 as exhibited in

Figs. 4-41a, 4-41b. All semicircles parameters respond to the changes in sodium activity as depicted in Fig. 4-42. They shift towards lower impedances as the sodium activity decreases. This is due to the increasing impact of the electronic short-circuit on the total resistance of the material with decreasing sodium chemical potential.

Owing to the complexity of the impedance technique, it is difficult to attribute exactly which part of a high frequency semi circle represents the bulk property of the material. It is assumed that the low frequency intersection of the high frequency semicircle i.e. Z_1Z_2 (Fig. 4-41b) represents the total bulk resistance of the sample.

The conductivities σ_1 and σ_2 that are calculated using Eq. 2-81, the parameters Z_1, Z_2 and the geometrical shape of the sample are plotted as a function of the sodium activity at T = 650 and 450 °C and displayed in Fig. 4-43.

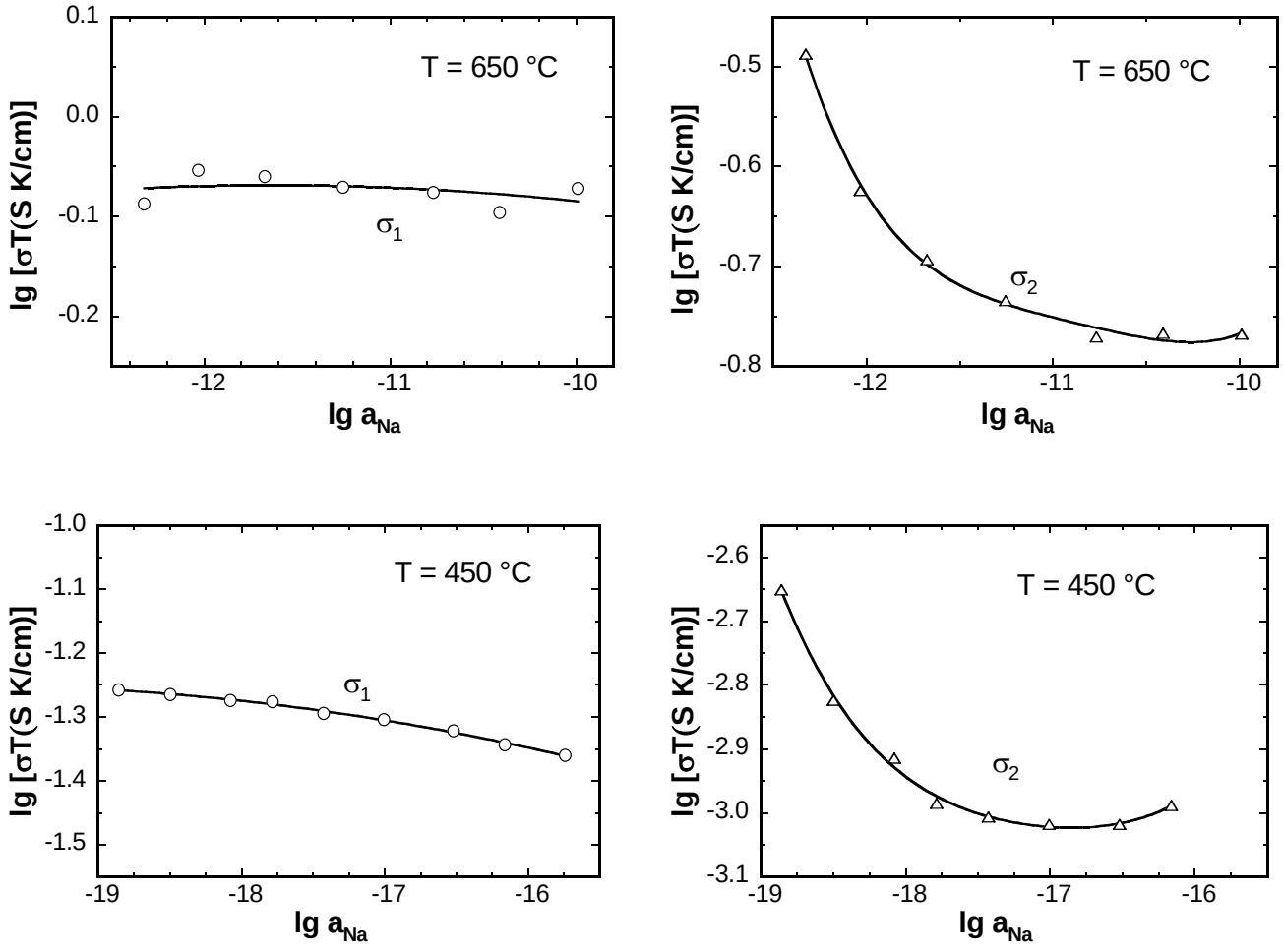

Fig. 4-43 Influence of sodium activity on the conductivities σ_1 (left) and σ_2 (right) of cell (I) at T = 450 °C and 650 °C

It is discernible that log σ_1 is nearly independent of the sodium chemical potential whereas log σ_2 varies exponentially in the whole range of the temperature interval covered in the present study proving that some changes in the total conductivity of Na_2CO_3 takes place under the condition of measurement. This could be interpreted by an activity depending change of the conductivities that Na_2CO_3 behaves as a mixed ionic-electronic conductor. The present findings qualitatively substantiate the findings obtained by thermoelectric power investigations (section 4.3).

In Fig. 4-44 σ_1 (curve 1) and σ_2 (curve 2) at the lowest sodium activity that is for the partial pressure of O_2 and CO_2 {p_{O_2} = 0.15 (bar), p_{CO_2} = 0.852 (bar)} are plotted as a function of the inverse temperature. The data are compared with the only available data on the total conductivity of Na_2CO_3 in the literature [43] (curve 3).

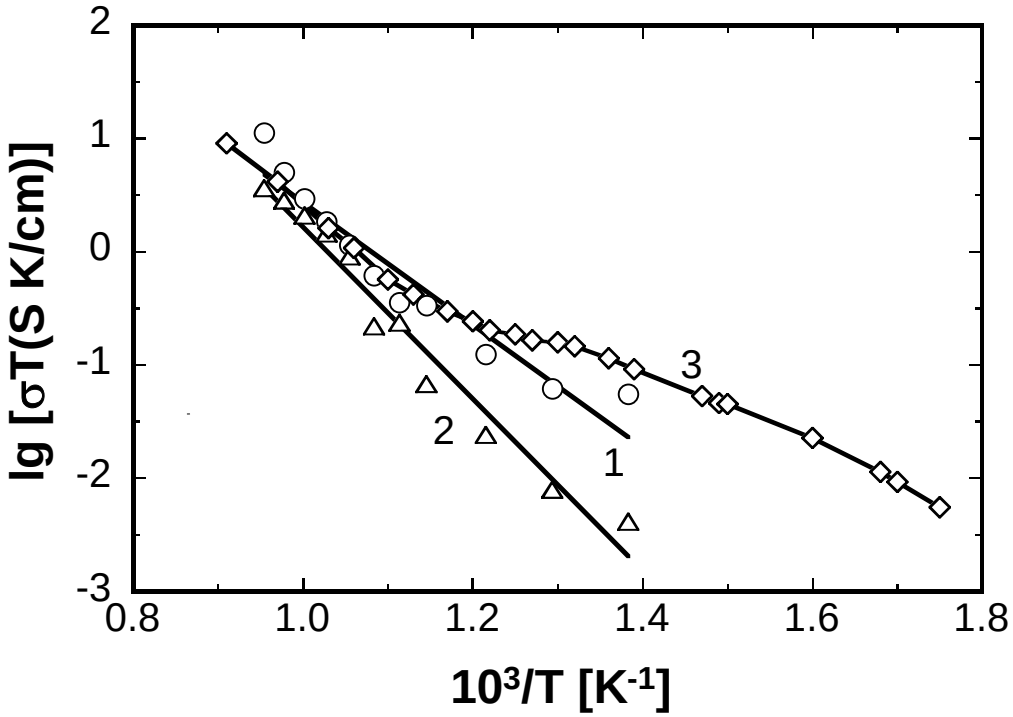

Fig. 4-44 Total conductivity of Na_2CO_3 as a function of the temperature (σ_1: curve 1, σ_2: curve 2) in comparison with literature data (curve 3 [43])

As evident from Fig. 4-44 the measured conductivities as far as the magnitude and temperature dependence is concerned are in fair agreement with the literature data [43]. The deviation of the data becomes larger as the temperature is decreasing. Since the literature data were measured in the ambient air, the chemical potential of sodium could not considered as well defined due to the uncertainty in the CO_2 partial pressure. However, in the present investigations the sodium activity is definitely fixed by

establishment of the partial pressures of CO_2, O_2 gas mixtures. Moreover, in [43] the impedance measurements were performed only at one fixed frequency which may be erroneously interpreted as pointed out by [114, 115].

Thus the conductivity measurement points out that Na_2CO_3 is a mixed conductor in the sodium activity region covered in the investigation in qualitative agreement with the previous observation by thermoelectric power technique (section 4.3).

5. Conclusions and Outlook

1. In the present investigation the thermodynamic stability of NASICON has been determined by solid state potentiometric technique without the impact of the electronic transference.
2. The thermodynamic activity of Na_2O was obtained in a wide range of the chemical potential and temperature interval (350-550 °C).
3. For the first time the establishment of the phase equilibrium in NASICON was characterized in-situ in a wide region of the sodium activity. The findings indicate the phase equilibrium in NASICON is composition independent under the applied measuring conditions.
4. The thermoelectric power was determined for the cation conducting solid electrolytes NASICON, Na-beta-alumina, K-beta-alumina, Na_2CO_3 and K_2CO_3 under a large interval of the temperature and the chemical potential. The metal chemical potential region covered was 6-7 orders of magnitude.
5. The numerical values of the p-electronic conduction parameter $a_{\oplus}$ were obtained by evaluating the ε vs. log a_{Me} relationship. It was demonstrated that the materials become electronically conductive under the condition of the measurements.
6. It was found that the p-electronic conduction parameter of Na-beta-alumina and K-beta-alumina is not a constant with respect to the chemical potential of the neutral species. The findings confirm the previous conclusions drawn by Näfe and co-workers [7-14] that $a_{\oplus}$ may adapt to the chemical potential in the surroundings of the solid electrolyte.
7. Na_2CO_3 was characterised by impedance spectroscopy measurements under different sodium activities and temperatures. The results are in qualitative agreement with the conclusion drawn from the thermoelectric power measurements underlining that Na_2CO_3 behaves as a mixed ionic-electronic conductor.

Even though the findings on the thermodynamic stability of NASICON indicate the existence of a univariant phase equilibrium, nothing is known regarding the co-existing phases in this material. For that reason further work should be focussed on the characterization of the composition of the phases taking part in the equilibrium. The

future work should also aim at the understanding of the possible phase transitions at low temperatures.

In the present work a non-negligible voltage under zero temperature gradient was observed for all the investigated materials in the whole spectrum of the chemical potential and the temperature. However, the cause of the origin of the offset voltage has not been understood. It remains unclear whether the occurrence of the offset voltage influences the thermoelectric power of the materials. Hence systematic study should be done to understand the evolution of the offset voltage and its relevance for the thermoelectric power.

The reasons for the adaptation of the p-electronic conduction parameter ($a_{\oplus}$) with the surroundings are not known yet. In addition, it is still an open question under which conditions $a_{\oplus}$ becomes independent of the surroundings and which factors govern the dependency.

To underline the general relevance of the observed phenomenon regarding $a_{\oplus}$ future work should be expanded to other cation conducting solid electrolytes and to a wider range of activities.

6. Summary

Under certain circumstances the electronic conductivity of the solid electrolyte may play a pivotal role for the behaviour of a solid state galvanic cell. Quantitatively, the extent of the electronic conductivity is expressed by the electronic conduction parameters, $a_{\oplus}$ and $a_{\ominus}$, that denote the alkali metal activities at which the n and p-type electronic conductivities, respectively, of the electrolyte are equal to its ionic conductivity. Previous findings [1-11] demonstrated the existence of a finite, non-negligible electronic conductivity in various alkali metal ion conductors like Na-beta-alumina (NBA), K-beta-alumina (KBA) and NASICON when these materials are employed as solid electrolytes in potentiometric CO_2 sensors or for certain thermodynamic investigations. Particularly, a number of previous studies [2, 5, 7, 10] brought into the light the tendency of the p-type electronic conduction parameter $a_{\oplus}$ to adapt to the chemical potential of those species that represent the neutral counterpart of the mobile ion of the electrolyte. These findings are in contradiction [2] with the basic assumptions of the conventional defect chemical considerations underlying the Schmalzried-Wagner theory of mixed ionic-electronic conduction. Because of the fundamental relevance, they were supposed to be substantiated further, at best by an experimental approach independent of the previously applied ones.

Thermoelectric power measurements, under certain prerequisites, allow to determine the proportion of the electronic charge carriers transport in the total conductivity of a mixed ionic-electronically conducting material. Moreover, this technique has an inherent advantage over the isothermal potentiometric technique insofar as the two surfaces of the solid electrolyte need not be exposed to different electrode media as the voltage is primarily generated due to a temperature gradient. This makes the approach an essential and so far disregarded tool to clarify the above mentioned unconventional phenomenon regarding $a_{\oplus}$.

The objective of the present work is the quantitative determination of the p-electronic conduction parameter $a_{\oplus}$ of several sodium and potassium ion-conducting solid electrolytes, namely NBA, KBA, NASICON, Na_2CO_3 and K_2CO_3, by thermoelectric power measurements under a possibly wide spectrum of the chemical potential of the potential determining species and temperature. The measurements aimed at finding further evidence for the dependence of the p-electronic conduction parameter on the surroundings as was first described by Näfe [2]. In addition, impedance spectroscopy studies were designed to characterize the conduction properties of some exemplary

materials by another measuring technique and to independently check the results of the thermoelectric power measurements, at least qualitatively. In view of the paucity of the knowledge regarding the stability of the constituent phases of NASICON and because of the relevance of this topic for the characterization of the electronic conduction parameter of this material, the thermodynamic stability of NASICON was determined as another task to be fulfilled within the present work.

For the thermoelectric power measurements, the following thermo-cells have been considered:

$Pt \mid CO_2, O_2, Au \mid Na_2CO_3 \mid Au, O_2, CO_2 \mid Pt$ (I)

$Pt \mid CO_2, O_2, Na_2CO_3\ (Au) \mid NASICON \mid Na_2CO_3\ (Au), O_2, CO_2 \mid Pt$ (II)

$Pt \mid CO_2, O_2, K_2CO_3\ (Au) \mid KBA \mid K_2CO_3\ (Au), O_2, CO_2 \mid Pt$ (III)

$Pt \mid CO_2, O_2, Au \mid K_2CO_3 \mid Au, O_2, CO_2 \mid Pt$ (IV)

$Pt \mid O_2, NaSi_yO_{2y+0.5}, SiO_2\ (Au) \mid NBA \mid NaSi_yO_{2y+0.5}, SiO_2\ (Au), O_2 \mid Pt$ (V)

$Pt \mid O_2, Na_2MoO_4, Na_2MoO_7\ (Au) \mid NBA \mid Na_2MoO_4, Na_2MoO_7\ (Au), O_2 \mid Pt$ (VI)

$Pt \mid O_2, KSi_yO_{2y+0.5}, SiO_2\ (Au) \mid KBA \mid KSi_yO_{2y+0.5}, SiO_2\ (Au), O_2 \mid Pt$ (VII)

$Pt \mid CO_2, O_2 \mid Na_2CO_3\ (Au) \mid NASICON\ (Au) \mid YSZ \mid O_2\ (CO_2) \mid Pt$ (VIII)

The measurements were carried out over the temperature range 698-923 K and under an interval of the sodium and potassium chemical potential that has been accomplished by using different kinds of electrodes e.g. $Me_2CO_3/CO_2/O_2$, $MeSi_yO_{2y+0.5}/SiO_2/O_2$ (Me = Na, K) and $Na_2MoO_4/Na_2MoO_7/O_2$. Their thermodynamic activities have been varied by using various compositions of CO_2-O_2-Ar gases in equilibrium with Me_2CO_3 and by using O_2-Ar, H_2-H_2O-Ar gases in equilibrium with $MeSi_yO_{2y+0.5}$ and molybdate (Me = Na, K). Thereby 3 orders of magnitude of the metal activity have been realized in the case of metal carbonates, 3-4 orders in the case of the silicates and one order in the case of sodium molybdate. By combining the results of the measurements a range of about 6-7 orders of magnitude in the thermodynamic activity has been altogether covered.

For the impedance measurements a SOLARTRON 1255B system was used. The total impedance of Na_2CO_3 employed as solid electrolyte in cell (I) was measured under various temperatures and, in particular, various sodium activities to get independent information about the conduction properties in addition to that of the thermoelectric power measurements.

The characterization of the thermodynamic stability of NASICON has been performed by a new type of cell voltage measurements on the solid electrolyte galvanic cell (VIII). The measuring principle is based on that of an oxygen concentration cell with yttria stabilized zirconia (YSZ) as an oxygen ion conducting solid electrolyte. The oxygen chemical potential established at the interface YSZ/NASICON is related to the activity of Na_2O dissolved in NASICON thereby providing an information about the thermodynamic stability of the constituent phases of NASICON.

The thermoelectric power (ε), defined as the derivative of the voltage of a thermo-cell with respect to the temperature gradient ΔT, was evaluated as a function of the alkaline metal activity a_{Na} and a_K, respectively, as well as the temperature. As concerns the dependence of the thermo voltage on ΔT from which the thermoelectric power data were derived, it is linear for cells (I)-(VII) in the complete interval of sodium and potassium activity as well as temperature. The thermoelectric power as a function of the chemical potential significantly deviates from the behaviour expected for a solid electrolyte with predominant ionic conduction. Then the ε vs. log a_{Me} relationship should be a straight line with the slope –R/F. The deviation from linearity is most significant in the region of low chemical potential. As concerns the non-linear shape of the ε vs. log a_{Me} dependence, the experimental observations are in agreement with previous findings on Na-beta-alumina with $Na_2CO_3/CO_2/O_2$ electrode [4]. By simulating the field of experimental data $\varepsilon = f(a_{Me}, T)$ using a non-linear curve fit algorithm, which is based on a redefined version of the classical Wagner equation, the p-electronic conduction parameter $a_\oplus$ for the materials was determined. The logarithm of $a_\oplus$ plotted as a function of the inverse temperature provides a linear relationship in accordance with theoretical expectation. In all cases the temperature dependence of $a_\oplus$ runs largely parallel to the temperature dependence of the electrode activities of the thermo-cells indicating that $a_\oplus$ is related to the chemical potential in the ambience of the electrolyte. This could finally be confirmed in detail by the studies on NBA and KBA for which $a_\oplus$ under different levels of the alkali metal activity was obtained. Here the p-type electronic conduction parameter proved to be not a constant but unambiguously changed with changing sodium or potassium chemical potential. The results are in complete agreement with previous findings based on other experimental approaches thus re-proving the peculiar property of the electronic conduction parameter of heavily doped mixed ionic-electronic conductors. Thus they demonstrate that the solid electrolyte materials used in the study behave as mixed conductors depending on the conditions of measurement, which is in

apparent contradiction to many reports on using these materials as pure ionic conductor in potentiometric solid state CO_2 sensors or for thermodynamic characterization.

The non-constancy of $a_{\oplus}$ may be understood as the consequence of a minor change of the composition of the electrolyte material under the impact of different levels of the chemical potential of the alkali metal in the surroundings. This is an expression of a certain degree of non-stoichiometry of the electrolyte due to which its nature as a solvent of all defects changes. Hence the equilibrium constants determining the relevant defect equilibria changes as well and so does $a_{\oplus}$ resulting from them.

In the thermoelectric measurements quite a small but finite thermo voltage under a zero temperature gradient termed as an offset voltage, was observed. The offset voltage that finally does not interfere the magnitude of the thermo power but in general contradicts the theoretical expectation slightly changes with the metal activity as well as the temperature and has a typical value of about 1-3 mV. The exact reason for the generation of the offset voltage is not yet understood and needs to be studied further. It could be assumed to result from a non-balanced distribution of the ions and electrons in the solid due to an incomplete equilibration with the surroundings [8]. As then even under isothermal conditions a flux of charge carriers may flow, an extremely low voltage decays especially at the polarization resistance of the electrodes.

The results of the impedance measurement on Na_2CO_3 indicate that changes in the total conductivity of the material take place as a function of the sodium activity. The conductivity increases with decreasing thermodynamic activity which is a typical phenomenon of a mixed ionic-electronic conductor. Thus the results are in qualitative agreement with the conclusions drawn from the thermoelectric power measurements about the role of the electronic conductivity.

The thermodynamic studies on NASICON accomplished by potentiometric measurements on cell configuration (VIII) proved for the first time the existence of a univariant phase equilibrium in the solid. This outcome is all the more profound as the establishment of the phase equilibrium was checked in-situ within a large interval of the composition of the phase mixture. It provides a solid basis for the comparison of the present data with the only source of data known in the literature [12] and for the interpretation of the apparent differences. As concerns the nature of the coexisting phases in the solid material nothing is known so far which is why further work should be focused on that aspect.

Literature

[1] M. Steinbrück, H. Näfe, Solid State Ionics **67** (1994) 271.

[2] H. Näfe, Sensors Actuators B **21** (1994) 79.

[3] S. Gollhofer, Dissertation, Universität Stuttgart (2002).

[4] K. Shqau, Dissertation, Universität Stuttgart (2003).

[5] H. Näfe, Solid State Ionics **113-115** (1998) 205.

[6] H. Näfe, M. Fritz, W. J. Lorenz, Solid State Ionics **74** (1994) 275.

[7] H. Näfe, S. Gollhofer, F. Aldinger, Mater. Res. Soc. Symp. Proc. **548** (1999) 52

[8] H. Näfe, J. Electrochem. Soc. **144** (1997) 3922.

[9] K. Shqau, H. Näfe, F. Aldinger, F. M. Figueiredo, Electrochemica Acta **49** (2004) 2691.

[10] H. Näfe, Sensors Actuators **B 105** (2005) 119.

[11] H. Näfe, M. Steinbrück, J. Electrochemical Soc. **141** (1994) 2779.

[12] G. M. Kale, K. T. Jacob, J. Mater. Res. **4 (2)** (1989) 417.

7. Zusammenfassung

Unter bestimmten Bedingungen kann die elektronische Leitfähigkeit des Festelektrolyten von zentraler Bedeutung für das Verhalten einer galvanischen Festelektrolytzelle sein. Das Ausmaß dieser Leitfähigkeit wird quantitativ durch die elektronischen Leitungsparameter $a_{\oplus}$ and $a_{\ominus}$ zum Ausdruck gebracht. Das sind jene Alkalimetallaktivitäten, bei denen die p- oder n-Leitfähigkeit des Festelektrolyten seiner ionischen Leitfähigkeit entspricht.

Die Ergebnisse früherer Arbeiten [1-11] haben gezeigt, daß in verschiedenen Alkalimetallionenleitern, wie Na-beta-Al_2O_3 (NBA), K-beta-Al_2O_3 (KBA) und NASICON, eine endliche, nicht vernachlässigbare elektronische Leitfähigkeit auftritt, wenn diese Materialien als feste Elektrolyte in potentiometrischen CO_2-Sensoren oder für thermodynamische Untersuchungen eingesetzt werden. Insbesondere hat sich aus den bisherigen Untersuchungen [2, 5, 7, 10] die Tendenz des p-Elektronenleitungsparameters $a_{\oplus}$ abgezeichnet, sich an das chemische Potential jener Spezies anzupassen, die das ungeladene Pendant zu den beweglichen Ionen des Festelektrolyten darstellen. Diese Beobachtungen stehen im Widerspruch zu den grundlegenden Annahmen der herkömmlichen defektchemischen Betrachtungen, die der Schmalzried-Wagner-Theorie der ionisch-elektronischen Mischleitung zugrunde liegen [2]. Wegen ihrer Bedeutung sollten die Messeffekte weiter vertieft werden, günstigenfalls durch eine experimentelle Vorgehensweise, die unabhängig von den bisher praktizierten ist.

Thermokraftmessungen erlauben unter bestimmten Bedingungen die Bestimmung des Anteils des elektronischen Ladungstransports an der Gesamtleitfähigkeit eines gemischt-leitenden Mediums. Darüber hinaus hat diese Technik gegenüber isothermen potentiometrischen Zellspannungsmessungen den Vorteil, daß die beiden Oberflächen des Elektrolyten nicht unterschiedlichen Elektrodensystemen ausgesetzt werden müssen, da die Spannung primär durch einen Temperaturgradienten verursacht wird. Das macht sie zu einem wesentlichen und bisher unbeachtet gebliebenen Werkzeug zur Aufklärung des oben erwähnten ungewöhnlichen Phänomens zum Verhalten von $a_{\oplus}$.

Das Ziel der vorliegenden Arbeit ist die quantitative Bestimmung des p-Elektronenleitungsparameters $a_{\oplus}$ verschiedener natrium- und kaliumionenleitender Festelektrolyte, wie NBA, KBA, NASICON, Na_2CO_3 und K_2CO_3, durch Messung der thermoelektrischen Kraft innerhalb eines möglichst großen Bereiches des chemischen

Potentials der potentialbestimmenden Spezies und darüberhinaus auch der Temperatur. Die Untersuchungen zielten auf weitere experimentelle Belege für die Abhängigkeit des p-Elektronenleitungsparameters von der Umgebung des Festelektrolyten ab, wie dies erstmals von Näfe [2] beschrieben worden ist. Zusätzlich sollten impedanzspektroskopische Untersuchungen durchgeführt werden, mit denen an einem exemplarisch gewählten Material die Leitungseigenschaften mittels einer weiteren Methode auf unabhängige Art und Weise charakterisiert und so die Aussagen der Thermokraftmessungen zumindest qualitativ überprüft werden können. Wegen des Fehlens verläßlicher Daten zur Phasenstabilität von NASICON ganz allgemein und wegen der Bedeutung solcher Daten für die Charakterisierung der Elektronenleitungseigenschaften dieses Materials wurde die Bestimmung der thermodynamischen Stabilität von NASICON als eine weitere Aufgabe dieser Arbeit angesehen.
Für die thermoelektrischen Untersuchungen wurden folgende Thermo zellen verwendet:

Pt | CO_2, O_2, Au | Na_2CO_3 | Au, O_2, CO_2 | Pt (I)

Pt | CO_2, O_2, Na_2CO_3 (Au) | NASICON | Na_2CO_3 (Au), O_2, CO_2 | Pt (II)

Pt | CO_2, O_2, K_2CO_3 (Au) | KBA | K_2CO_3 (Au), O_2, CO_2 | Pt (III)

Pt | CO_2, O_2, Au | K_2CO_3 | Au, O_2, CO_2 | Pt (IV)

Pt | O_2, $NaSi_yO_{2y+0.5}$, SiO_2 (Au) | NBA | $NaSi_yO_{2y+0.5}$, SiO_2 (Au), O_2 | Pt (V)

Pt | O_2, Na_2MoO_4, Na_2MoO_7 (Au) | NBA | Na_2MoO_4, Na_2MoO_7 (Au), O_2 | Pt (VI)

Pt | O_2, $KSi_yO_{2y+0.5}$, SiO_2 (Au) | KBA | $KSi_yO_{2y+0.5}$, SiO_2 (Au), O_2 | Pt (VII)

Pt | CO_2, O_2 | Na_2CO_3 (Au) | NASICON (Au) | YSZ | O_2 (CO_2) | Pt (VIII)

Die Messungen wurden innerhalb des Temperaturintervalls 698-923 K und über einen weiten Bereich des chemischen Potentials von Natrium bzw. Kalium durchgeführt, letzteres durch die Verwendung unterschiedlicher Elektrodensysteme: $Me_2CO_3/CO_2/O_2$, $MeSi_yO_{2y+0.5}/SiO_2/O_2$ (Me = Na, K) und $Na_2MoO_4/Na_2MoO_7/O_2$. Die thermodynamischen Aktivitäten dieser Elektroden wurden durch variierende Zusammensetzungen von Gasgemischen realisiert, und zwar von CO_2-O_2-Ar im Gleichgewicht mit Me_2CO_3 und von O_2-Ar sowie H_2-H_2O-Ar im Gleichgewicht mit $MeSi_yO_{2y+0.5}$ (Me = Na, K) bzw. Na-Molybdat. Dadurch gelang es, die Alaklimetallaktivität im Falle der Carbonate über 3 Zehnerpotenzen hinweg zu variieren, im Falle der Alkalisilikate über 3-4 Zehnerpotenzen und im Falle des Natriummolybdats über eine Zehnerpotenz. Durch Kombination der Meßergebnisse konnte somit ein Bereich von insgesamt 6-7 Zehnerpotenzen

hinsichtlich des chemischen Potentials in der Umgebung des Elektrolyten überstrichen werden.

Für die Impedanzmessungen wurde das Meßsystem SOLARTRON 1255B verwendet. In diesem Falle diente Na_2CO_3 als Festelektrolyt (Zelle (I)), dessen Impedanz bei verschiedenen Temperaturen, insbesondere aber variierenden Natriumaktivitäten ermittelt wurde, um so unabhängig von den thermoelektrischen Untersuchungen zusätzlich Informationen über die Leitungseigenschaften zu erhalten.

Die Charakterisierung der thermodynamischen Stabilität von NASICON wurde durch eine neuartige Form potentiometrischer Zellspannungsmessungen mit Hilfe von Zelle (VIII) realisiert. Das Meßprinzip basiert auf dem einer Sauerstoffkonzentrationskette mit yttriumoxidstabilisiertem ZrO_2 (YSZ) als sauerstoffionenleitendem Festelektrolyt. Auf diese Weise wird das chemische Potential des Sauerstoffs, das sich an der Phasengrenze YSZ/NASICON einstellt, mit der Aktivität des im NASICON gelösten Na_2O in Beziehung gesetzt, woraus sich eine Information über die thermodynamische Stabilität der in NASICON dominierenden Phasen ergibt, die ihrerseits mit der Komponente Na_2O im Gleichgewicht stehen.

Die thermoelektrische Kraft (ε), die als Differentialquotient der Spannung einer Thermozelle hinsichtlich des Temperaturgradienten ΔT definiert ist, wurde als Funktion der Alkalimetallaktivität a_{Na} bzw. a_K und der Temperatur ausgewertet. Was die Abhängigkeit der Thermospannung vom Temperaturgradienten anbelangt, so ist diese für die Zellen (I)-(VII) im gesamten Intervall der Natrium- und Kaliumaktivität sowie der Temperatur linear, woraus sich auf einfache Weise die Thermokraftdaten ermitteln lassen. Diese weichen eindeutig von dem für einen Festelektrolyten mit überwiegender Ionenleitung erwarteten Verhalten ab, wonach die ε-log a_{Me}-Beziehung durch eine Gerade mit der Steigung –R/F repräsentiert sein sollte. Die Abweichung von der Geraden wird mit abnehmender Alkalimetallaktivität immer ausgeprägter. Hinsichtlich dieses nichtlinearen Zusammenhangs entsprechen die Beobachtungen den früher bereits gemachten Erfahrungen an Na-beta-Al_2O_3 mit $Na_2CO_3/CO_2/O_2$ als Elektrode [4]. Durch Beschreibung des Feldes experimenteller Daten, $\varepsilon = f(a_{Me}, T)$ mittels eines Zusammenhangs, der auf einer erweiterten Fassung der auf Wagner zurückgehenden klassischen Beziehungen basiert, und durch Anwendung eines Algorithmus zur nichtlinearen Regression wurde aus den Daten der p-Leitungsparameter $a_\oplus$ für die jeweiligen Materialien bestimmt. Trägt man den Logarithmus von $a_\oplus$ als Funktion der inversen Temperatur auf, so ergibt sich in Übereinstimmung mit den theoretischen Erwartungen ein linearer Zusammenhang. In allen betrachteten Fällen verläuft die

Temperaturabhängigkeit von $a_{\oplus}$ weitgehend parallel zur Temperaturabhängigkeit der Aktivität der in den Thermozellen eingesetzten Elektrodensysteme. Das deutet darauf hin, daß $a_{\oplus}$ mit dem jeweils in der Umgebung des Elektrolyten vorherrschenden chemischen Potential in Beziehung steht, was schließlich im einzelnen durch die Untersuchungen an den Materialien NBA und KBA bestätigt werden konnte. In diesen Fällen war $a_{\oplus}$ bei stark unterschiedlichen Alkalimetallaktivitäten ermittelt worden. Dabei erwies sich der p-Elektronenleitungsparameter als nicht konstant, sondern änderte sich unzweideutig mit dem sich ändernden chemischen Potential des Natriums bzw. Kaliums. Die Ergebnisse stimmen mit früheren Beobachtungen auf der Basis anderer experimenteller Methoden überein und belegen erneut das ungewöhnliche Verhalten des Elektronenleitungsparameters in einem gezielt dotierten Mischleiter. Sie demonstrieren somit, daß die untersuchten Festelektrolyte in Abhängigkeit von den jeweiligen Bedingungen gemischte Leiter sein können, was im Widerspruch zu vielen Angaben aus der Literatur steht, wo dieselben Materialien bei ihrer Verwendung in CO_2 Sensoren und für thermodynamische Messungen ohne Einschränkung als reine Ionenleiter angesehen werden.

Die Nichtkonstanz von $a_{\oplus}$ kann als Folge einer geringfügigen Änderung der Zusammensetzung des Festelektrolyten unter dem Einfluß unterschiedlicher Niveaus des chemischen Potentials des Alkalimetalls in der Umgebung des Elektrolyten verstanden werden. Dies ist Ausdruck eines gewissen Grades von Nichtstöchiometrie im Elektrolyten, durch die sich seine Natur als Lösungsmittel für alle beteiligten Defekte ändert. Infolge dessen ändern sich auch die Gleichgewichtskonstanten für die relevanten Defektgleichgewichte, aus denen unter anderem auch $a_{\oplus}$ hervorgeht.

Während der thermoelektrischen Messungen tritt eine sehr kleine, aber endliche Thermospannung selbst bei verschwindendem Temperaturgradienten, das heißt bei $\Delta T = 0$, auf. Diese Offset-Spannung, die zwar nicht die Größe der Thermokraft verfälscht, aber dennoch den theoretischen Erwartungen widerspricht, ändert sich interessanterweise leicht mit der Metallaktivität und der Temperatur. Sie bewegt sich zwischen 1 und 3 mV. Die Entstehung dieser Spannung ist unklar und bedarf weiterer Aufklärung. Denkbar ist, daß sie aus einer gegebenenfalls nicht völlig im Gleichgewicht befindlichen Verteilung der Ladungsträger über den Querschnitt des Festelektrolyten hinweg resultiert [8]. Dann kann auch unter isothermen Bedingungen ein äußerst geringfügiger Strom fließen, der zu einem Spannungsabfall vor allem an den Elektrodenwiderständen führt.

Die Ergebnisse der impedanzspektroskopischen Messungen an Na_2CO_3 weisen darauf hin, daß mit der Natriumaktivität Änderungen in der Gesamtleitfähigkeit des Materials einhergehen. Die Leitfähigkeit steigt mit fallender thermodynamischer Aktivität, was typisch für einen Mischleiter ist. Die Ergebnisse stehen qualitativ mit den Schlußfolgerungen aus den thermoelektrischen Messungen über die Rolle der elektronischen Leitfähigkeit im Einklang.

Die thermodynamischen Untersuchungen an NASICON belegten zum ersten Mal die Existenz eines univarianten Phasengleichgewichtes in dem Festkörper. Diese Erkenntnis ist um so profunder, als die Einstellung des Gleichgewichts in-situ und innerhalb eines großen Intervalls der Zusammensetzung des Phasengemisches überprüft wurde. So ergibt sich eine solide Grundlage für den Vergleich der vorliegenden mit den einzigen in der Literatur verfügbaren Daten [12] sowie für die Interpretation der auftretenden Unterschiede. Zur Natur der in dem Festkörper koexistierenden Phasen kann derzeit nichts gesagt werden. Dieser Aspekt muß weiteren Untersuchungen vorbehalten bleiben.

Literatur

[1] M. Steinbrück, H. Näfe, Solid State Ionics **67** (1994) 271.
[2] H. Näfe, Sensors Actuators B **21** (1994) 79.
[3] S. Gollhofer, Dissertation, Universität Stuttgart (2002).
[4] K. Shqau, Dissertation, Universität Stuttgart (2003).
[5] H. Näfe, Solid State Ionics **113-115** (1998) 205.
[6] H. Näfe, M. Fritz, W. J. Lorenz, Solid State Ionics **74** (1994) 275.
[7] H. Näfe, S. Gollhofer, F. Aldinger, Mater. Res. Soc. Symp. Proc. **548** (1999) 52
[8] H. Näfe, J. Electrochem. Soc. **144** (1997) 3922.
[9] K. Shqau, H. Näfe, F. Aldinger, F. M. Figueiredo, Electrochemica Acta **49** (2004) 2691.
[10] H. Näfe, Sensors Actuators **B 105** (2005) 119.
[11] H. Näfe, M. Steinbrück, J. Electrochemical Soc. **141** (1994) 2779.
[12] G. M. Kale, K. T. Jacob, J. Mater. Res. **4 (2)** (1989) 417.

8. References

[1] L. C. De Jonghe, L. Feldman, A. Beuchele, J. Mater. Sci. **16** (1981) 780.

[2] A. V. Virkar, J. Mater. Sci. **20** (1985) 552.

[3] N. Weber, Energy Conv. **14** (1974) 1.

[4] C. Sun, Z. Guo, Guisuanyan Xuebao **9** (1981) 444.

[5] O. Takikawa, A. Imai, M. Harata, Solid State Ionics **7** (1982) 101.

[6] M. Fritz, M. R. Barbosa, G. Staikov, W. J. Lorenz, M. Steinbrück, R. Knödler, Solid State Ionics **62** (1993) 273.

[7] H. Näfe, M. Steinbrück, J. Electrochemical Soc. **141** (1994) 2779.

[8] M. Steinbrück, H. Näfe, Solid State Ionics **67** (1994) 271.

[9] H. Näfe, Sensor Actuators B **21** (1994) 79.

[10] H. Näfe, Solid State Ionics **68** (1994) 249.

[11] H. Näfe, Solid State Ionics **113-115** (1998) 205.

[12] H. Näfe, M. Fritz, W. J. Lorenz, Solid State Ionics **74** (1994) 275.

[13] H. Näfe, S. Gollhofer, F. Aldinger, Mater. Res. Soc. Symp. Proc. **548** (1999) 521.

[14] H. Näfe, S. Gollhofer, F. Aldinger, J. Electrochem. Soc. **149** (2002) E311.

[15] K. Shqau, H. Näfe, F. Aldinger, F. M. Figueiredo, Electrochemica Acta, **49** (2004) 2691.

[16] K. Shqau, H. Näfe, (to be published).

[17] C. Wagner, Prog. Solid State Chem. **7** (1972) 1.

[18] H. Näfe, Lecture notes, (Spring 2003) (unpublished).

[19] N. Tallan, I. Bransky, J. Electrochem. Soc. **118** (1971) 345.

[20] H. Kuwato, H. Sato, Solid State Ionics **5** (1981) 187.

[21] A. Schiraldi, P. Baldini, P. Ross, J. Electrochem. Soc. **130** (1983) 2490.

[22] R. Subasri, H. Näfe, F. Aldinger, J. Solid State Electrochem. **6** (2002) 259.

[23] K. Shqau, Dissertation, Universität Stuttgart (2003).

[24] K. S. Goto, Solid state electrochemistry and its applications to sensors and electronic devices, Material Science Monographs 45, Elsevier, Amsterdam-Oxford-New York-Tokyo (1988), pp 12.

[25] S. Geller, Solid Electrolytes, Topics in Applied Physics, Springer-Verlag, Berlin-Heidelberg-New York (1977), pp 15.

[26] J. L. Briant, G. C. Farrington, J. Solid State Chemistry **33** (1980) 385.

[27] W.L. Roth, R.E. Benenson, V.K. Tikku, J.L. Briant, B. Dunn, Solid State Ionics **5** (1981) 163.

[28] T. Kodama, I. Ogino, O. Nakamura, Y. Miyake, Osaka Kogyo Gijutsu Shikensho Kiho **26** (1975) 113.

[29] J. H. Kennedy, Solid Electrolytes, Editors: S. Geller, Springer-Verlag, Berlin-Heidelberg-New York (1977) 105.

[30] T. Cole, N. Weber, T. K. Hunt, Proc. Int. Conf. Fast Ion Trans. Solids, Editor: P. Vashishta, Elsevier North-Holland, Inc., Lake Geneva, Wisconsin, U.S.A. (1979) 277.

[31] W. Jakubowski, D. H. Whitmore, J. Am. Ceram. Soc. **62** (1979) 381.

[32] M. Steinbrück, V. Heinzel, F. Huber, W. Peppler, M. Voss, H. Will, Proc. 28th Intersociety Energy Conversion Engineering Conf. **1** (Am. Chem. Soc., Washington, DC, 1993) p. 1.799.

[33] Ionotec Ltd., Internet Homepage.

[34] S. E. Omrod, D.L. Kirk, J. Phys. D **10** (1977) 1497.

[35] A. Hachtel, Dissertation, Universität Stuttgart (1988).

[36] A. V. Virkar, G. R. Miller, R. S. Gordon, J. Am. Ceram. Soc. **61** (1978) 250.

[37] Ph. Colomban, E. Mouchon, Solid State Ionics **53-56** (1992) 813.

[38] J. P. Boilot, J. P. Salanié, G. Desplanches, D. Le Potier, Mat. Res. Bull. **14** (1979) 1469.

[39] J. R. Dygas, M. E. Brodwin, Solid State Ionics **18-19** (1986) 981.

[40] R. O. Fuentes, F. M. Figueiredo, M. R. Soares, F. M. Marques, J. Euro. Ceram. Soc. **25 (4)** (2005) 455.

[41] S. Y. Andersen, J. S. Lundsgaard, Solid State Ionics **14** (1984) 73.

[42] O. Bohnke, S. Ronchetti, D. Mazza, Solid State Ionics **122** (1999) 127.

[43] P. Cerisier, F. Roux, J. Solid State Chem. **22** (1977) 245.

[44] S. Brosda, H. J. M. Bouwmeester, U. Guth, Solid State Ionics **101-103** (1997) 1201.

[45] P. Cerisier, F. Roux, Solid State Communications **26** (1978) 661.

[46] F. A. Kröger, H. J. Vink, Solid State Physics, **3**, Editors: F. Seitz, D. Turnbull, Academic Press, New York (1956), pp 307.

[47] F. A. Kröger, H. J. Vink, J. Phys. Chem. Solids **5** (1958) 208.

[48] H. Näfe, M. Steinbrück, J. Electrochem. Soc. **141 (10)** (1994) 2779.

[49] J. H. Kennedy, A. F. Sammells, J. Electrochem. Soc. **119** (1972) 1609.

[50] I. W. Jones, L. J. Miles, Proc. Brit. Ceram. Soc. **19** (1971) 161.

[51] A. Imai, M. Harata, Electrochem. Soc. Meeting Abst. (1970) 277.

[52] W. L. Worrel, Solid Electrolytes, Editors: S. Geller, Springer-Verlag, Berlin-Heidelberg-New York (1977) 143.

[53] W. L. Bragg, C. Gottfried, J. West, Z. Kristallogr. **77** (1931) 255.

[54] C. A. Beevers, M. A. S. Ross, Z. Kristallorg. **95** (1937) 59.

[55] M. Bettman, L. L. Terner, Inorg. Chem. **10** (1971) 1442.

[56] J. Felsche, Naturwissenschaften **54** (1967) 621.

[57] C. R. Peters, H. Bettman, J. W. Moore, M. D. Glick, Acta Cryst. **B27** (1971) 1826.

[58] W.L. Roth, Trans. Am. Cryst. Assoc. **11**, (1975).

[59] W.L. Roth, J. Solid State Chem. **4** (1972) 60.

[60] P. D. Dernier, J. P. Remeika, J. Solid State Chem. **17** (1976) 245.

[61] H. Y-P. Hong, Mat. Res. Bull. **11** (1976) 173.

[62] J. B. Goodenough, et al., Mat. Res. Bull. **11** (1976) 203.

[63] J. Zarzycki, Faraday Soc. Discuss. **32** (1961) 38.

[64] A. Reismann, J. Am. Chem. Soc. **80** (1958) 3558.

[65] A. T. Ward, G. J. Janz, Electrochimica Acta **10** (1965) 849.

[66] W. Van Aalst, J. Den Hollander, W. J. A. M. Peterse, P. M. De Wolff, Acta. Cryst. **B32** (1976) 47.

[67] S. J. Schneider, E. M. Levin, J. Am. Ceram. Soc.-Discussions and Notes **56 (4)** (1973) 218.

[68] H. Schmalzried, Z. Elektrochem. 66 (1962) 572.

[69] H. Näfe, Proc. Electroceramics IV **2** (1994) 745.

[70] NIST-JANAF Thermochemical Tables, 4th Edition, National Institute of Standards and Technology New York (1998).

[71] H. Näfe, J. Electrochem. Soc. **151 (5)** (2004) J-27.

[72] N. Karpukhina, H. Näfe (to be published).

[73] R. Amin, Dissertation, Universität Stuttgart (2005).

[74] C. Wagner, Advances in Electrochemistry and Electrochemical Engineering, Editor: P. Delahay **4** (Interscience, New York, 1966) 1.

[75] H. Rickert, C. Wagner, Ber. Bunsenges. Phys. Chem. **67** (1971) 621.

[76] C. Wagner, Z. Phys. Chem. B **21** (1933) 25.

[77] C. Wagner, Z. Elektrochem. **60** (1956) 4.

[78] W. Dürselen, Mitteilungsblatt Chem. Ges. DDR **19** (1972) 57.

[79] W. Dürselen, H. H. Möbius, Z. Phys. Chem. **258** (1977) 181.

[80] Landolt-Bornstein, Vol. **2,** part 6, Springer, Berlin, Heidelberg New York (1959) 931.

[81] F. A. Kröger, The chemistry of imperfect crystals, Vol. **3**, North-Holland/American Elsevier (1974) 191.

[82] G. M. Kale, K. T. Jacob, J. Mater. Res. **4 (2)** (1989) 417.

[83] H. Näfe, F. Meyer, F. Aldinger, Electrochimica Acta **45** (2000) 1631.

[84] K. Shqau, H. Näfe, J. Am. Ceram. Soc. **88 (10)** (2005) 2894.

[85] J. Yang, H. Näfe, F. Aldinger, J. Am. Ceram. Soc. **88** [10] (2005) 2897.

[86] H. Näfe, Solid State Ionics **93** (1997) 117.

[87] J. E. Bauerle, J. Phys. Chem. Solids **30** (1969) 2657.

[88] H. Näfe, Solid State Ionics **13** (1984) 255.

[89] J. R. Macdonald, Impedance Spectroscopy: Emphasizing Solid Materials and Systems, Wiley-Interscience Publication New York (1987).

[90] JCPDS, Powder Diffraction Files Int. Centre for Diffraction Data Newton Square, USA (1998).

[91] D. W. Johnson, S. M. Grundstaff, W. W. Rhodes, Bull. Am. Ceram. Soc. 58 (9) (1979) 849.

[92] G. E. Youngblood, A. V. Virkar, W. R. Cannon, R. S. Gordon, Am. Ceram. Soc. Bulletin 56 (1) (1977) 206.

[93] E. Groschuff, Z. anorg. Chem. **58** (1908) 117.

[94] H. Näfe, Z. Metallkd. **94** (2003) 962.

[95] T. Maruyama, X. Y. Ye, Y. Saito, Solid State Ionics **23** (1987) 113.

[96] F. Salam, S. Bredikhin, P. Birke, W. Weppner, Solid State Ionics **110** (1988) 319.

[97] T. Maruyama, Materials Science and Engineering, **A146** (1991) 81.

[98] S. Yao, Y. Shimizu, N. Miura, N. Yamazoe, J. Electrochem. Soc. **139** (1992) 1384.

[99] N. Miura, S. Yao, Y. Shimizu, N. Yamazoe, Sensor and Actuators B **13** (1993) 387.

[100] N. Miura, S. Yao, Y. Shimizu, N. Yamazoe, Solid State Ionics **70-71** (1994) 572.

[101] G.M. Kale, A.J. Davidson, D.J. Fray, Solid State Ionics **86-88** (1996) 1107.

[102] S. D. Choi, W. Y. Chung, D. D. Lee, Sensor and Actuators B **35-36** (1996) 263.

[103] M. A.-Porta, R.V. Kumar, Sensor and Actuators B **71** (2000) 173.

[104] J. Ramírez-Salgado, P. Fabry, Solid State Ionics **158** (2003) 297.

[105] Y. Shimizu, N. Yamashita, Sensor and Actuators B **64** (2000) 102.

[106] L. Zhang, D. J. Fray, J. C. Dekeyser, F. de Schutter, Met. Trans., **27B** (1996) 794.

[107] R. J. Brisley, D. J. Fray, Met. Trans., **14B** (1983) 435.

[108] M. Gauthier, A. Chamberland, J. Electrochem. Soc. **124** (1977) 1579.

[109] M. Itoh, E. Sugimoto, Z. Kozuka, Trans. Jap. Inst. Met. **25** (1984) 504.

[110] T. Maruyama, S. Sasaki, Y. Saito, Solid State Ionics **23** (1987) 107.

[111] R. Akila, K. T. Jacob, Sensor Actuators **16** (1989) 311.

[112] J. Liu, W. Weppner, Eur. J. Solid State Inorg. Chem. **28** (1991) 1151.

[113] H. H. Möbius, P. Shuk, W. Zastrow, Fresenius, J. Anal. Chem. **356** (1996) 221.

[114] E. Schouler, A. Hammou, M. Kleitz, Mat. Res. Bull. **11** (1976) 1137.

[115] C. E. McGinley, P. Hancok, J. Mater. Sci. **6** (1971) 260.

[116] J. Jaffray, M. Martin, J. Phys. Rad. **14** (1953) 553.

[117] E. Brouns, J. W. Visser, Acta Crystallogr. **17** (1964) 614.

[118] G. C. Dubbeldam, P. M. De Wolff, Acta Crystallogr. **B25** (1969) 2665.

[119] H. Näfe, J. Electrochemical Soc. **144** (1997) 3922.

Curriculum Vitae

Family name	Gautam
First name	Devendraprakash
Date of birth	25.06.1978
Place of birth	Deori Hatai, India
Nationality	Indian
Gender	Male

Education and working experience:

July 1994-June 1996	Higher Secondary School
July 1996-June 1999	Bachelor of Science Nagpur University, Nagpur, India
August 1999-June 2001	Master of Science Nagpur University, Nagpur, India **Project title**: "Fabrication of electrochemical oxygen gas sensor''
July 2001-April 2002	Teaching Assistant at Department of Physics Nagpur University, Nagpur, India
June 2002-present	Pursuing Ph.D. (Material Science)at the Max-Planck-Institut für Metallforschung affiliated to University of Stuttgart, Stuttgart, Germany **Thesis title**: "Characterization of the conduction properties of alkali metal ion conducting solid electrolytes using thermoelectric measurements''